ABSTRACT

PENLEY, CHRISTOPHER RANDY. Cesium Neutral Beam and Surface Oxidation Effects on SIMS Analysis at Surface of Silicon. (Under the direction of Dr. Dieter P. Griffis.)

The effects of sample aging and unintended cesium contamination on measurements of low dose P implants in Si using SIMS were investigated. The goal of the sample aging part of this study was to investigate changes over time in the apparent phosphorus surface concentration that have been observed in SIMS depth profiles of low dose ($\leq$1E13at/cm^2) phosphorus implanted silicon samples. The impetus for the cesium exposure study is to determine whether unintended cesium contamination occurring during SIMS analysis contributes to the observed changes in the apparent P concentrations in subsequent analyses.

The changes in apparent (i.e. as measured by SIMS) phosphorus surface concentration which occur over time may be affected by surface oxidation, diffusion, and/or the influence of adjacent prior analyses. It is not clear whether the apparent increase in P surface concentration observed in SIMS depth profiles results from redistribution of the implanted dose, contamination from the environment, a change in P secondary ion yield, or a combination of these and/or other factors.

The increase in P concentration was particularly apparent for the lowest dose (1E12at/cm^2) P implanted samples measured, especially those which had been stored in heat and exposed to Cs due to previous analyses of the same wafer piece. This effect was less apparent as implanted dose increases and was not measurable on samples having 1E14at/cm^2 dose. There is also evidence that redistribution occurs in heat without Cs exposure, but at a much slower pace. Thus, the use of low dose P implants without any pre or post processing as standards for P dose measurements or other P quantification experiments is problematic.

With regard to using pre or post processing methods for mitigating any aging problems in low dose P implants in Si, the use of pre-amorphization is problematic since the depth of the implant is drastically reduced causing potential problems with obtaining sufficient data points for generation of a useful RSF. However, preliminary results indicate that either pre-cleaning followed by RTA or implantation through a 50Å oxide can provide wafers that improve results when these samples are used for low dose P implant standards.

The second part of this study examined depth profiles of sample surfaces that have been previously exposed to Cs primary beam. Depth profiles of these samples clearly showed significant Cs contamination (a few tenths of an atomic percent) as far as 300μm away from the previously analyzed crater. It was shown that this level is sufficient to significantly affect P redistribution and/or P secondary ion yield for samples previously exposed to Cs and/or stored in heat.

For wafers without any pre or post processing, results indicate that in order to achieve high precision quantitative measurement of P in low dose P implanted Si samples, samples should be stored in a cool dry environment and that samples previously exposed to Cs should not be used.

Additionally, if a new piece of standard can be used for each analysis, the RTA method appears to produce a useful standard. If Cs exposure cannot be avoided, it is recommended that a depth beyond that affected by the P increase be selected and that only the dose at greater than the selected depth be integrated to avoid any risk of the potentially deleterious effects of surface Cs.

Cesium Neutral Beam and Surface Oxidation Effects on SIMS Analysis at Surface of Silicon

by
Christopher Randy Penley

A thesis submitted to the Graduate Faculty of
North Carolina State University
In partial fulfillment of the
Requirements for the Degree of
Master of Science

Materials Science and Engineering

Raleigh, North Carolina

2008

APPROVED BY:

John M. Mackenzie Committee Member	Phillip E. Russell Committee Member
Dieter P. Griffis Committee Member	J. Michael Rigsbee Chair of Advisory Committee

DEDICATION

To my parents and my wife…

For your love and support…

BIOGRAPHY

Christopher Penley was born in Hickory, North Carolina. He went to Lenoir-Rhyne College in Hickory, North Carolina in 2001 and graduated with a Bachelor of Science degree in Physics with a minor in Mathematics in 2005. In the fall of 2005, he began work on his Masters degree in Materials Science and Engineering at North Carolina State University in Raleigh, North Carolina under the direction of Dr. Phillip E. Russell and Dr. Dieter P. Griffis.

ACKNOWLEDGEMENTS

I would like to express my sincere gratitude to the following:

- Dr. Dieter P. Griffis and Dr. Phillip E. Russell, for providing me with this excellent opportunity, guidance, and support with this research.
- Fred Stevie for his expert guidance and mentorship with his encouragement and support throughout my research.
- Dr. J. Michael Rigsbee and Dr. John M. Mackenzie for being my committee members and evaluating my work.
- Dr. Dale Batchelor, Roberto Garcia, and Chuck Mooney for their encouragement, guidance, and technical assistance.
- The Analytical Instrumentation Facility graduate students for their support and assistance.
- Intel Corporation for providing the financial support and samples utilized in this research.
- My parents and my sisters for their love and support.
- My wife, Amanda, for her love, patience, and support.

TABLE OF CONTENTS

LIST OF FIGURES ..... **viii**

LIST OF TABLES ..... **xiv**

1 Introduction and Overview **1**

1.1 Structure of the Thesis 1

1.2 Research Motivation and Thesis Goal 1

1.3 References 4

2 Semiconductor Processing **5**

2.1 Introduction 5

2.2 Ion Implantation 6

2.3 References 10

3 Secondary Ion Mass Spectrometry (SIMS) **12**

3.1 Introduction 12

3.2 Technique Overview 12

3.2.1 Static versus Dynamic SIMS 14

3.2.2 SIMS Analysis Methods 15

3.3 Fundamental Concepts in SIMS Related to Depth Profiling 16

3.3.1 Crater Depth and Topography Measurement 16

3.3.2 The Transient Region 17

3.3.3 Sensitivity and Depth Resolution 19

3.4 SIMS Quantification 28

3.4.1 Secondary Ion Yields 28

3.4.2 Relative Sensitivity Factor (RSF) 32

3.5 References 35

4 SIMS Instrumentation **38**

4.1 Introduction 38

4.2 Mass Analyzers 38

4.2.1 Time of Flight (TOF) Analyzers 39

4.2.2 Quadrupole Mass Analyzers 42
4.2.3 Magnetic Sector Analyzers 45
4.3 CAMECA IMS-6F 48
4.3.1 Ion Sources 49
4.3.1.1 Cs Microbeam Source 49
4.3.1.2 Duoplasmatron 51
4.3.2 The Primary Ion Column 53
4.3.3 Mass Spectrometer 53
4.3.4 Secondary Ion Detection 56
4.3.4.1 Faraday Cup 56
4.3.4.2 Electron Multiplier 57
4.3.4.3 Microchannel Plate/Fluorescent Screen 58
4.4 Tencor P-20 Stylus Profilometer 59
4.5 References 60
5 SIMS Depth Profiling of Phosphorus Implants under Cs^+ Bombardment 63
5.1 Introduction 63
5.2 Experiment 64
5.3 Results and Discussion 70
5.3.1 Effects on Different Phosphorus Implant Doses in Silicon 70
5.3.2 Effects on Phosphorus Implants in Silicon Exposed to Different Processing Methods 77
5.4 Summary 90
5.5 References 93
6 Quantification and the Effects of Cesium Surface Contamination in Si under Cs^+ Bombardment 94
6.1 Introduction 94
6.2 Experimental Method 94

6.3 Results and Discussion 96
6.3.1 Mechanisms for Cs Contamination on the Sample Surface....96
6.3.2 Visual Observation....97
6.3.3 Quantitative Analysis of Cs Contaminated Si 98
6.3.4 Quantification of Cs Contamination via Secondary Sputtering and Redeposition 100
6.3.5 Quantification of the Cs Surface Concentration Induced by Adjacent SIMS Analysis 102
6.4 Summary 106
6.5 References....107
7 Conclusions and Future Work 109
7.1 Summary 109
7.2 Future Work 110
APPENDIX....111

LIST OF FIGURES

Figure 1-1. Comparison of Moore's Law (dotted line) with the actual developments in the semiconductor industry.[1,2] 2

Figure 2-1. Dose and energy requirements of major implantation applications.[1] 7

Figure 3-1. Schematic of the SIMS technique.[2] 12

Figure 3-2. Collision cascades after the primary ion bombards the sample surface.[4] 13

Figure 3-3. Profile of O in Si using O_2^+ illustrating the typical surface transient region with O_2^+ bombardment at 5.5keV.[2] The projected range of the primary ion bombardment of O_2^+ into Si is represented by the dotted line. 18

Figure 3-4. Illustration of sensitivity, depth resolution, and dynamic range from the acquisition of a SIMS depth profile.[13] 20

Figure 3-5. Depth profile of P in Si for Cs^+ bombardment and high mass resolution.[2] Detection limits shown by arrows for Cs^+ and for O_2^+ bombardment at low and high mass resolution. 21

Figure 3-6. B implanted (9.6E13 atoms/cm^3, 35keV) into Si, profiled with different primary ion beam currents. Raw and processed data are shown on the left and right, respectively. Detection limits are represented by the dashed lines...23

Figure 3-7. Parameters for depth resolution.[2] 24

Figure 3-8. Increasing the O_2^+ primary beam energy increases the distortion of the depth profile and decreases the depth resolution. 25

Figure 3-9. TRIM simulation of cesium and oxygen implantation into silicon at different energies and incident angles. E_i is the impact energy of the ions, α is the angle of incidence, R_p is the projected range, and ΔR_p is the straggle. 26

Figure 3-10. The data presented illustrates the raster and gate relationship to depth profile shape and depth resolution.[2] 28

Figure 3-11. Comparing literature results of the variations of the silicon work function after cesium exposure.[50] 31

Figure 3-12. Variations of RSF's in Si matrix under O_2^+ and Cs^+ bombardment.[2] 32

Figure 3-13. P in Si depth profile illustrating the conversion of raw data to reduced data.[2] 35

Figure 4-1. A time of flight (TOF) mass spectrometer with a reflectron.[6] 40

Figure 4-2. Schematic of the TRIFT system for TOF-SIMS. 41

Figure 4-3. Schematic of quadrupole mass spectrometer.[5] 44

Figure 4-4. Schematic of a magnetic sector double focusing mass analyzer.[17] 46

Figure 4-5. High mass resolution spectrum of P in amorphous Si.[15] 48

Figure 4-6. Schematic of the CAMECA IMS-6F magnetic sector SIMS used in the research. 49

Figure 4-7. Schematic of a Cs microbeam surface ionization source.[27] 51

Figure 4-8. Schematic of a duoplasmatron.[31] 52

Figure 4-9. Schematic of the CAMECA IMS-6F primary ion column. 53

Figure 4-10. Trajectory of ions with different energies. The energy dispersion produced by the electrostatic sector and the magnetic prism work to cancel each other. Blue, red, yellow colors correspond to high, medium, low energies, respectively.[32] 54

Figure 4-11. Mass separation of ions with the same energy but different trajectories.[32] 55

Figure 4-12. Schematic of the Faraday cup in the CAMECA IMS-6F.[33] 57

Figure 4-13. (a) Illustration of a discrete-dynode electron multiplier with; (b) an expanded view showing the cascade effect at each successive dynode.[34,35] 58

Figure 4-14. Schematic of a microchannel plate device coupled to a fluorescent screen.....59

Figure 5-1. Sample 353 (P 1.8E13 at/cm^2, 35keV) as implanted and after 5 years.....64

Figure 5-2. (left) Illustrates inconsistent Si signals with the alpha 1 setting and (right) the stable Si signal using alpha 2. 68

Figure 5-3. Depth profiles of sample 341 (P in Si of 1E13 atoms/cm^2, 35keV) unexposed and exposed to Cesium. The sample unexposed to Cs is represented by the as received depth profile of sample 341. The sample previously exposed to Cs has been analyzed 7 times and stored in an oven at 100°C over 31 weeks.....71

Figure 5-4. Depth profiles of sample 471 (P in Si of 1E12 atoms/cm^2, 35keV) as received, CsEx and CsNo samples after 31 weeks stored at 100°C.....73

Figure 5-5. Depth profiles of sample 471 (P in Si of 1E12 atoms/cm^2, 35keV) as received, CsEx and CsNo samples after 31 weeks stored in a dessicator with water. 74

Figure 5-6. Depth profiles of sample 471 (P in Si of 1E12 atoms/cm^2, 35keV) as received, CsEx and CsNo samples after 31 weeks stored in an ambient laboratory environment. 75

Figure 5-7. Depth profiles of sample 471 (P in Si of 1E12 atoms/cm^2, 35keV) as received, CsEx and CsNo samples after 31 weeks stored in a dry dessicator....75

Figure 5-8. Depth profiles of sample 471 (P in Si of 1E12 atoms/cm^2, 35keV) as received and CsNo samples after 32 weeks stored under LN_2.....76

Figure 5-9. Depth profiles of samples 798, 672, 471 (P in Si of 1E12 atoms/cm^2, 35keV) as received. 78

Figure 5-10. Depth profiles of sample 839 (P in Si of 1E12 atoms/cm^2, 35keV through a 50Å oxide) as received, CsEx, and CsNo samples stored in a dry dessicator. ..80

Figure 5-11. Depth profiles of sample 839 (P in Si of 1E12 atoms/cm^2, 35keV through a 50Å oxide) as received, CsEx, and CsNo samples stored at 200°C.....81

Figure 5-12. Depth profiles of sample 840 (P in Si of 1E12 atoms/cm^2, 35keV after RTA) as received, CsEx, and CsNo samples stored in a dry dessicator. 82

Figure 5-13. Depth profiles of sample 840 (P in Si of 1E12 atoms/cm^2, 35keV after RTA) as received, CsEx, and CsNo samples stored at 200°C. 82

Figure 5-14. Depth profiles of sample 805 (P in Si of 1E12 atoms/cm^2, 35keV after pre-amorphization) as received, CsEx, and CsNo samples stored in a dry dessicator. 83

Figure 5-15. Depth profiles of sample 805 (P in Si of 1E12 atoms/cm^2, 35keV after pre-amorphization) as received, CsEx, and CsNo samples stored at 200°C. 84

Figure 5-16. Depth profiles of sample 471 (P in Si of 1E12 atoms/cm^2, 35keV) and 805 (P in Si of 1E12 atoms/cm^2, 35keV after pre-amorphization) obtained from as received wafers. 85

Figure 5-17. Depth profiles of sample 839 (P in Si of 1E12 atoms/cm^2, 35keV through a 50Å oxide) as received, CsEx, and CsNo samples stored in LN_2. 86

Figure 5-18. Depth profiles of sample 840 (P in Si of 1E12 atoms/cm^2, 35keV after RTA) as received, CsEx, and CsNo samples stored in LN_2. 87

Figure 6-1. Depth profile of native Si implanted with $1x10^{14}$ atoms/cm^2 Cs at 400keV used as a standard to quantify the Cs concentration.....95

Figure 6-2. Illustration of the memory effect.....97

Figure 6-3. Cs depth profiles obtained from a Si wafer implanted with $1x10^{14}$ atoms/cm^2 P at 35keV across two different areas: exposed and unexposed to Cesium in relation to the sample holder drawings. 99

Figure 6-4. Sample holder image (left) and the Si [100] sample areas in reference to the discussion above (right). 99

Figure 6-5. Physical layout of the SIMS sample holder used to examine for secondary sputtering and redeposition on previously unanalyzed areas. 100

Figure 6-6. Depth profiles of fresh Si [100] samples; exposed and unexposed to secondary sources of cesium. 101

Figure 6-7. Physical layout of the post pre-sputtering SIMS craters (blue) on the silicon sample in terms of distance from the center of the original SIMS crater (red): craters in the x (1,500μm) and y (10,000μm) regions are equally separated from each other.....102

Figure 6-8. Cs concentration profiles on Si surface that was pre-sputtered by Cs primary ions.....103

Figure 6-9. Cs^+ and Si^+ depth profiles of the Si surface which was pre-sputtered by Cs primary ions.....104

Figure 6-10. Surface Cs concentration with respect to the distance from the pre-sputtered crater by Cs primary ions on a Si [100] sample. 106

Figure A-1. Depth profiles of sample 344 (P in Si of 1E14 atoms/cm^2, 35keV) as received, CsEx and CsNo samples after 31 weeks stored in an oven at 100°C.....112

Figure A-2. Depth profiles of sample 344 (P in Si of 1E14 atoms/cm^2, 35keV) as received, CsEx and CsNo samples after 31 weeks stored in a dessicator with water. 112

Figure A-3. Depth profiles of sample 344 (P in Si of 1E14 atoms/cm^2, 35keV) as received and CsNo samples after 32 weeks stored under LN_2.....113

Figure A-4. Depth profiles of sample 341 (P in Si of 1E13 atoms/cm^2, 35keV) as received, CsEx and CsNo samples after 31 weeks stored in an oven at 100°C.....113

Figure A-5. Depth profiles of sample 341 (P in Si of 1E13 atoms/cm^2, 35keV) as received, CsEx and CsNo samples after 31 weeks stored in a dessicator with water. 114

Figure A-6. Depth profiles of sample 341 (P in Si of 1E13 atoms/cm^2, 35keV) as received, CsEx and CsNo samples after 31 weeks stored in an ambient laboratory environment. 114

Figure A-7. Depth profiles of sample 341 (P in Si of 1E13 atoms/cm^2, 35keV) as received, CsEx and CsNo samples after 31 weeks stored in a dry dessicator. 115

Figure A-8. Depth profiles of sample 341 (P in Si of 1E13 atoms/cm^2, 35keV) as received and CsNo samples after 32 weeks stored under LN_2. 115

LIST OF TABLES

Table 5-1. Descriptions of wafers and standards analyzed to determine the effects on different P implant doses in Si 65

Table 5-2. Descriptions of wafers implanted with 1.0E12 at/cm^2 P at 35keV and the bulk doped standard analyzed to determine the effects of different processing methods. 66

Table 5-3. The storage conditions used for the P implant aging study. 66

Table 5-4. CAMECA IMS-6F analysis conditions used for the P implant aging study depth profiles. 67

Table 5-5. Calculated doses of wafers 839, 840, and 805. 89

Table 5-6. Results from the earlier phosphorus implant aging study (wafers 344, 341, and 471). Yes and No refer to the presence or absence of observed changes in P surface concentration. 91

Table 6-1. Analysis conditions used for the Cesium neutral beam study. 95

1 Introduction and Overview

1.1 Structure of the Thesis

Chapter one describes the motivation and objective of this work. Chapter two discusses background information on semiconductor processing with the focus on ion implantation. Chapter three describes secondary ion mass spectrometry (SIMS) and the fundamentals of the SIMS technique with emphasis on the near surface analyses of low dose phosphorus (P) implanted into silicon (Si) wafers. Chapter four discusses the instrumentation and experimental methods used in this research. Chapter five concentrates on SIMS analyses of phosphorus implanted in silicon with cesium primary ion bombardment. Chapter six discusses aspects of quantification of the surface cesium contamination observed during SIMS analyses under cesium bombardment. Conclusions and future work are given in chapter seven.

1.2 Research Motivation and Thesis Goal

The continued rapid growth of the semiconductor industry requires decreasing the size of integrated circuit (ICs) components. Scaling down the physical dimensions of device components is desired for increased density and performance of integrated circuits. Smaller IC components yield higher speed and low power consumption due to smaller resistances, capacitances and inductances. IC technology has advanced from small scale integration (SSI) to medium scale integration (MSI), to large scale integration (LSI), to very large scale integration (VLSI) and finally to ultra large scale integration (ULSI). There were 2 to 100 devices on SSI ICs. For ULSI technology, more than five million devices are on a single chip. This growth in the number of devices on a chip was predicted by Gordon Moore (Intel co-founder) in 1965. This principle is known as Moore's Law, stating that the number of transistors on a chip doubles about every two years.[1] Figure 1-1 illustrates the actual growth in the number of transistors integrated on a chip as a function of time. It shows the trend of exponential growth has continued and the prediction by Moore has been accurate.

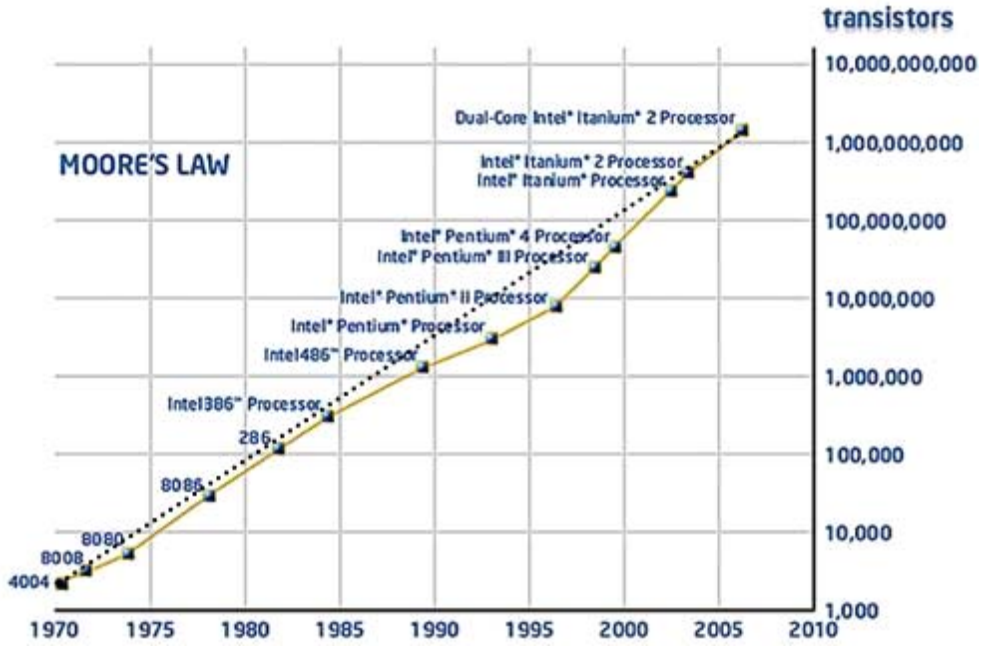

Figure 1-1. Comparison of Moore's Law (dotted line) with the actual developments in the semiconductor industry.[1,2]

In the past few years, the device component sizes have decreased to less than 100nm. These advances in semiconductor manufacturing technology have led to the integration of millions of transistors on a single IC. In order to accommodate the increasing number of devices onto an IC, it has been necessary to reduce the dimensions of the various parts that make up the IC. Transistor scaling typically involves more than the linear reduction of the transistor width and length. For example, source/drain (S/D) junction depth and gate dielectric thickness are also typically reduced to produce devices with the desired electrical characteristics.[3]

The next generation of devices contains components having dimensions on the order of 32nm. Recently, the first fully functional chips using 32nm process technology were introduced by Intel allowing integration of more than 1 billion transistors on one chip. These devices require that ions be implanted significantly closer to the surface, often at depths less than 20nm, to obtain the desired performance according to the International Technology Roadmap for Semiconductors (ITRS).[4] The fabrication of devices with these decreasing

junction depths requires ultra low energy (ULE) and low dose implantation. These ultra low energy implants, with energies less than 1keV, will place the ion implanted species closer to the surface. Additionally, as transistor dimensions are decreased, the power supply voltages at which they operate are also reduced. If supply voltages are not scaled accordingly, the possibility of failure increases for the IC. This is due to increased possibility of rupturing the gate dielectric, which is caused by the increase in the electric field across the scaled down gate dielectric. However, reducing supply voltages reduces the obtainable IC performance. To compensate for lowering the overall performance of the IC, it is desirable to reduce the threshold voltage (V_t).[3] Threshold voltages can not always be scaled down in comparable steps because of limiting factors in ion implanter technology.

Modern implanter technology provides high and medium dose implants which are consistently accurate. However, implanter calibration at medium doses does not always scale down to the lower doses required for reducing the V_t. Lowering of the implant dose increases the significance of implanter beam leakage currents and other errors on the implanted ion dose. A leakage current of 1% of the actual beam current is insignificant for medium dose implantation but can result in a 100% error for an implant dose that has been lowered by two orders of magnitude.[5] In modern semiconductor technology, the ability to control the V_t is crucial to IC miniaturization. Therefore, careful tailoring of the dopant concentration profile is required to control the threshold voltage. Control of the dopant profile is accomplished by performing low dose implantation.[6] For example: medium energy, low dose phosphorus implants are used to adjust a threshold voltage for high V_t p-channel field effect transistors (p-FETs) and flash memory cells.[5,7] Ultra low energy and low dose implantation monitoring have exposed some of the limitations of SIMS characterization. The P aging study (see Chapter 5) will concentrate on measurement of low dose P implantation using SIMS and on development of an accurate and reproducible SIMS characterization method for low dose P in Si.

SIMS is the most widely used characterization technique for P depth profiling because SIMS has the ability to provide true elemental depth profiles with both high sensitivity and depth resolution.[8] Accurate depth profiles of P in Si are possible with SIMS

as a result of the technique's ability to provide the high mass resolution ($m/\Delta m \approx 4000$) required to eliminate a mass interference between ^{30}SiH and ^{31}P.

The goal of this thesis is to investigate changes over time in the apparent phosphorus (P) surface concentration that have been observed in SIMS depth profiles of low dose phosphorus implanted silicon samples. Possible explanations for the changes in apparent P distribution over time are surface oxidation, diffusion, and/or the influence of adjacent prior analyses. Therefore, two aspects of SIMS depth profiling of low dose phosphorus are investigated in this study: phosphorus implant aging and the effect of unintended cesium contamination of the sample surface. The impetus for the cesium exposure study is to determine whether unintended cesium contamination occurring during analysis contributes to the observed changes in the real or apparent P concentrations.

1.3 References

[1] G. Moore, Electronics **38**, 114 (1965).

[2] Moore's Law, The Future - Technology & Research at Intel. 21 September 2007 < http://www.intel.com/technology/mooreslaw/>.

[3] K.R. Mistry and I.R. Post. "Method of fabricating dual threshold voltage n-channel and p-channel MOSFETS with a single extra masked implant operation." US Patent 6693331. 17 Feb. 2004.

[4] International Technology Roadmap for Semiconductors, update (2006).

[5] A. Short, K. Bala, and H. Glawischnig. in Proceedings of the 11th International Conference on Ion Implantation. Austin, TX, 202 (1996).

[6] J.S. Brown, B.C. Colwill, T.B. Hook, D. Hoyniak, "Method for forming a retrograde implant." US Patent 6610585. 26 Aug. 2003.

[7] C. Hsu and C. Chen, "Method for forming a flash memory cell with improved drain erase performance." US Patent 6261906. 17 July 2001.

[8] P.K. Chu, Y. Gao, and J.W. Erickson, J. Vac. Sci. Technol. B **16**, 197 (1998).

2 Semiconductor Processing

2.1 Introduction

Silicon is the most important semiconductor material for the electronics industry. Most integrated circuits are fabricated on silicon wafers because of its unique electrical properties. Typically, there are over 350 process steps required to make an integrated circuit. For the purpose of this study, only ion implantation will be discussed. In single crystal silicon the atomic density is $5x10^{22}$ atoms/cm^3. This known value provides a baseline for comparison to determine the concentration of impurities including dopants in silicon. The application of a semiconductor circuit or device is strongly dependent on the amount of electrical current that can be accommodated by the material, the direction of the current and the doping polarity. Increasing the current carrying capacity requires increasing the amount of mobile carriers through doping the semiconductor.

Ion implantation is widely used as the doping technique for silicon integrated circuits because it provides a clear advantage over alternative techniques (e.g. diffusion) in all but extreme cases. The accuracy and precision of introducing a specific dose or number of dopant atoms into silicon is far greater with ion implantation in comparison to alternative methods. In addition, the desired depth of the implanted dopants can be predictably obtained by controlling the ion implant energy. However, as the semiconductor industry strives to improve on today's technology, it has been necessary to continually decrease the device sizes on integrated circuits. This advancement of semiconductor processing requires implants to be ever closer to the Si surface. Low energy implantation methods are used to reduce junction depths. Precise low doses are required to carefully tailor the dopant concentration profile to obtain desired threshold voltages. Both ULE and/or low dose implantation are techniques used to obtain maximum performance for integrated circuits. As dopant depths become more shallow and as dopant doses become lower, characterization becomes more difficult.

2.2 Ion Implantation

Ion implantation refers to the bombardment of a solid substrate with ions accelerated to kinetic energies ranging from low energies (for example 500eV) to more than 3MeV. The technique's applications require doses and energies spanning several orders of magnitude. Most implants fall within one of the boxes in Figure 2-1.[1] Ultra shallow implants used for source-drain contacts/extensions require low energies, less than 1keV, while deeper implants used to produce wells in semiconductors require high energy, greater than 1MeV,implantation.

The ion implantation method is used to introduce atoms into the surface layer of solid materials. As the ions enter the crystal, they create a cascade of damage that may displace a thousand atoms for each implanted ion. The cascading effect occurs as ions lose energy to the lattice atoms as a result of the electronic and nuclear stopping power of the material being implanted, and the implanted ions finally come to rest at some depth in the material.[2] The most common application for ion implantation is the doping of silicon during device fabrication. Ion implantation was introduced into semiconductor processing over three decades ago because it can provide precisely controlled amounts of virtually any element into any solid material. Implantation energy can be selected to scale the depth and beam current can be adjusted to provide control of dose concentrations. Ion implantation has become the dominant tool for introducing dopants into the silicon crystal to change the electrical properties of the silicon. This trend is expected to continue well into the future as miniaturization of the individual transistors in integrated circuits continues.

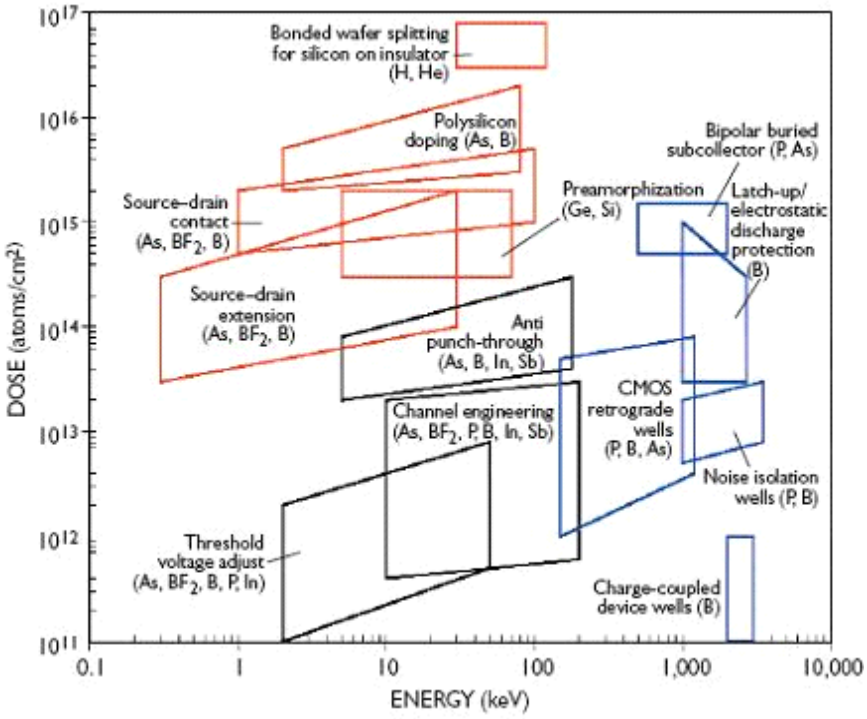

Figure 2-1. Dose and energy requirements of major implantation applications.[1]

For dopant control in the 10^{14} to 10^{18} atoms/cm^3 range, implantation offers an advantage over other techniques (e.g. diffusion). Doses can be accurately controlled because it is essentially based upon the implanter's ion beam current, charge and implantation time:

$$\phi = \frac{1}{A}\int \frac{I}{q} dt \qquad \textbf{Equation 2-1}$$

where ϕ is the dose (atoms/cm^2), A (cm^2) the beam area, I (amperes) the measured beam current, q the charge per ion (equal to one electronic charge = 1.6 x 10^{-19} coulomb), and t (sec) the implant duration. Introducing a specific dose or number of dopant atoms into silicon crystal is possible because the electrical charge on the ion allows the implanter current to be measured by collection of charges in a Faraday cup. Ion current measurements are very accurate and can be carried out over a wide range of doses. 10^{12} cm^{-2} to 10^{16} cm^{-2} are routine values of the number of dopant atoms introduced during semiconductor processing illustrating that a wide range of doses is possible since increasing the dose simply requires a

longer implant time or a higher beam current.[3] The implanted dopant's depth distribution profile is controlled by changing the implantation energy.

Computer programs (e.g. TRIM) have been developed to simulate ion stopping and ion distribution enabling precise prediction of the placement of ions during implantation.[4] The distribution of implanted ions in the solid substrate depends on the energy, angle of implantation and the mass relationship between the ion to be implanted and the substrate matrix atoms which are involved in the collision processes.[1,5] The implanted ion undergoes scattering events with electrons and atomic nuclei in the target, with the implanted ion losing energy until it comes to rest. The total path length of the ion is called the range, R. The maximum implanted ion concentration occurs at the depth at which a typical implanted ion stops. This depth is called the projected range, R_p. Due to the random nature of ion implantation, an individual ion may undergo more or less scattering events than the typical ion causing ions to stop at different distances below the surface. Recoil mixing or knock-on effects of target atoms also occur during the implantation process and must be considered. The combination of the above effects gives rise to a distribution of ions where most ions are within a standard deviation $\pm\Delta R_p$ (straggle) of the projected range. The depth distribution of ion ranges can be described statistically by a symmetric Gaussian distribution function given by [3,6]

$$C(x) = C_p \exp\left[-\frac{(x - R_p)^2}{2\Delta R_p^2} \right] \qquad \textbf{Equation 2-2}$$

where R_p is the average projected range, ΔR_p is the straggle about the range, and C_p is the peak concentration where the Gaussian is centered. Therefore, Monte Carlo simulations (e.g. TRIM) can be used to model the random nature of the ion distribution for ion implantation.

For silicon and other crystalline materials, crystal structure also plays an important role. Crystalline symmetry can affect the implant profile. The channeling effect occurs during implantation into crystalline solids as a result of some implanted species entering an open "channel" in the crystal lattice between rows of atoms.[7] As a result, some implanted species penetrate the solid more deeply than other species which encounter more collisions

with atoms in the lattice. Channeling can produce unexpectedly deep profiles or unusual profile shapes. The phenomenon of ion channeling is often characterized by a deviation from the Gaussian shape of the implant in the form of a tail, as seen in SIMS depth profiles.[8,9] The channeling tail has been well characterized for phosphorus in silicon. [8-10] The depth profiles of other dopants (i.e. boron and arsenic) in Si have also shown significant channeling can occur.[11] Implementing techniques to reduce channeling effects has become increasingly important as ULE and low dose implantation proliferate. In silicon technology ion implantation processes reduce channeling by incorporating wafer tilting (most commonly by ≈7°), rotation, implanting through a thin amorphous layer (e.g. oxide) and pre-amorphization.[2,3,6,9-13] Pre-amorphization uses a high dose implant (e.g. Si) prior to the actual dopant implant to destroy the crystalline structure and thereby eliminate channeling.

The most commonly implanted species in silicon (Si) are boron (B), phosphorus (P) and arsenic (As). Boron is the dominant p-type (acceptor) dopant in silicon semiconductor technology. It is probably the element that has been most commonly analyzed by SIMS. Phosphorus and arsenic, which contribute an extra electron to the crystal, are the dominant n-type (donor) dopants in silicon. These three dopants are impurity atoms that supply holes or electrons, which move freely through the crystal. However, introducing these dopant elements with ion implantation can cause amorphization or unwanted defects such as vacancies and interstitials. Vacancies and interstitials can combine with the dopants to form electrically inactive areas. Therefore, a post implant anneal is required to restore the damaged crystal. As a result of the post implant anneal the dopant atoms move to substitutional sites and become electrically active. Also, annealing allows the silicon atoms displaced by the implant to become substitutional, thus removing defects that trap carriers and/or affect their mobility. With the use of ion implantation to accurately control the doping concentration, the free electron and hole concentrations can be precisely controlled and therefore the electrical characteristics of the silicon can be controlled [3] Other implants used in the semiconductor process include: indium (In) and antimony (Sb) as dopants, Si for pre-amorphization, BF_2 to implant B without channeling effects, and deuterium (D) for interfaces.

Secondary ion mass spectrometry (SIMS) is the most widely used technique for characterizing the concentration and in-depth distribution of ion implanted species, both before and after processing.[14] SIMS is capable of providing in depth characterization of all of the previously discussed dopants in Si. However, advancements in semiconductor processing require ever smaller components and layers. Therefore, ion implantation parameters continue to change in order to obtain dopants implanted with the lower energies and smaller doses needed for the development of the smaller features required for modern semiconductors. As ULE and low dose implantation methods are used for dopants in Si, it is necessary for the characterization techniques and methods to improve.

2.3 References

[1] L.Rubin and J. Poate, The Industrial Physicist **9**, 12 (2003).

[2] S. Tian, M. Morris, S. Morris, B. Obradovic, G. Wang, A.F. Tashch, and C. Snell, IEEE Transactions on Electron Devices **45**, 1226 (1998).

[3] J.D. Plummer, M.D. Deal, and P.B. Griffin, *Silicon VLSI Technology: Fundamentals, Practice and Modeling*, Prentice Hall, New Jersey (2000).

[4] J.F. Ziegler, J.P. Biersack and U. Littmark, *The Stopping and Range of Ions in Solids*, Pergamon Press, NY (1985).

[5] M. Schulz, Appl. Phys. **4**, 91 (1974).

[6] S.M. Sze, Ed., *VLSI Technology*, McGraw Hill, New York (1983).

[7] D.V. Morgan, Ed., *Channeling: Theory, Observation and Applications*, Wiley, New York (1973).

[8] G. Dearnaley, Nature **256**, 701 (1975).

[9] R.A. Moline, J. Appl. Phys. **42**, 3553 (1971).

[10] P. Blood, G. Dearnaley, and M.A. Wilkins, J. Appl. Phys. **45**, 5123 (1974).

[11] S.R. Walther, S. Mehta, J. Weeman, A. Grouillet, and D. Brown, "Dopant channeling as a function of implant angle for low energy applications," p. 126, Proc. 13th Int. Conf. Ion Implant. Tech., 1999.

[12] V.G.K. Reddi and J.D Sansbury, J. Appl. Phys. **44**, 2951 (1973).

[13] J.W. Mayer, International Electron Devices Meeting **19**, 3 (1973).

[14] V.K.F. Chia, *Materials and Process Characterization of Ion Implantation*, edited by M.I. Current and C.B. Yarling, Ion Beam Press (1997).

3 Secondary Ion Mass Spectrometry (SIMS)

3.1 Introduction

In 1910, J.J. Thomson observed and identified the emission of positive secondary ions when he bombarded a metal surface with primary ions in a discharge tube.[1] This discovery lead to the development of Secondary Ion Mass Spectrometry (SIMS) in the 1960's. The SIMS technique has made enormous advancements and has become a leading technique for surface and thin-film analysis during the last 40 years. SIMS can be used to provide elemental and molecular characterization of the surface and near surface region of solids. It is commonly used to determine dopant and trace contaminate levels in semiconductors. This chapter will outline basic principles of the SIMS technique.

3.2 Technique Overview

In SIMS, a surface is bombarded with energetic primary ions under ultra high vacuum conditions. During bombardment, various atoms and molecules are sputtered from the surface. Most of these sputtered species are in the form of neutral atoms and molecules, but some of the sputtered species are ionized and extracted by an electric field into a mass spectrometer. These ionized secondary ions are then mass separated and detected. A schematic of the SIMS technique is shown in Figure 3-1.[2]

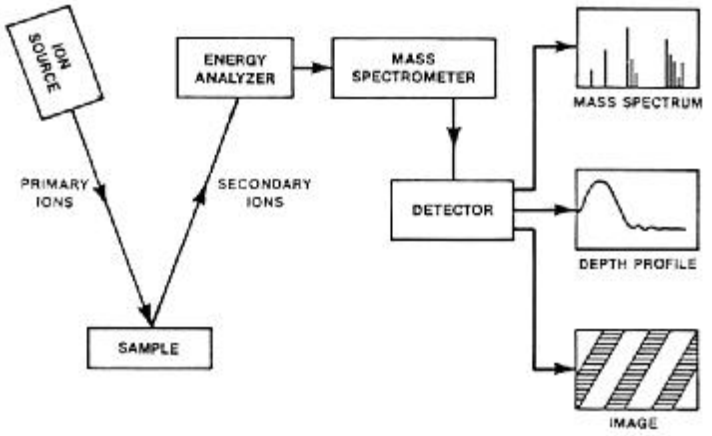

Figure 3-1. Schematic of the SIMS technique.[2]

Considered in more detail, the SIMS energetic primary ions strikes the sample surface and penetrates, as in ion implantation, coming to a rest at an average depth equal to the projected range (R_p). Primary beam energies used range from approximately 200eV to over 30keV, with energy dependent on analysis requirements. The incident ions are usually oxygen or cesium since these elements provide secondary ion yield enhancement of electropositive and electronegative elements, respectively.[3] Bombarding primary ions cause a collision cascade which transfers energy to near-surface atoms or molecules sufficient to cause them to leave the surface. The escape depth of sputtered species is only a few angstroms. The formation of the collision cascade is illustrated in Figure 3-2 and shows some ejected species as ions.[4] Secondary ions are extracted by an electric field, mass analyzed, and subsequently detected and counted using an electron multiplier or a Faraday cup, or displayed using a channel plate/fluorescent screen for imaging.

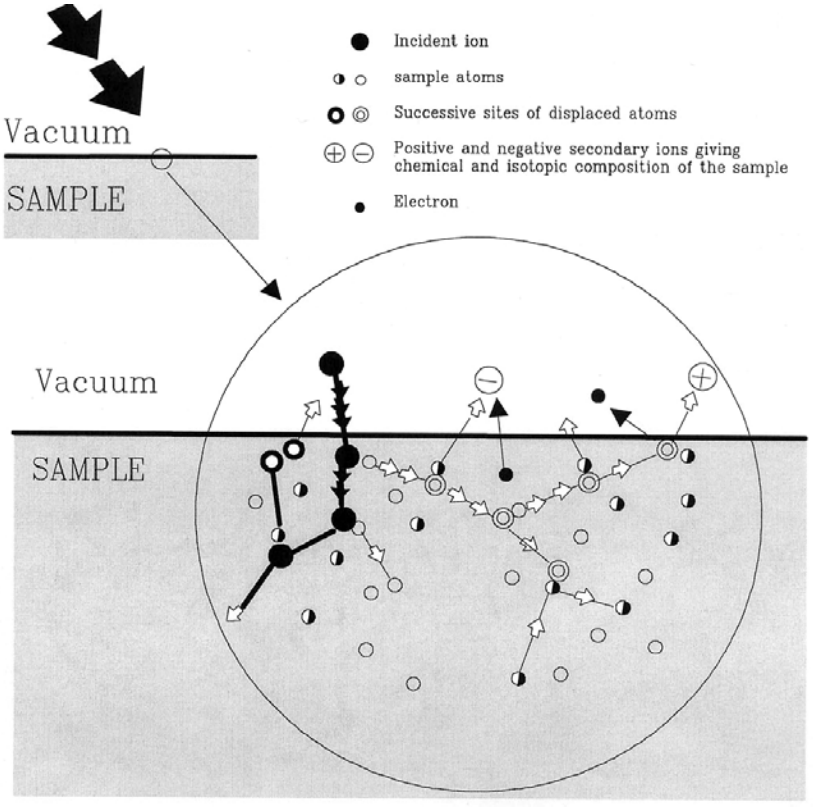

Figure 3-2. Collision cascades after the primary ion bombards the sample surface.[4]

3.2.1 Static versus Dynamic SIMS

In SIMS, according to the ratio of the erosion time for one monolayer, t_M, to the recording time for a mass spectrum, t_A, two modes may be classified: "static SIMS" ($t_M/t_A >> 1$), which removes a fraction of the first monolayer,[5] and "dynamic SIMS" ($t_M/t_A < 1$), which is used to measure depth profiles.[6] TOF instruments can be used for depth profiling however, they are generally used to provide chemical analysis of the sample surface. This mode is referred to as "static SIMS".[7] In static SIMS, a mass spectrum is obtained using a very low primary ion beam intensity providing a mode for surface analysis of the top monolayer of the sample. Static SIMS uses a very low primary ion beam dose ($< 10^{13}$ at/cm^2) to limit the amount of damage to the sample surface. Static SIMS requires that less than 1% of the surface is disturbed (sputtered) such that ionization events originate from a pristine area of the surface. This results in the quasistatic analysis of the surface monolayer. Therefore, mass spectra and imaging can provide molecular information on the surface chemistry. Quadrupole and magnetic sector SIMS instruments are usually operated in dynamic SIMS mode to obtain quantitative elemental and isotopic information as a function of depth. Dynamic SIMS uses a high primary ion beam intensity, exceeding 10^{13} at/cm^2. High beam intensity results in rapid material removal and surfaces implanted with primary ion species to enhance ion yield (see section 3.4.1). Therefore, the secondary ion intensity is maximized for high sensitivity trace impurity analysis of the near surface region (0 to 10μm depths). In dynamic SIMS the sample surface undergoes bombardment-induced erosion to measurable depths by scanning the ion beam in a raster pattern.[8] While sputtering the secondary ion intensities are continuously acquired on the basis of mass-to-charge ratios of elements for which information is desired, in a cyclic manner (the selected mass-to-charge ratio intensities are acquired and then the sequence is repeated for a period of time required to sputter to a specific depth) resulting in a depth profile. Also, dynamic SIMS can use mass spectra and secondary ion imaging to provide elemental and isotopic information.

3.2.2 SIMS Analysis Methods

There are three types of SIMS data that are commonly acquired: secondary ion images, mass spectra and depth profiles. Secondary ion images are acquired to visualize the distribution of individual species on the surface. For secondary ion imaging, either the monitored secondary ions are detected by an ion sensitive image amplifier such as a channel plate/fluorescent screen (ion microscope mode) or by mapping of the secondary ion intensity versus beam position (ion microprobe mode). Images provide the lateral distribution of the selected secondary ion species. A mass spectrum is acquired by scanning through a range of masses as a function of mass to charge ratio and measuring the secondary ion intensity at each mass. Mass spectra are commonly used for impurity or contaminated surveys that can be used for quantitative comparison of samples of the same matrix acquired using the same instrumental conditions. Depth profiles are the most commonly used SIMS technique and can provide quantitative information in depth impurity profiles. Depth profiles are used to determine the intensity (or concentration) of selected secondary ions as a function of time (or depth) from the surface. For depth profiling, a depth scale is typically obtained by measurement of the crater created by sputtering or by applying a known sputtering rate for the material. Quantification is usually achieved by applying conversion factors obtained from analysis of ion implanted or bulk doped standards under similar analytical conditions. The application of conversion factor commonly called the relative sensitivity factors (RSFs) allows for quantitative analysis of depth profiles.

SIMS is able to analyze all elements in the periodic table including isotopes. SIMS can provide high elemental sensitivity down to parts per million (ppm) and even parts per billion (ppb) depending on analytical conditions and the element being analyzed as a function of depth. For example, the atom density of silicon is 5.0×10^{22} at/cm^3. This translates to 1ppb for B in Si at approximately 5.0×10^{13} at/cm^3. SIMS analyses can typically provide depth resolutions of 10-20nm, although good depth resolutions of less than 3nm have been achieved.[9] Also, SIMS has excellent dynamic range, $>10^5$ for many analyses. As semiconductor devices are produced with ever smaller dimensions, SIMS serves as a critical analytical technique for dopant characterization due to its high sensitivity, good depth

resolution, and high dynamic range. However, SIMS requires standards for quantification and is destructive to the analyzed samples.

The different types of SIMS mass analyzers, with emphasis on the CAMECA IMS-6F Magnetic Sector SIMS used in this project, will be described in sections 4.2 and 4.3, respectively.

3.3 Fundamental Concepts in SIMS Related to Depth Profiling

3.3.1 Crater Depth and Topography Measurement

In SIMS depth profiling, the raw data is in the form of secondary ion intensity versus sputtering time. A depth scale for each profile is traditionally calibrated by measuring the final crater depth with a stylus profilometer and obtaining the sputter rate by dividing the crater depth by the final analysis time. Assuming the sample is homogenous and the primary beam has a constant density and current, then the sputtering rate should be uniform throughout the analysis. Therefore, the average sputter rate is applied to the whole profile to convert the profile from intensity versus time to intensity versus depth. For accurate depth calibration in SIMS depth profiles, differences in sputter rates for each layer of multiple layered samples is required. It is also important to monitor crater bottom roughness due to sample surface and ion bombardment.[2,10] Crater depths larger than 10 nanometers can be measured using a stylus profilometer. Atomic force microscopy should be used for measuring depths below 10 nanometers.

A smooth sample surface is critical for obtaining uniform sputtering, good depth resolution and an accurate crater depth measurement. Sputtering a rough sample surface creates a crater bottom with similar topography to the surface. However, differential sputtering can create crater bottom roughness even on smooth samples. In many cases, ion bombardment induced surface topography takes the form of ripples at the bottom of the crater.[11] Surface topography may be reduced using a different angle of incidence and/or by sample rotation.[12] Limiting surface topography will help produce a smooth and evenly sputtered crater and improve the depth resolution of the data.

3.3.2 The Transient Region

At the beginning of a depth profile, SIMS analysis generates secondary ions from the top monolayers of the bombarded sample. Secondary ion emission, atomic as well as molecular, can provide the elemental composition (dynamic SIMS) and chemical identification (static SIMS) of the near surface (transient) region of the sample. Obtaining accurate quantitative elemental analysis in the near surface region ($\leq$ 50nm) has become increasingly important as the semiconductor industry strives to produce ever shallower devices. A smaller semiconductor device requires increasingly shallow implant depths which require the use of lower implant energies. Thus, precise and accurate SIMS measurements for semiconductor devices become more difficult to obtain with the peak concentration of shallow implants positioned in the transient region. Ion yield and sputter rate changes at the surface or in the near surface region must be accounted for to correctly interpret data at the beginning of a depth profile. Understanding the results in the near surface region requires knowledge of the projected ion range of the implanted species and primary ion beam into each specific sample and the consideration of secondary ion yield enhancement due to contamination.

In a SIMS depth profile, the transient region corresponds to the depth (time) over which the ion yield and sputter rate are changing and have not reached their equilibrium values.[13] The changes in ion yield and sputter rate within the transient region are the result of primary ion bombardment, changes in sample composition from the surface layers to the bulk or contamination of the sample. The width of the transient region is dependent on the analysis impact energy, mass of the primary ion, and the substrate. Lower primary ion impact energies reduce the transient zone width by reducing the projected range (R_p) of the primary ions, reducing the SIMS primary ion dose it takes to achieve a constant primary ion surface concentration, and thus a steady ion yield and sputter rate. Figure 3-3 schematically displays a typical transient region with O_2^+ bombardment at 5.5keV.[2] The figure illustrates the presence of surface oxide, R_p (dotted line) of O_2^+ into Si at 5.5keV, and the equilibration depth showing O non-uniformity at the beginning of a depth profile. Changes in the secondary ion yield and sputter rate are observed while depth profiling through the transient

region and quantification becomes problematic within the transient region.[14] Quantification is difficult in the transient region because relative sensitivity factors and sputter rates can change quickly. However, once the equilibration depth has been reached, constant secondary ion yields and sputter rates are observed and accurate quantification is possible.

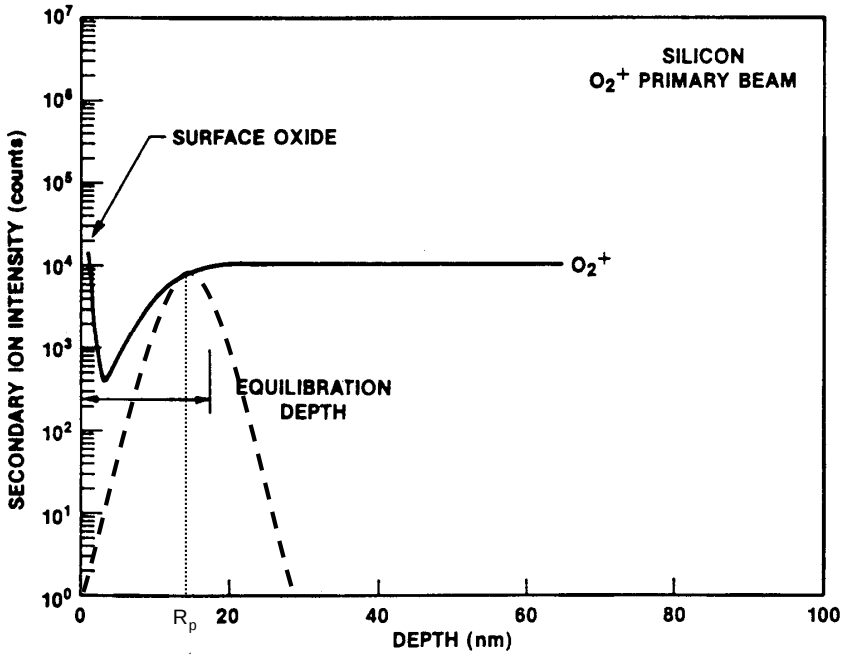

Figure 3-3. Profile of O in Si using O_2^+ illustrating the typical surface transient region with O_2^+ bombardment at 5.5keV.[2] The projected range of the primary ion bombardment of O_2^+ into Si is represented by the dotted line.

The depth at which the primary ions are implanted into the sample being analyzed is relevant to SIMS as it can be used to determine the amount of damage formed in the near surface region. The atom density of the primary species is not at equilibrium until the depth corresponding to the projected range of the primary beam has been sputtered away. However, in some cases with normalization to bulk doped standards, quantitative elemental concentrations can be obtained from the transient region.[15,16] In addition to primary ion beam effects, another factor influencing near surface analysis is the secondary ion yield enhancement due to oxygen from a native oxide.[17,18] A surface native oxide is present on many samples as it develops almost immediately after a fresh surface is exposed to air. The

presence of surface native oxide can be the cause of a secondary ion intensity peak not directly relatable to dopant concentration, a common feature for a SIMS depth profile, in the pre-equilibrium region. The peak at or near the surface occurs because of variation in the secondary ion yield.[19-21] As a result, oxygen should be monitored during a SIMS depth profile on a new material to characterize the surface oxide which can affect SIMS quantification in the pre-equilibrium region.

Another variation in near surface analysis may be due to neutral beam sputtering. Neutrals are formed in the primary ion column and as the primary beam strikes the last aperture. A significant neutral beam can impinge the sample surface and sputter away the uppermost monolayers, or contaminate regions outside of the rastered area. Therefore, previous analyses on a sample may affect adjacent areas used in future analyses. Contaminated surfaces can lead to inaccurate quantification of the near surface region. Other sources of near surface analysis problems are caused by surface defects, mishandling, and storage conditions of samples creating contamination.[2] Therefore, careful preparation and consideration of the analysis conditions are vital for accurate SIMS measurements of the near surface region.

3.3.3 Sensitivity and Depth Resolution

Secondary ion mass spectrometry is considered one of the most important analytical techniques for accurately characterizing ion implants due to its high sensitivity and good depth resolution. Figure 3-4 illustrates how the sensitivity, depth resolution, and dynamic range are determined. Both sensitivity and depth resolution are important in the quantification of SIMS depth profiles of low dose ($\leq$1E13atoms/cm^2) phosphorus implanted silicon samples. Analysis of these samples requires the detection of low phosphorus concentration and the study of effects near the surface. As the implant energy is decreased, the critical depth for analysis becomes tens of nanometers or less, requiring good SIMS depth resolution to obtain accurate quantification. Instrument parameters that affect sensitivity and depth resolution are the primary beam species, primary beam energy, and angle of incidence. Sputter rate also affects sensitivity.

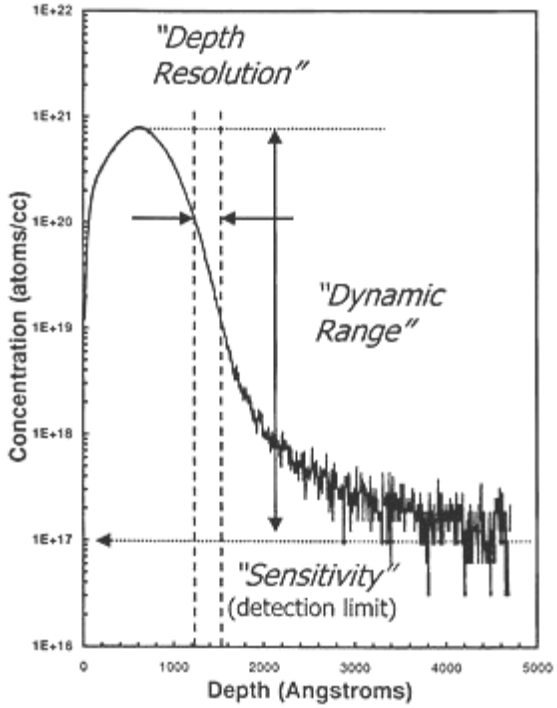

Figure 3-4. Illustration of sensitivity, depth resolution, and dynamic range from the acquisition of a SIMS depth profile.[13]

Detection sensitivity is the minimum measurable atom density for a particular species in a matrix, determined by the either the lack of detectable signal or by the background intensity for the specific mass being analyzed. Dynamic SIMS provides excellent detection limits, less that $1x10^{16}$ atoms/cm^3 for most elements, depending on instrumental background signals, mass interferences, ionization probability, and count rate. Instrumental background signal contributes to poor detection limits. This can be due to a poor vacuum in the case of residual gas species (H, C, N, O) or due to contaminated components of the instrument. Contamination occurs as a result of prior analyses and consists of material previously sputtered onto instrument components. A contaminated instrument creates a background signal of the element being analyzed that does not originate from the sample (memory effect). Ideally, elimination of instrument contamination can be achieved with the use of application specific instruments where an instrument is dedicated to one matrix. However, practical alternative methods utilize sputtering the matrix to be analyzed until the surface

causing the memory effect is coated with the sputtered material, use of voltage offset, and/or monitor molecular species.

Any elements that may be in the matrix, in the vacuum or contributed by the instrument need to be considered in a check for mass interferences. These interferences influence the detection limit since an unknown interference would result in a signal level not truly indicative of the level of impurity in the sample. Eliminating mass interferences is typically achieved in magnetic sector instruments by use of mass resolution sufficient to separate the interference from the mass of interest. The mass interferences of most interest for P in Si matrix is $^{1}H^{30}Si$ requiring a mass resolution of approximately 4000M/ΔMto achieve separation. Figure 3-5 shows a depth profile of P in Si for Cs^{+} bombardment and high mass resolution.[2] Detection limits are shown for Cs^{+} and for O_2^{+} bombardment at low and high mass resolution. Detection limit with O_2^{+} is improved with high mass resolution. Use of Cs^{+} with high mass resolution provides the highest secondary ion yield and detection.

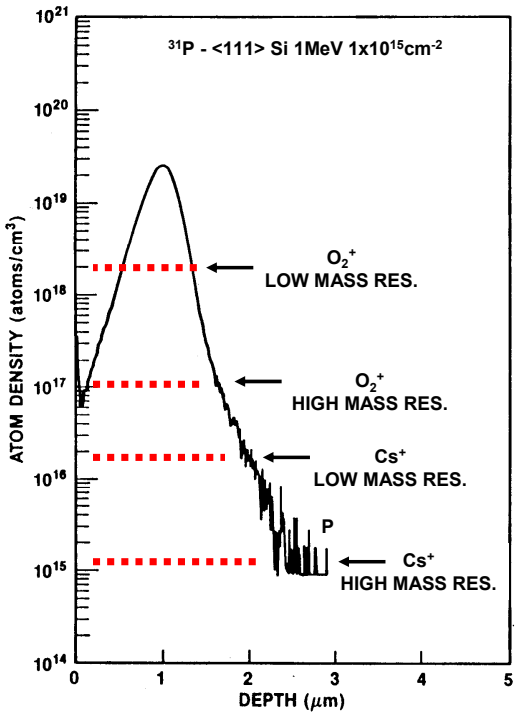

Figure 3-5. Depth profile of P in Si for Cs^{+} bombardment and high mass resolution.[2] Detection limits shown by arrows for Cs^{+} and for O_2^{+} bombardment at low and high mass resolution.

Detection limits are also affected by factors including useful yield, detector efficiency and sputter rate. The useful yield of the mass spectrometer is defined as the ratio of the number of secondary ions detected to the number of atoms sputtered from the sample. Useful yields are dependent on extraction efficiency, which is the ratio of atoms extracted from the sample and focused into the entrance aperture in route to the mass spectrometer. Useful yields also depend on instrument transmission, which is the fraction of sputtered atoms transmitted through the mass spectrometer and reaching the detector. In addition to the extraction efficiency and instrument transmission being vital to the useful yield, they also influence the amount of sputtered atoms hitting the detector. Ion detectors with high conversion efficiency provide an advantage in terms of the detection sensitivity. The detector efficiency varies with the velocity and the measured mass to charge ratio of secondary ions. SIMS instruments can have several types of detectors, including Faraday cup, electron multiplier, and ion image detector which will be discussed in detail in Chapter 4 (section 4.3.4). Sputter rate of the material affects the secondary ion count rate. If a material is sputtered faster and the detected area is kept constant, the secondary ion generation and thus the secondary ion count rate will increase. The count rate of a species in a depth profiling analysis is directly proportional to the primary ion current impinging on the analyzed area.[22] Therefore, increasing the current density of the primary beam improves the detection limit by increasing the secondary ions emitted. Figure 3-6 displays depth profiles of a boron implant (9.6E13 atoms/cm^2, 30keV) in silicon acquired with a high and a low primary ion beam current to illustrate the effect of primary ion beam current on count rate and detection limit. The depth profiles show the count rate and detection limit at low (20nA) and high (200nA) primary beam current with a raster x,y dimension of 160μm and a detected area of 60μm diameter. The plots show a higher count rate and an improved detection limit with use of a higher primary ion beam density.

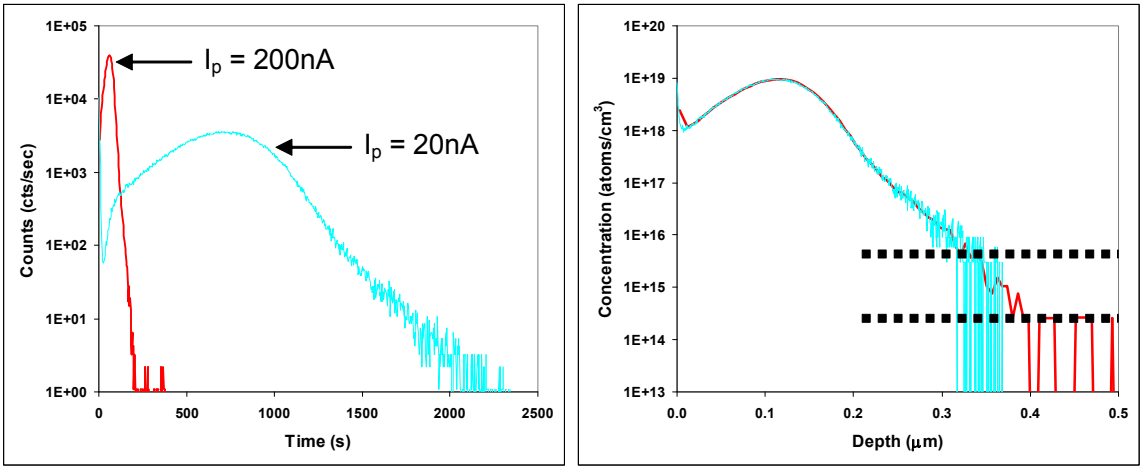

Figure 3-6. B implanted (9.6E13 atoms/cm^3, 35keV) into Si, profiled with different primary ion beam currents. Raw and processed data are shown on the left and right, respectively. Detection limits are represented by the dashed lines.

The ability to resolve interfaces and multilayer structures in a depth profile is dependent on the depth resolution. The depth resolution achieved at an interface is most commonly expressed in terms of the measured width of the transition between two layers when sputtering. The interface width is defined as the depth over which the measured analytical intensity changes from 84% to 16% of the maximum signal which may be represented as Δt (in terms of sputtering time) or Δz (in terms of depth z), as shown in Figure 3-7.[2] The error function is the derivative of the interface curve and the +/- 1 sigma points correspond to 84% and 16% of maximum intensity.

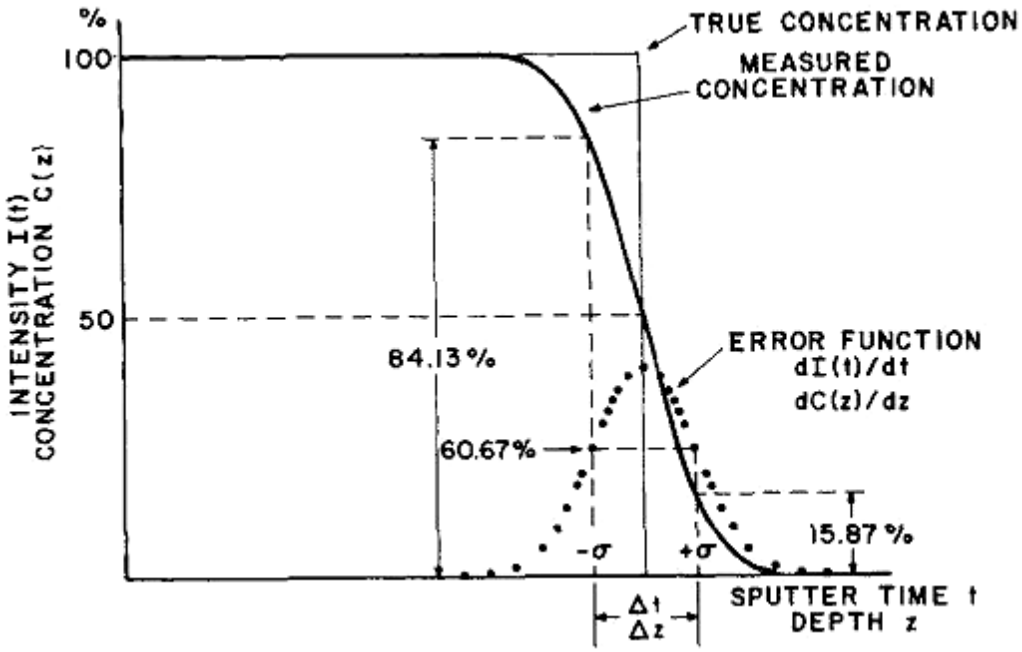

Figure 3-7. Parameters for depth resolution.[2]

Depth resolution depends on three factors related to the sputtering process: atomic mixing effects, non uniform sputtering, and crater edge effects within the analyzed area. The atomic mixing effect includes three different ion beam mixing processes: recoil mixing, cascade mixing, and radiation-enhanced diffusion.[2] The mixing occurs as the primary beam sputters the sample with energetic particles producing a series of collisions via the collision cascade. The mixing depth is approximately the projected range plus the straggle of the primary ion beam. The depth of the mixing region is dependent on the impact conditions which include the primary beam energy, species, and the angle of incidence. The use of lower primary beam energy minimizes the cascade mixing depth and thus provides a higher depth resolution (see Figure 3-8).[23] Also, using a primary species with a higher mass and larger incident angle from normal can reduce the mixing region and improve the depth resolution.

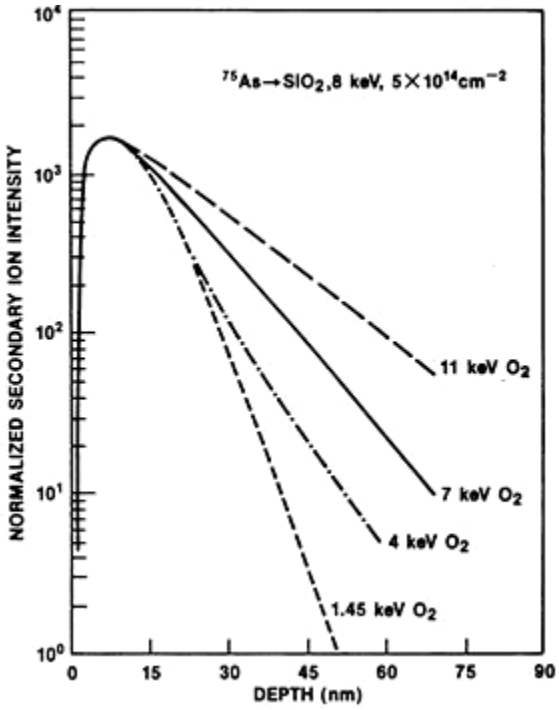

Figure 3-8. Increasing the O_2^+ primary beam energy increases the distortion of the depth profile and decreases the depth resolution.

Monte Carlo simulations can be used to predict the range and distribution of implanted ions within the target. The ion-solid interaction region is referred to as the mixing region. The depth of the mixing region is proportional to the projected range plus the straggle of the primary ion beam into a target. TRIM (Transport of Ions in Matter) is a widely used Monte Carlo program for simulation of ion implantation and bombardment.[24] The depth of the mixing region depends on the energy, the species and the angle of impact of the primary beam. Lower primary beam energies produce a shallower mixing region and thus higher depth resolution. Figure 3-9 is a TRIM simulation of cesium and oxygen implantation into Si. Figure 3-9 (a) and (b) can be used to compare the Cs^+ penetration at high (14.5keV) and low (6.0keV) impact energies, (b) and (c) compare Cs^+ and O_2^+ penetration at the same impact energy with angle of incidence of 27.3°, and (c) and (d) relates the incident angle of 27.3° and 50.0° using O_2^+ penetration at the same impact energy. Comparison of these plots clearly demonstrates that penetration increases with higher energy

ion bombardment. At the same impact energy and angle of incidence, the depth of the cesium mixing region is shallower than oxygen because of its larger atomic size. Also, the simulations show that a larger incidence angle relative to the normal reduces the mixing region. Therefore, for higher depth resolution, a low energy Cs^+ ion beam at a high angle with respect to normal will provide better results than O_2^+ at a similar energy and angle of incidence.

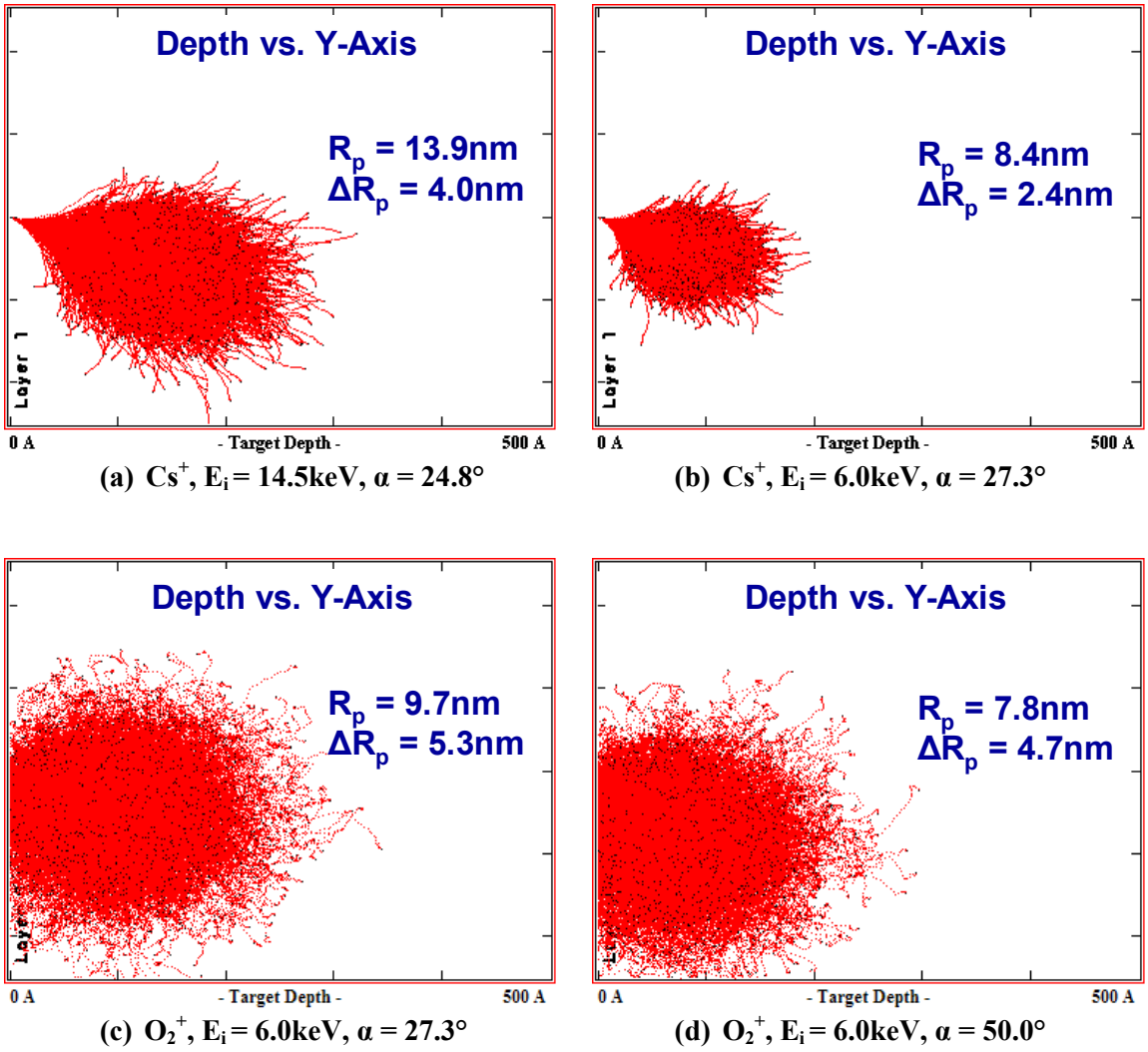

(a) Cs^+, E_i = 14.5keV, α = 24.8°

(b) Cs^+, E_i = 6.0keV, α = 27.3°

(c) O_2^+, E_i = 6.0keV, α = 27.3°

(d) O_2^+, E_i = 6.0keV, α = 50.0°

Figure 3-9. TRIM simulation of cesium and oxygen implantation into silicon at different energies and incident angles. E_i is the impact energy of the ions, α is the angle of incidence, R_p is the projected range, and ΔR_p is the straggle.

Non uniform sputtering of the analyzed area degrades the depth resolution. Therefore, the sample and the sputtered crater must be flat in the area of the analysis in order to avoid ion detection from various depths distorting the depth profile. When the crater depth increases, depth resolution will decrease if ion bombardment causes topography formation. Topography formation varies with substrate, bombarding species, energy and angle of interest.

Also, depth resolution depends on the ability to reject secondary ions originating from crater edges. Crater edge effects can be reduced with optimum raster and gate conditions. A generally accepted standard usually requires the detected (i.e. gated) area to be smaller than the rastered area by at least a factor of 3 to reduce crater edge effects. This reduces side-wall contributions allowing only ions from the center of a flat bottomed crater to be detected by rejecting ions which are emitted from the crater walls where various depths are exposed to the sputtering beam.[2,22,25] A flat bottomed crater is attained by sweeping a focused primary beam in a uniform, overlapping raster pattern over a selected region. Gating is then carried out via optical and/or electronic apertures. An optical aperture can be used to select secondary ions from the center of the crater while rejecting ions from the crater edges. Electronic gating can also be used or added to optical gating to further improve the rejection of ions outside the region of interest. Figure 3-10 illustrates the effect of the relationship of the raster and gating to depth profile shape and depth resolution.[2] Profile A (raster = 220μm x 220μm) is more accurate because data is only from the central flat portion of the crater with ions which are emitted from the crater walls being rejected. The shaded area represents a 60μm diameter detected area. Profile B (raster = 80μm x 80μm) illustrates the distortion introduced by too small a ratio of rastered area to detected area. The size of the gated area relative to the raster size used for profile B is insufficient to reject sidewall contributions. Optimal depth resolution is obtained by controlling all of the above.

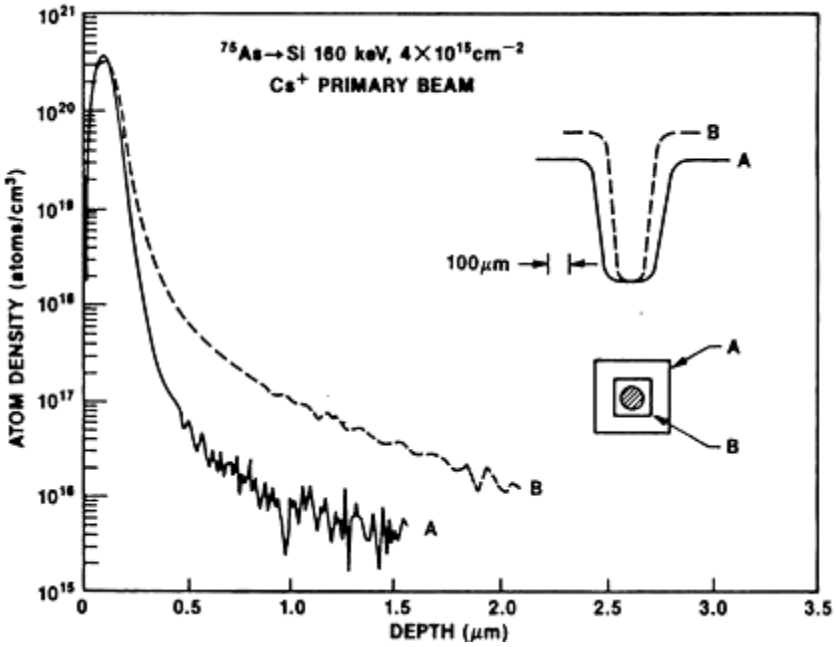

Figure 3-10. The data presented illustrates the raster and gate relationship to depth profile shape and depth resolution.[2]

Determining optimum analysis conditions for depth profiling requires consideration of the elements to be monitored and the relative importance of detection sensitivity versus depth resolution. The requirements for high sensitivity and high depth resolution are generally mutually exclusive. Improving the depth resolution will be at the expense of sensitivity and the resulting detection limit. For example, improved depth resolution is seen as impact energy is decreased, but lower impact energy decreases the sensitivity. These considerations influence the best analytical conditions utilized for analyzing the mass of interest.

3.4 SIMS Quantification

3.4.1 Secondary Ion Yields

Secondary ion yields are dependent on the element of interest, the primary ion species used and the sample matrix (matrix effects), and can vary by over six orders of magnitude.

Previous SIMS studies have demonstrated secondary ion yield dependence can be significantly influenced by altering the surface chemistry through the use of chemically active elements (i.e. O_2^+ or Cs^+) as the primary ion species.[26-31] Oxygen bombardment (O_2^+ or O^-) provides enhanced positive ion yields for the electropositive elements via surface oxidation.[28] Use of Cs as the primary ion improves negative ion yield by lowering the surface work function. Differences in positive ion yields obtained using oxygen can be correlated with the ionization potential. Negative ion yields obtained with Cs correlate with electron affinity. The secondary ion yield enhancements obtained using O_2^+ and Cs^+ are complementary and provide high SIMS sensitivity across most of the periodic table.

It has been known for many years that negative secondary ion yield is strongly enhanced in the presence of alkali metals at the surface emission site of the ions.[29] SIMS utilizes this information to increase the detection sensitivity of electronegative elements as negative ions.[2] This is typically accomplished by bombarding the sample with cesium primary ions.[29-31] As the Cs^+ primary ion beam is used to sputter a specimen, some of the primary ions are implanted into the near surface layer of the substrate. Thus, the near surface region of the bombarded specimen contains significant amount of cesium. This implies that the means of ion yield enhancement involves the surface or near-surface sample chemistry. The amount of cesium coverage at the surface depends on a variety of parameters such as the primary ion beam's energy and incidence angle and the sputtering yield of the sample.[32,33] It is well known that the ion yield enhancement is attributed to a lowering of the surface work function, Φ, induced by the deposition of alkali metals. When absorbed on a solid surface, the alkaline atoms form partly ionic bonds with the surface atoms, creating a dipolar layer. In this case, the layer produces an electric field and reduces the work function of the target.[34] Current theoretical models of secondary ion-emission predict an exponential dependence of the ionization probability of sputtered particles on the surface work function, Φ, as follows

$$P^+ \propto \exp\left(-\frac{(IP - \varphi)}{\varepsilon_0}\right),\ P^- \propto \exp\left(-\frac{(\varphi - A)}{\varepsilon_0}\right) \qquad \textbf{Equation 3-1}$$

in the case of positive secondary ions and negative secondary ions, respectively. The parameter IP is the ionization potential, A is the atom's electron affinity, and ε_0 depends on the normal component of the ion emission velocity.[35,36] The effect of evaporated cesium on secondary ions yields has been studied in detail and the validity of Equation 3-1 has been established with several static alkali-metal adsorption experiments.[37-41] In these static conditions, the cesium surface concentration can be easily controlled and measured, without altering the surface states, by Auger Electron Spectroscopy (AES). However, SIMS analyses usually operate under dynamic conditions. The problem is much more complex in dynamic conditions where cesium ions are used as the primary beam to perform analyses such as depth profiles. Under these conditions, it is difficult to measure and control the cesium surface concentration during depth profiles and quantify variations in Φ for the target. Thus, an accurate value for the ionization probability of the sputtered particles may be difficult to obtain.

Previous research has concluded cesium surface concentration achieved during cesium bombardment is directly related to the substrate's sputtering yield (Y) of cesium in the material in accordance with the following equation:

$$[\mathrm{Cs}]_{\max} \propto \frac{1}{1+Y}.$$ [26,42-45] **Equation 3-2**

Unfortunately, little information is available as to the equilibrium Cs concentration that has accumulated at the surface upon dynamic Cs^+ bombardment. Therefore, changes in Φ and predictions of the Cs^+ yield variations in different substrates (e.g. in a depth profile analysis) are not feasible.[46] These problems are illustrated by the disparity in the existing results for quantifying Cs surface concentration under dynamic conditions.[33,44-49] Different methods have been used to measure the Cs surface concentration. Gnaser and Wirtz measured the work function variations as a function of energy distributions with magnetic sector instruments.[45-47] Using the work function variations, Cs surface concentrations were calculated. Villegas and Kudriavtsev examined the changes of the work function caused by alkali ion sputtering. Villegas and Kudriavtsev used the idea of a dipole layer forming between Si-Cs dipoles. The partly ionic character of Si-Cs bond increases the surface

binding energy of Cs and, as a consequence, its surface concentration.[48,49] AES has been used as a method of analyzing surface cesium concentration after cesium ion bombardment.[44] For interpretation of SIMS data analysis, it is important to know the real value of the work function. Unfortunately, the difficulty and variance in methods of calculating the work function for dynamic SIMS analyses has led to discrepancies between the reported Cs surface concentrations.

Brison et al. concluded that for fixed surface cesium coverage, the work function is lower for the highest energies (Figure 3-11).[50] This effect is due to the fact that cesium ions are implanted deeper for analyzing with a high energy beam than for lower ones (see Figure 3-9). Cesium implantation modifies the lattice and becomes comparable to alloy formation through bonding of implanted Cs atoms to Si target atoms, leading to an increase in the polarizability of cesium.[48,50] The silicon work function decreases linearly with the cesium surface concentration for coverage below 10%. The decrease is about -1.0eV for 10% of cesium in the surface.[50] Yu discovered that deposition of cesium on silicon results in a lowering of the work function by more than 3eV using low energy ion bombardment. However, the surface Cs atom concentration ranged from 20% to 30%.[38]

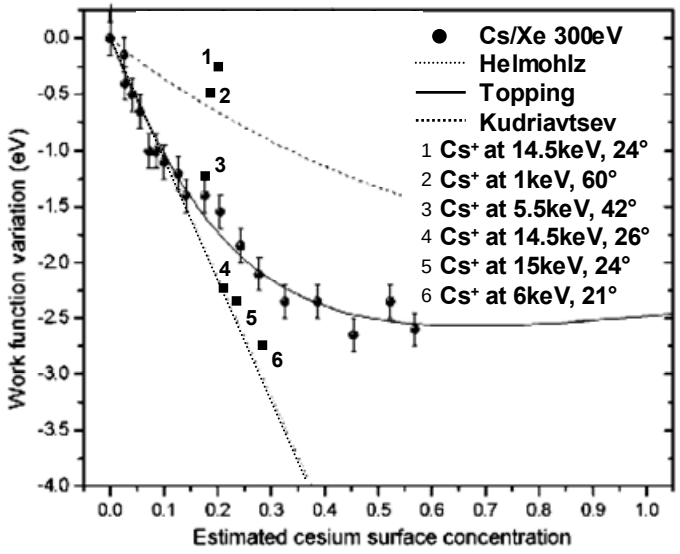

Figure 3-11. Comparing literature results of the variations of the silicon work function after cesium exposure.[50]

3.4.2 Relative Sensitivity Factor (RSF)

The relative sensitivity factor (RSF) approach is the most widely used calibration technique for quantitative analysis in SIMS. The RSF is derived from analysis of standards and provides a calibration factor to convert secondary ion counts to concentration. The RSF is inversely proportional to ion yield. Figure 3-12 illustrates the variation of RSF in a Si matrix under O_2^+ and Cs^+ bombardment.[2]

Using RSFs for SIMS quantification requires standards. Standards can be either an implanted standard (known dose) usually containing only one isotope or a bulk doped standard (known concentration) usually containing all isotopes at natural abundances. Ion implanted standards can be created for all naturally occurring elements and isotopes in any solid matrix. Analysis of a standard can be used to determine the RSF and detection limit for a particular element in a particular matrix under a specific set of experimental conditions.

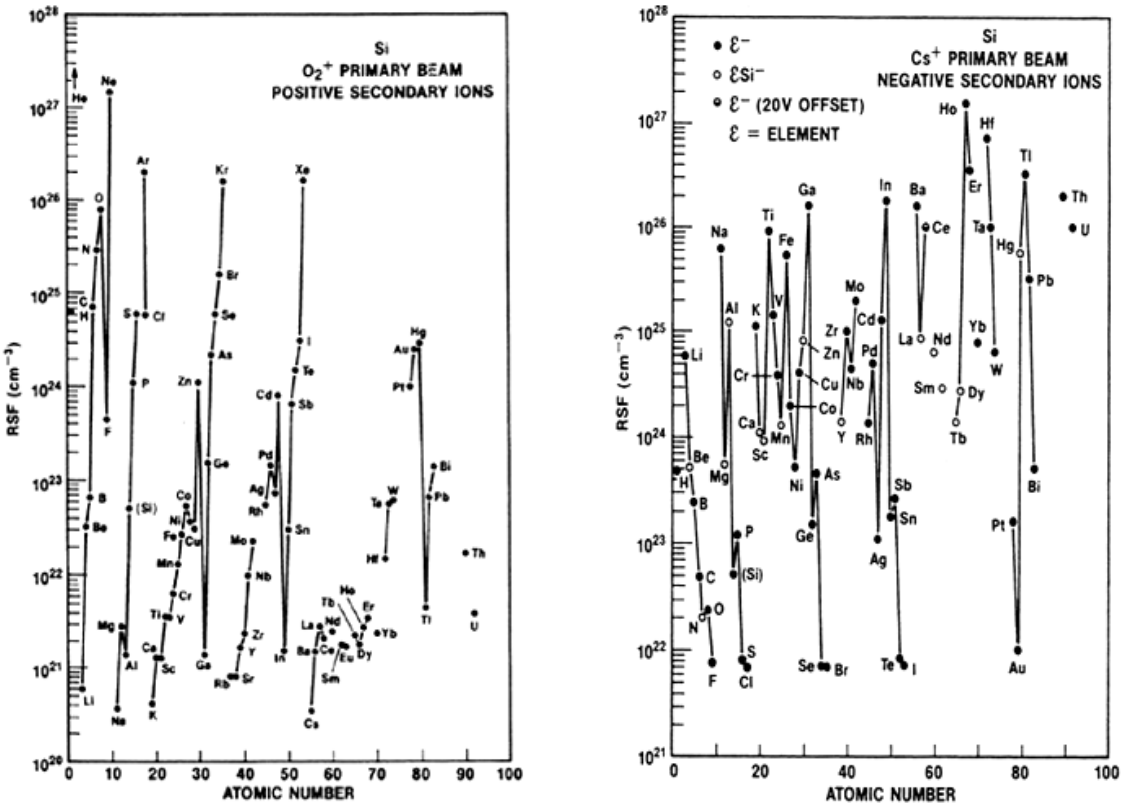

Figure 3-12. Variations of RSF's in Si matrix under O_2^+ and Cs^+ bombardment.[2]

The sensitivity factor is defined according to:

$$\frac{I_m}{C_m} = RSF_i \frac{I_i}{C_i}, \qquad \textbf{Equation 3-3}$$

where I_m and C_m are the secondary ion intensity and concentration of the matrix element and I_i and C_i are the secondary ion intensity and concentration of element *i*. RSF_i is the relative sensitivity factor of element *i* in matrix *m*.

In trace element analysis, the matrix concentration is assumed to remain constant. The matrix concentration can be combined with the elemental RSF_i to give a more appropriate RSF:

$$RSF = C_m RSF_i = C_i \frac{I_m}{I_i} \qquad \textbf{Equation 3-4}$$

The RSF is a function of the element of interest and the sample matrix. If the RSF is known for a specific matrix, then the elemental concentration can be calculated:

$$C_i = \frac{I_i}{I_m} RSF\ . \qquad \textbf{Equation 3-5}$$

Two types of standards are commonly used to compute the RSF value required for the quantification of a species of interest, *i*, in a depth profile. An RSF can be calculated using either an external standard sample of the same matrix that has been implanted with a known dose or bulk doped with a known concentration of this species of interest.

From an ion implanted standard, the RSF is computed using knowledge of the implanted dose, ϕ, of the species of interest and the sum of the ratios I_i/I_m obtained by point by point integration of this ratio over the depth profile, as indicated in the relationship:[2]

$$RSF = \frac{\phi}{\int \frac{I_i}{I_m}}, \qquad \textbf{Equation 3-6}$$

Ion implanted standards used to measure RSF values for quantitative SIMS analysis must match in both impurity and matrix composition and the implanted sample must be homogeneous to ensure repeatability. The ion implant dose should be high enough to obtain

a secondary ion intensity with sufficient signal to noise and the impurity should be implanted sufficiently deeply to place a sufficient fraction of the implanted ions far from the surface to avoid dose calculation errors caused by surface effects.

From a bulk doped standard, the RSF is computed from the ratio I_m/I_i of a given data point N corresponding to a known concentration, C_k, with the relationship:

$$RSF = C_k \cdot \frac{I_m(N)}{I_i(N)}, \qquad \textbf{Equation 3-7}$$

There are two options for the concentration method. The RSF value can be calculated from a known concentration set either for a given data point or for a mean value of several data points over the depth profile.

Depth profiles provide the secondary ion count rate of selected elements as a function of time. Figure 3-13 shows the raw data for a measurement of phosphorus in a silicon matrix. Also, as shown in Figure 3-13,the shaded area is the total signal ($\int I_i$) from the P implant (3.681×10^6 P ions). Raw data can be converted to concentration (atoms/cm^3) of the species of interest as a function of depth using an RSF, a crater depth measurement, and the measured Si matrix and impurity intensities (cts/sec). The x-axis is converted into depth by using a profilometer (discussed in section 4.4) to measure the crater depth and to calculate the sputtering rate. A previously calculated RSF is used to execute the conversion of the y-axis from secondary ion intensity into concentration (see Equation 3-5). An example of converting raw data to reduced data is shown in Figure 3-13.[2]

In this study, the RSF approach was the calibration technique used for SIMS quantification. RSFs were calculated using average P/Si ratios obtained from bulk doped P in Si samples selected for use as standards.

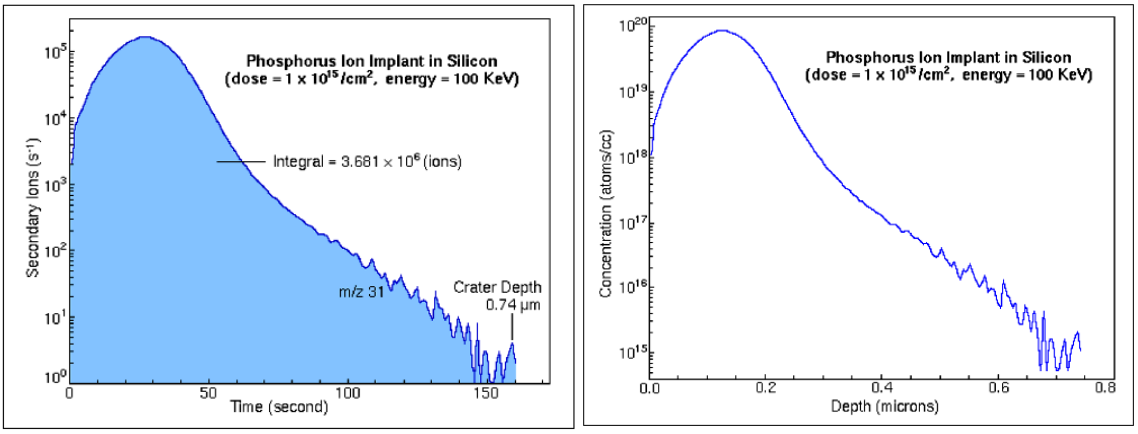

Figure 3-13. P in Si depth profile illustrating the conversion of raw data to reduced data.[2]

3.5 References

[1] J. J. Thomson, Phil. Mag. **20**, 752 (1910).

[2] R. G. Wilson, F. A. Stevie, and C. W. Magee, *Secondary Ion Mass Spectrometry: A Practical Handbook for Depth Profiling and Bulk Impurity Analysis*, Wiley, New York (1989).

[3] R. Zhang and T. F. Kuech, Appl. Phys. Lett. **72**, 1611 (1998).

[4] CAMECA, IMS-6F User's Guide**,** 1-5 (1996).

[5] A. Benninghoven, Z. Physik. **230**, 403 (1970).

[6] H.W.Werner, in *Quant. Analysis with* EMP *and* SIMS, Jill-Conf. **8**, 239 (1973).

[7] A. Benninghoven, F. G. Rudenauer, and H. E. Werner, *Secondary Ion Mass Spectrometry, Basic Concepts, Instrumental Aspects, Applications and Trends*, Wiley, New York, p.290 (1987).

[8] P.C. Zalm, Mikrochim. Acta **132**, 243 (2000).

[9] B. G. Yacobi, D. B. Holt, Lawrence L. Kazmerski, *Microanalysis of Solids*, Springer, New York (1994).

[10] B.W. Schueler and D.F. Reich, J. Vac. Sci. Technol. B **18**, 496 (2000).

[11] R.M. Bradley and J.M.E. Harper, J. Vac. Sci. Technol. A **6**, 2390 (1988).

[12] E.-H. Cirlin, J.J. Vajo, R.E. Doty, and T.C. Hasenberg, J. Vac. Sci. Technol. A **9**, 1395 (1991).

[13] Joe Bennett, Sematech.

[14] V.K.F. Chia, G.R. Mount, M.J. Edgell, and C.W. Magee, J. Vac. Sci. Technol. B **17**, 2345 (1999).

[15] S.R. Bryan, R.W. Linton and D.P. Griffis, J. Vac. Sci. Technol. A **5**, 9 (1987).

[16] K. Wittmaack and W. Wach, Nucl. Instru. Methods **191**, 327 (1981).

[17] G. Slodzian and J.-F. Hennequin,C.R.Acad. Sci. Paris B **263**, 1246 (1996).

[18] C. A. Andersen, Int . J . Mass Spectrom . Ion Phys . **2**, 61 (1969).

[19] K. Wittmaack, Int. J. Mass Spectrom. Ion Phys **17**, 39 (1975).

[20] J.B. Clegg, Surf. Interface Anal. **10**, 332 (1987).

[21] K. Wittmaack, Surf. Interface Anal. **26,** 290 (1998).

[22] C.W. Magee and R.E. Honig, Surf. Interface Anal. **4**, 35 (1982).

[23] W. Vandervorst, H.E. Maes, and R.F. De Keersmaecker, J. Appl. Phys. **56**, 1425 (1984).

[24] J.F. Ziegler, J.P. Biersack and U. Littmark, *The Stopping and Range of Ions in Solids*, Pergamon Press, NY (1985).

[25] J.A. McHugh. Methods of Surface Analysis, A.W. Czanerna, Ed., Elsevier, Amsterdam (1975).

[26] V.R. Deline, C.A. Evans, Jr. and P. Williams, Appl. Phys. Lett. **33**, 578 (1978).

[27] V.R. Deline, W. Katz, C.A. Evans, Jr. and P. Williams, Appl. Phys. Lett. **33**, 832 (1978).

[28] C.A. Andersen, Int. J. Mass Spectrosc. Ion Phys. **3**, 413 (1970).

[29] V.E. Krohn, J. Appl. Phys. **33**, 3523 (1962).

[30] H.A. Storms, K.F. Brown, and J.D. Stein, Anal. Chem. **49**, 2023 (1977).

[31] P. Williams, R.K. Lewis, C.A. Evans, Jr., and P.R. Hanley, Anal. Chem. **49**, 1399 (1977).

[32] G.S. Tompa, W.E. Carr, and M. Seidl, Surf. Sci. **198**, 431 (1988).

[33] N. Menzel and K. Wittmaack, Nucl. Instrum. Methods **191**, 235 (1981).

[34] R.W. Gurney, Phys. Rev **47**, 479 (1935).

[35] J.K. Norskov and B.L. Lundquist, Phys. Rev. B **19**, 5661 (1979).

[36] N.D. Lang, Phys. Rev. B **27**, 2019 (1983).

[37] Ming L. Yu, Phys. Rev. Lett. **40**, 574 (1978).

[38] Ming L. Yu, Phys. Rev. B **26**, 4731 (1982).

[39] Ming L. Yu, Phys. Rev. B **29**, 2311 (1984).

[40] J.E. Ortega, E.M. Oelling, J. Ferron, and R. Miranda, Phys. Rev. B **36**, 6212 (1987).

[41] Ming L. Yu, in *Sputtering by Particle Bombardment III*, edited by R. Behrisch and K. Wittmaack (Spring, Berlin, 1991), p.91.

[42] F. Schulz, K. Wittmaack, Rad. Eff. **29**, 31 (1976).

[43] P. van der Heide, C. Lupu, A. Kutana, and J.W. Rabalais, Appl. Surf. Sci. **231**, 90 (2004).

[44] J.E. Chelgren, W. Katz, V.R. Deline, C.A. Evans, R.J. Blattner, and P. Williams, J. Vac. Sci. Technol. **16**, 324 (1979).

[45] H. Gnaser, Phys. Rev. B **54**, 16458 (1996).

[46] H. Gnaser, Phys. Rev. B **54**, 17141 (1996).

[47] T. Wirtz, H.-N. Migeon, Surf. Sci. **561**, 200 (2004).

[48] Y. Kudriavtsev, R. Asomoza, Appl. Surf. Sci. **167**, 12 (2000).

[49] A. Villegas, Y. Kudriavtsev, A. Godines, and R. Asomoza, Appl. Surf. Sci. **203**, 94 (2003).

[50] J. Brison, N. Mine, S. Poisseroux, B. Douhard, R.G. Vitchev, and L. Houssiau, Surf. Sci. **601**, 1467 (2007).

4 SIMS Instrumentation

4.1 Introduction

A typical SIMS instrument consists of the following basic components: ion sources to produce energetic primary ions such as O_2^+, O^-, Cs^+, Ga^+, Au^+, Bi^+, C_{60}^+; ion optics to transport and direct a focused ion beam at the sample; a sample stage and exchange system to mount and insert samples; an electric field, biased to extract either positive or negative secondary ions from the sample surface; energy filters to reduce energy dispersion of extracted secondary ions; a mass spectrometer to separate secondary ions according to their mass to charge ratio and detectors to measure secondary ion intensities for display or counting. Additionally, most SIMS instruments utilize ultra high vacuum (UHV) conditions, typically less than 10^{-9} Torr, and a computer system. UHV ensures secondary ions can move undisturbed to detectors and minimizes contamination of the sample surface by background gas particles during analyses. A computer system is required to control mass switching, acquiring secondary ion intensity data, displaying and processing data.

Secondary ion mass spectrometry (SIMS) is considered one of the most important analytical techniques for accurately determining dopant profiles in Si and other semiconductor materials. In this study, SIMS meets most of the requirements of good depth resolution, high sensitivity, and excellent detection limit for the analysis of ^{31}P in Si.

4.2 Mass Analyzers

The secondary ions that have been extracted from the sample and have passed through an energy analyzer are separated based on mass to charge ratios by mass analyzers. There are three types of mass analyzers commonly used for SIMS instruments: time of flight (TOF), quadrupole, and magnetic sector.

4.2.1 Time of Flight (TOF) Analyzers

In TOF-SIMS, a pulsed beam of ions impinges on the surface of a sample to remove particles from the outermost layers. Typical primary ions include liquid metal ion sources (LMIS) such as Ga, Au, and Bi, or Cs, or cluster ions such as C_{60}. The primary column provides a pulse of ions which impinges on the sample surface generating a pulse of secondary ions which are accelerated into a flight tube. The time it takes for ions to reach the detector at the end of the flight tube determines the mass to charge ratio. A mass spectrum is then recorded as the ions impinge on the detector. A TOF mass spectrometer determines the mass by the exact time it takes secondary ions of different masses to reach the detector. Pulsed primary ions are required for TOF in contrast to the continuous or DC ion beams typical in magnetic sector and quadrupole SIMS.

The theory behind a time of flight mass analyzer begins with understanding the potential energy of a charged particle in an electric field is related to the charge of the particle and to the strength of the electric field:

$$E_p = qV \qquad \textbf{Equation 4-1}$$

where E_p is potential energy, q is the charge of the particle, and V is the voltage. When the charged particle is accelerated into the field-free drift tube by the voltage, V, the ions potential energy is converted to kinetic energy. Thus, the same kinetic energy, E_k, will enter the field-free drift region with velocities, v, according to their mass, m:

$$E_k = \frac{1}{2}mv^2 \qquad \textbf{Equation 4-2}$$

Therefore, the potential energy equals the kinetic energy, meaning that equations 4-1 and 4-2 are equal:

$$qV = \frac{1}{2}mv^2 \qquad \textbf{Equation 4-3}$$

The ion velocity after acceleration will not change as it moves in the field-free region of the flight tube. Therefore, the velocity of the ion, v, determines the flight time since the length of the flight tube, L, is known and the time of the flight of the ion, t, can be measured.

$$v = \frac{L}{t}$$ **Equation 4-4**

Substituting this expression for v into the kinetic energy relation provides the working equation for the time of flight mass spectrometer to be derived:

$$\frac{m}{q} = \frac{2Vt^2}{L^2}$$ **Equation 4-5**

Rearranging the equation to solve for the mass is then:

$$m = \frac{2qVt^2}{L^2}$$ **Equation 4-6**

Ions leaving the ion source of a time of flight mass spectrometer have neither exactly the same starting times nor exactly the same kinetic energies (similar to the "chromatic aberrations" discussed below for magnetic sector mass spectrometers). Therefore, secondary ions are not all emitted with the same energy but with an energy distribution which may be greater than 100eV. Various designs of TOF-SIMS spectrometers have been developed to compensate for these differences. Two types of analyzer systems, commercially available, are the reflectron and the TRIFT.

A reflectron is an ion optical device utilized to compensate for the spread in the kinetic energies by using a combination of ions passing through drift regions and a "mirror" or "reflectron," as shown in Figure 4-1.[5,6]

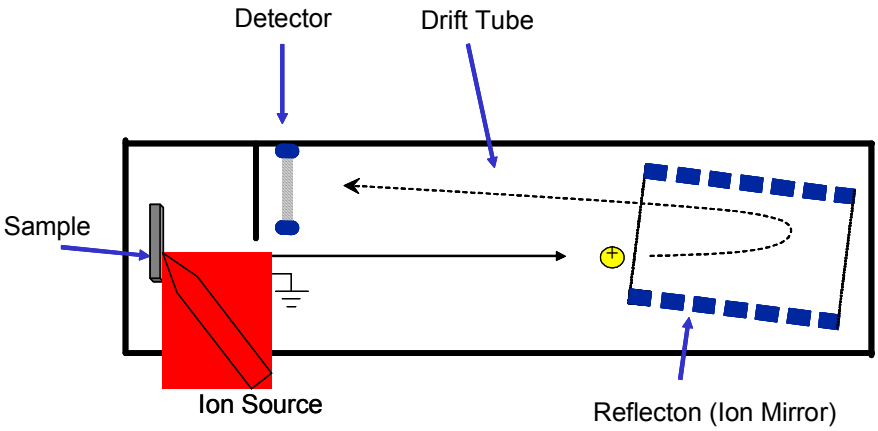

Figure 4-1. A time of flight (TOF) mass spectrometer with a reflectron.[6]

The reflectron acts as ion mirror, which extends the time of flight path without designing a larger instrument. The linear field reflectron allows ions with greater kinetic energies to penetrate deeper into the reflectron than ions with smaller kinetic energies. Therefore, ions that penetrate deeper will take longer to leave the reflectron. After reversing directions, the ions are accelerated out of the ion mirror and enter the drift region towards the detector. This mechanism allows energy variant ions to arrive at the detector simultaneously. The result is improved resolution in the time of flight mass spectrometer. A curved field reflectron assures the ideal detector position for the time of flight mass spectrometer does not vary with the mass-to-charge ratio. This improved design can provide a mass resolution of > 10,000 for time of flight mass spectrometers.[7-9]

TRIFT spectrometers were designed to transport a magnified secondary ion image from the sample to the detector and provide energy focusing for the time of flight.[10,11] Energy compensation in the TRIFT spectrometer is possible through the combination of electrostatic lenses and a group of three hemispherical electrostatic analyzers (ESAs), as shown in Figure 4-2.

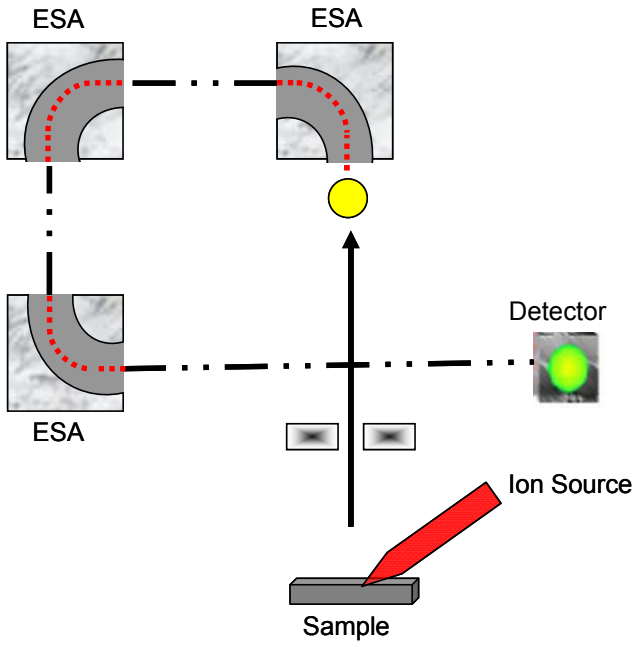

Figure 4-2. Schematic of the TRIFT system for TOF-SIMS.

Consider a TRIFT system with secondary ions starting from the sample with different energies. Ions disperse along the flight path and enter the first ESA. High-energy ions traverse the ESA closer to the outside sector, generating a longer flight path than low-energy ions. At the entrance of the second ESA, the beam is dispersed according to the ion energy, perpendicular to the spectrometer axis. Higher energy ions are still ahead of the low-energy ions until the center of the second ESA. After leaving the second ESA, the ions enter and are again deflected by the third ESA. Along the path to the detector, the high-energy ions catch up to the low-energy ions and they arrive at the detector simultaneously. The TRIFT system can provide a mass resolution that exceeds 15,000 for TOF-SIMS.[12]

TOF-SIMS is capable of shallow depth profiling with good depth resolution. Modern systems can be used to perform depth profiles that are micrometers deep. An ion gun is operated in the DC or continuous mode for sputtering. The same ion gun or a second ion gun is then operated in the pulsed mode for data acquisition. For ultra-shallow depth profiling (a few nm) the ion gun can be operated in AC or pulsed mode for sputtering. Depth profiling by TOF-SIMS allows monitoring of all species of interest simultaneously, and with high mass resolution.[13]

In a magnetic sector or quadrupole SIMS analyzer, the spectrometer scans through the mass range to record a mass spectrum. This is not a serious restriction if only one or two species are being monitored in a depth profile, but it is a problem with surface studies within "static" SIMS. By contrast, the TOF mass spectrometer is a parallel detection analyzer with a full mass spectrum recorded for each primary ion pulse. Thus the mass spectrometer does not scan through the mass range and thus no information is lost when recording a mass spectrum. As well as parallel detection, it has high mass resolution, high ion transmission, and the highest mass range of all SIMS analyzers discussed in this work.

4.2.2 Quadrupole Mass Analyzers

In a quadrupole SIMS, the sample is typically at low voltage or ground potential. The absence of a high sample potential allows for easy charge neutralization. Therefore, insulator analysis can often be more easily achieved using a quadrupole analyzer as compared to either

TOF or magnetic sector SIMS, both of which rely on high potentials to accelerate secondary ions from the sample surface.[14,15] When energetic primary ions bombard a sample, the secondary ions ejected from the sample surface are extracted by an extraction lens. A typical extraction voltage used in quadrupoles is around 300eV and the working distance is commonly 10mm. The polarity of the voltage in the extraction lens determines the polarity of the secondary ions that are extracted. Similar to the configuration of magnetic sector SIMS, an energy analyzer is used in combination with a mass analyzer, in this case, a quadrupole. The ions are then separated by the quadrupole mass analyzer according to their mass to charge ratio. The ions having a specific mass to charge ratio are allowed to pass through the quadrupole and enter the detector. Quadrupole based SIMS instruments do not use electromagnets and can achieve peak switching between selected ions faster than a magnetic sector because there is no hysteresis. Therefore, quadrupole mass analyzers are ideal for depth profiling of multiple masses over a large range. However, quadrupoles have a limited mass resolution, with typical systems providing a resolution of about 300 using the m/Δm 10% valley definition, and a typical mass range less than 400amu. They also have lower transmission.

Mass selection in quadrupoles is based on the potential φ(x,y) in a two-dimensional electrostatic quadrupole field of the general shape:

$$\varphi(x,y) = (V_{dc} + V_{ac}\omega t)\frac{x^2 - y^2}{r_0^2} \qquad \textbf{Equation 4-7}$$

Ideally, such a field is set up by an arrangement of four hyperbolic cylinders of infinite length when equal and opposite potentials represented by:

$$V = \pm(V_{dc} + V_{ac}\cos\omega t) \qquad \textbf{Equation 4-8}$$

are applied to adjacent cylinders. Instead of using hyperbolic cylinders, this geometry can be approximated with closely spaced circular rods with radius of:

$$r_r = 1.16 r_0 \qquad \textbf{Equation 4-9}$$

where $\pm V_{dc}$ are the dc voltages applied to positive and negative rods, respectively, V_{ac} is the amplitude of the ac component, ω is the circular frequency of the ac component, r_r is the rod radius, and r_0 is equal to the field radius (half distance along x- or y-direction between two rods.[3] Typical rods for a SIMS instrument are about 1cm in diameter and 20cm long. As shown schematically in Figure 4-3, ions enter from the left and radio frequency (RF) and direct current (DC) electric fields are applied to the rods, in pairs.[5] Alternating and direct voltages on the rods cause the ions to oscillate after entering the quadrupole. For a given set of voltages, ions with a specific mass to charge ratio have stable oscillations and will traverse through the rods. All other ions have unstable oscillations and will collide with the rods and will not reach the detector. By varying the electrical signals to a quadrupole it is possible to vary the range of the mass to charge ratio transmitted. Scanning over a range of voltages provides a mass spectrum. Unlike a magnetic sector which simultaneously disperses all the ions as a function of their mass to charge ratio, quadrupoles function by selective removal of ions and are often referred to as mass filters, rather than mass analyzers.

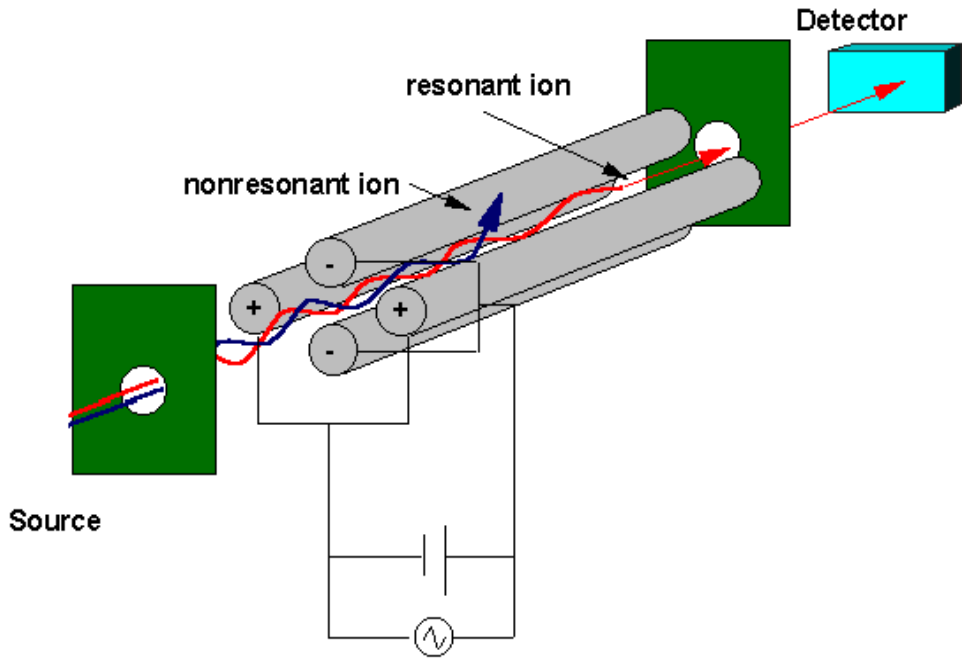

Figure 4-3. Schematic of quadrupole mass spectrometer.[5]

4.2.3 Magnetic Sector Analyzers

In SIMS, a surface is bombarded with energetic primary ions during which various atoms and molecules are sputtered from the sample surface. Most of these sputtered species are in the form of neutral atoms and molecules, but some of the sputtered species are ionized and extracted by an electric field into a mass spectrometer. The electric field is biased to extract either positive or negative secondary ions from the sample surface. These ionized secondary ions are then mass separated and detected. Magnetic sector analyzers separate the beam of secondary ions into its component parts according to their mass to charge ratios.[15]

A double focusing magnetic sector mass spectrometer provides high transmission of secondary ions. The configuration of a magnetic sector SIMS instrument is typically called a double focusing instrument because it uses both direction and velocity focusing. Thus, a diverging ion beam with ions of different energies is energy filtered and brought into focus followed by mass separation according to the mass to charge ratio.[16] For most SIMS magnetic sector instruments, the arrangement consists of an electrostatic energy analyzer followed by a magnetic field mass spectrometer. A schematic of the secondary ion column for a magnetic sector double focusing mass analyzer is shown in Figure 4-4.[17] Entrance and exit slits are arranged at ion beam crossovers for obtaining the highest mass resolution. Ion trajectories are illustrated by red (ions having the correct trajectory for transmission) and green colors (ions that do not have the correct energy or mass and thus do not pass through the spectrometer). A magnetic sector analyzer, used by itself, has trouble dealing with multiple energies because it is a momentum filter and thus to separate by mass to charge ratio, all ions must have the same energy. Chromatic aberrations are the result of separating ions of multiple energies as these ions do not have exactly the same velocity. Aberrations lead to a reduction in mass resolution. Thus, an electrostatic energy analyzer is used prior to the magnetic sector. The electrostatic analyzer (ESA) is used to select a desired energy range of the secondary ions extracted from the sample surface by applying a force perpendicular to the direction of ion motion that focuses ions according to their kinetic energy. The selected secondary ion energy range can be further narrowed using an energy slit. With this narrow range of secondary ion energies, a magnetic sector analyzer can then sort secondary ions

according to their momentum. In a double focusing magnetic sector mass spectrometer, the energy selection capability of the ESA can compensate the energy dispersion of ions leaving the sample. Therefore, a reduction in the chromatic aberrations occurs and allows a magnetic sector SIMS instrument to achieve higher mass resolution.

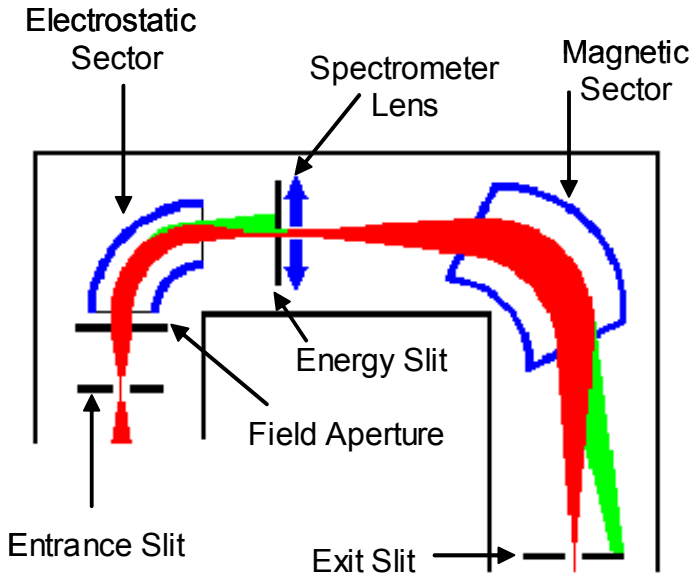

Figure 4-4. Schematic of a magnetic sector double focusing mass analyzer.[17]

A magnetic sector analyzer separates the beam of secondary ions, as the ion beam passes through the magnetic field, according to their mass to charge ratios. Magnetic sector SIMS, e.g. CAMECA IMS-6F, is achieved through holding the sample at a constant potential and extracting the secondary ions through the immersion lens. The sample potential can be changed, but the voltages on other secondary ion components must be changed accordingly. The immersion lens cover plate (4.5mm above the sample in the CAMECA F series instruments) is grounded creating a strong field to easily extract the secondary ions. The extracted secondary ions leaving the sample are accelerated to a kinetic energy given by:

$$\frac{1}{2}mv^2 = qV \qquad \textbf{Equation 4-10}$$

where m is the mass of the ion, v is its velocity, q is the charge of the ion and V is the secondary ion acceleration voltage.

The ions enter a magnetic sector flight tube between the poles of the magnet and are deflected by the magnetic field (B). The magnetic field is applied in a direction perpendicular to the direction of ion motion. When acceleration is applied perpendicular to the direction of motion of the ions, the velocity of the ions remains constant, but the ions travel in a circular path. Therefore, the ions in the magnetic sector follow an arc, the radius and angle of the arc varying with different ion optical designs. Only ions of mass to charge ratio that have equal centrifugal and centripetal forces pass through the flight tube as described by the Lorentz force law:

$$\frac{mv^2}{r} = qvB \qquad \textbf{Equation 4-11}$$

where r is the radius of curvature of the ion path.

From the above equations, a working equation for magnetic sector SIMS is obtained that provides the mass to charge ratio as a function of magnetic field and secondary ion acceleration voltage:

$$\frac{m}{q} = \frac{B^2 r^2}{2V} \qquad \textbf{Equation 4-12}$$

The magnetic field is varied to separate ions of equal energy according to their mass to charge ratios in magnetic sector spectrometers. Since these analyzers employ electromagnets, they can suffer from hysteresis during the rapid change of a magnetic field to detect multiple masses. Thus, the speed at which multiple masses can be selected is limited. When the magnetic sector spectrometer is being used for multiple ion detection, the magnetic field is changed in a stepwise manner to address a series of masses in turn. At each mass, a settling time must be introduced to compensate for the effect of hysteresis. In the case of multiple ion detection requiring rapid switching between masses, magnetic sector instruments are inferior quadrupole mass analyzers.

High mass resolution afforded by magnetic sector analyzers provides the ability to separate mass interferences. For example, ^{30}SiH and ^{31}P have the same nominal mass (31) with exact masses of 30.9816 and 30.9738, respectively. Mass resolution ($m/\Delta m = 31/.0078$) required for separating ^{30}SiH and ^{31}P is approximately 4000. Figure 4-5 illustrates a high mass resolution spectrum of P in amorphous Si analyzed using O_2^+ primary beam. The resolving power of a magnetic sector mass spectrometer is adjusted using the entrance and exit slit widths. Higher resolution is obtained by decreasing the slit widths; however, this results in decreasing the number of ions that reach the detector. For the CAMECA IMS-6F a practical mass resolution limit is approximately 10,000 using the $m/\Delta m$ 10% valley definition since the secondary ion transmission decreases with increasing mass resolution.

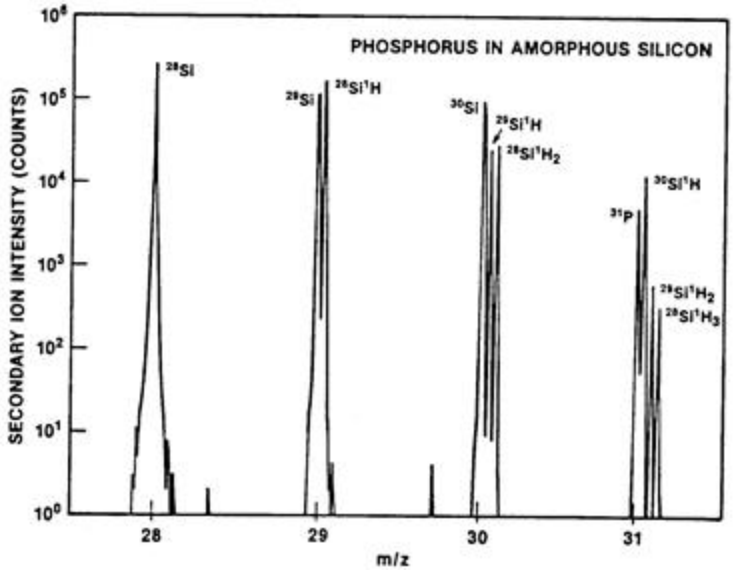

Figure 4-5. High mass resolution spectrum of P in amorphous Si.[15]

4.3 CAMECA IMS-6F

The SIMS instrumentation used in this research is a CAMECA IMS-6F electrostatic/magnetic sector SIMS (see Figure 4-6) equipped as follows. Two types of ion sources are used, a Cs^+ surface ionization source and a Duoplasmatron for O_2^+. Detectors used are a Faraday cup for high ion count rates, an electron multiplier for single ion counting

(less than 2E6 counts/second), and a microchannel plate/fluorescent screen for secondary ion imaging.

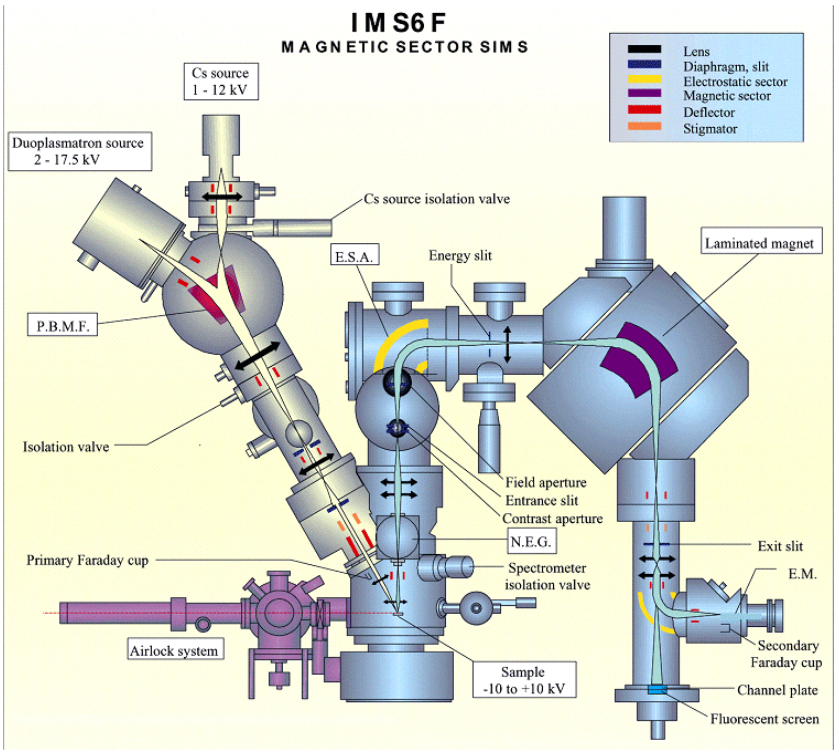

Figure 4-6. Schematic of the CAMECA IMS-6F magnetic sector SIMS used in the research.

4.3.1 Ion Sources

The CAMECA IMS-6F is equipped with two primary ion sources: a surface ionization Cs microbeam source and a duoplasmatron which is a cold cathode plasma ionization source.

4.3.1.1 Cs Microbeam Source

Cs^+, used for negative ion yield enhancement, is produced by the surface ionization Cs source. [18-20] In magnetic sector SIMS, the sample is negatively biased for extraction of negative secondary ions, and the positive primary ions are attracted towards the surface. The

positive primary potential and negative sample bias result in impact energies higher than the initial primary ion beam energy.

The Cs microbeam source is based on a surface ionization process. First considered by Langmuir and Kingdon, the phenomenon of surface ionization was described as the ionization of an atom with a low ionization potential becoming ionized in proximity of a hot metal surface. In 1923, it was shown that a heated tungsten filament in saturated cesium vapor converts all cesium atoms which strike it into cesium ions.[21,22] Further study showed an atom on the hot metal surface will be thermally ionized and the ionization probability is given approximately by the Langmuir-Saha equation:[23-26]

$$\alpha = \frac{g_+}{g_0} \exp\left[\frac{e(\Phi - I)}{kT}\right] \qquad \textbf{Equation 4-13}$$

where g_+ and g_0 are the statistical weight of the ion and atom states, *e* is the electronic charge, Φ is the work function of the metal, I is the ionization potential of the atom, k is the Boltzmann constant, and T is the temperature of the hot metal plate. For efficient positive ionization, the work function of the metal surface must be high. The ionization probability of alkali metals on a hot refractory metal surface can be close to 1. Ion sources based on the surface ionization principle generally exhibit a high degree of ion beam purity, low energy spread, but they are capable of ionizing only a limited number of elements.

In the vapor state, Cs forms positive Cs^+ ions when it comes into contact with the surface of a tungsten plate in the temperature range of 900°C to 1200°C. For the CAMECA IMS-6F, the preferred temperature is 1100°C for efficient ion emission. A schematic of the Cs microbeam surface ionization source in the CAMECA IMS-6F is shown in Figure 4-7.[27] A cesium carbonate tablet (Cs_2CO_3) is contained in a reservoir heated to a temperature of 400°C to release Cs vapor. The Cs vapor comes into contact with a tungsten plate in the ionizer. The plate has been heated to 1100°C by electron bombardment and converts the Cs vapor into Cs positive ions. The Cs^+ ions are extracted and accelerated with the generation of an electric field between the surface of the tungsten plate and the extraction electrode.

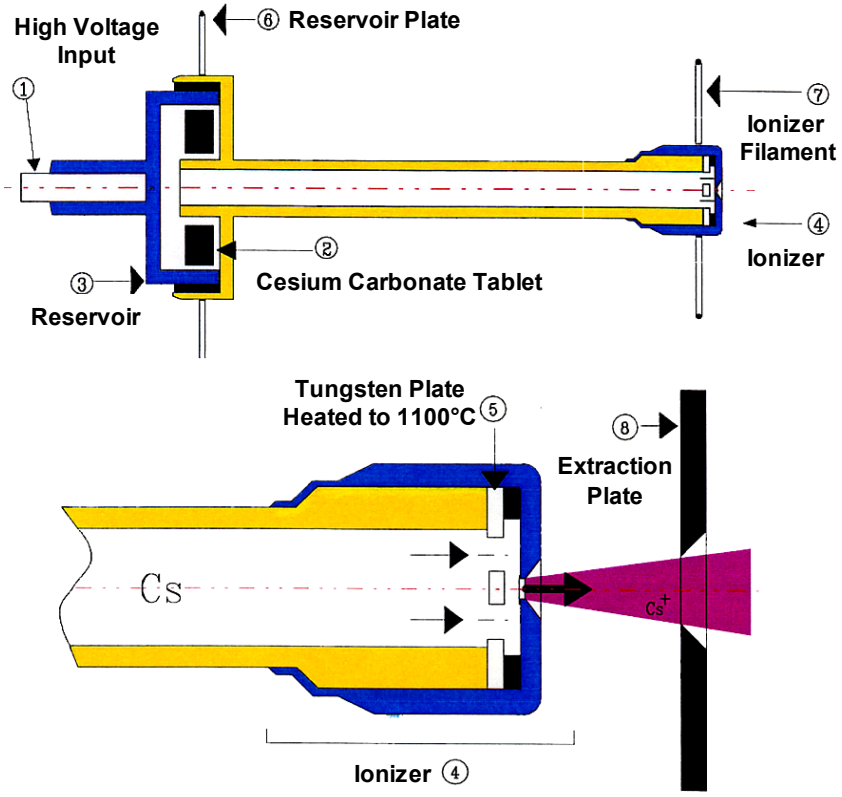

Figure 4-7. Schematic of a Cs microbeam surface ionization source.[27]

4.3.1.2 Duoplasmatron

It has been known for many years that the yield of positive secondary ions is enhanced by bombardment with electronegative species such as oxygen.[28,29] O_2^+ primary ions extracted by the duoplasmatron are used for positive secondary ion yield enhancement for the analysis of electropositive elements. Positive secondary ions are extracted from the sample which in magnetic sector SIMS requires a positive sample potential. The positive sample potential repels the incoming positive O_2^+ primary ions, so the primary incidence energy is always less than the primary beam energy.

This type of source was originally developed by von Ardenne in 1956 as a high current ion source, delivering high brightness and a good beam size (250μm) at a moderate cost.[30] A schematic of the duoplasmatron source of the CAMECA IMS-6F is shown in Figure 4-8.[31] Principal components of the source are a cathode, an anode, an intermediate

electrode, and a coil. Gas is introduced into the source at a low pressure to the hollow cathode through an adjustable leak. The anode is biased at several hundred volts relative to the cathode and a plasma is produced by an arc sustained between the cathode and anode. A conical intermediate electrode, at a floating potential, helps maintain the discharge close to the central axis. The plasma is concentrated close to the extraction hole in the anode by an electromagnetic coil produced magnetic field located between the intermediate electrode and anode. The plasma extends through the extraction hole and expands in a chamber due to the pressure difference between the duoplasmatron and the chamber of the gun. Primary ions are extracted from the plasma by a grounded extraction electrode (not shown in the figure). The source is called a duoplasmatron because the beam size is constricted by both the intermediate electrode and the action of the coil that surrounds the anode, intermediate electrode and cathode. Positive and negative ions can be extracted from the duoplasmatron according to the polarity of the extraction potential. Positive ions are prevalent when the cathode is centered on the anode aperture and negative ions are more abundant when the region close to the cathode is aligned with the anode aperture. Oxygen is the most commonly used gas species, which produces positive (O_2^+ and O^+) or negative (O_2^- and O^-) ions. O_2^+ and O^- are the most abundant species and are generally used.

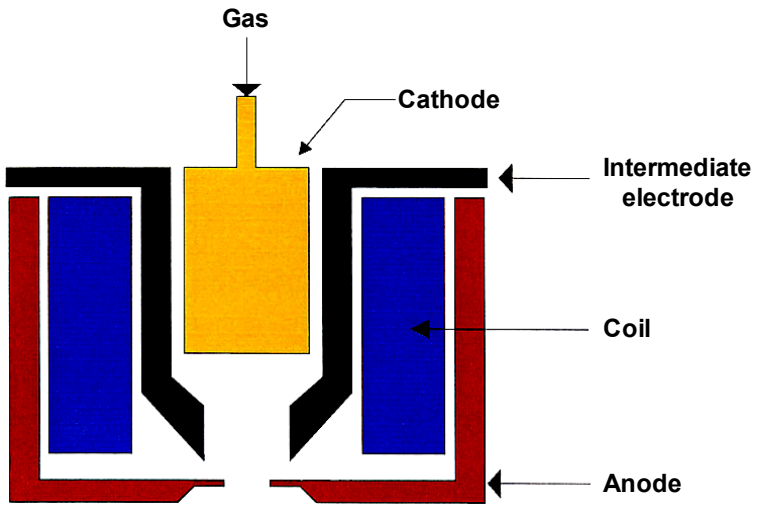

Figure 4-8. Schematic of a duoplasmatron.[31]

4.3.2 The Primary Ion Column

The primary ions generated by the ion source are accelerated toward the sample through the primary column (see Figure 4-9). Typical SIMS instrument columns consist of a mass filter, lenses, apertures, and deflection plates. These are used to filter, focus, shape, position and raster the primary beam. A primary beam mass filter (PBMF) after the ion source allows selection of either the Cs microbeam source or the duoplasmatron, eliminating any impurities in the gas or generated in the ion source. The electrostatic lenses and apertures control the intensity and shape of the primary beam.

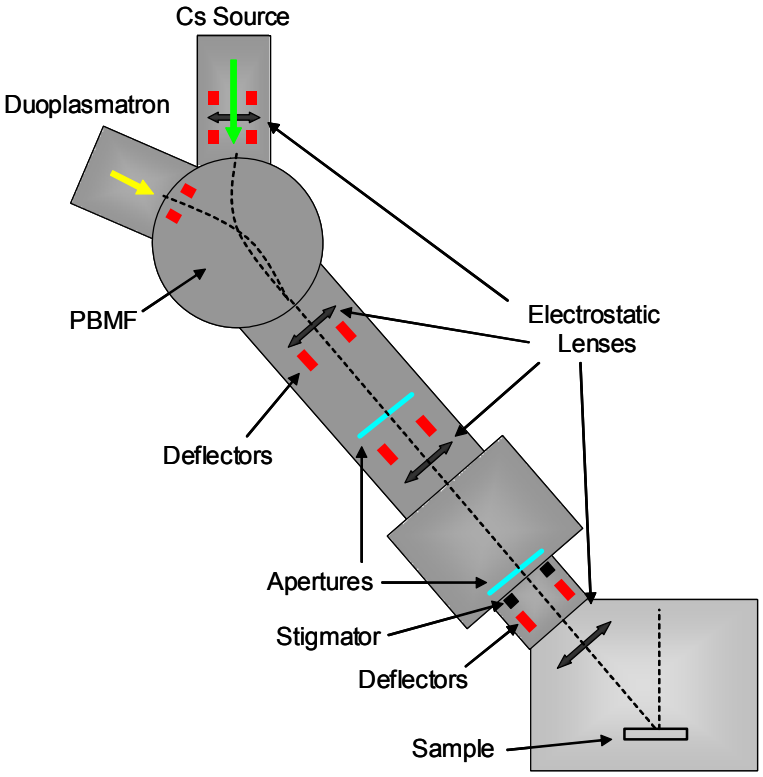

Figure 4-9. Schematic of the CAMECA IMS-6F primary ion column.

4.3.3 Mass Spectrometer

The mass spectrometer in the CAMECA IMS-6F is a double focusing electrostatic/magnetic sector. For a magnetic sector to function as a mass separation device,

all ions entering the magnetic sector must have similar kinetic energies. Therefore, the double focusing magnetic sector mass spectrometer uses an electrostatic sector for energy filtering to focus the initial energy spread of secondary ions into a monoenergetic beam. However, the initial energy spread of secondary ions will cause the particles of a given mass to experience an additional dispersion before entering the mass spectrometer. This is the equivalent of a "chromatic effect" and must be corrected in order to achieve a higher mass resolution.

In the CAMECA IMS-6F, achromatic mass separation is achieved by coupling a magnetic prism with an electrostatic sector through an electrostatic lens, the spectrometer lens, which compensates the energy dispersions produced by both prisms. The combination of the electrostatic sector and the spectrometer lens insures that ions with different initial energy will be focused to the same plane (cross-over) after exiting the magnetic sector (Figure 4-10).[32]

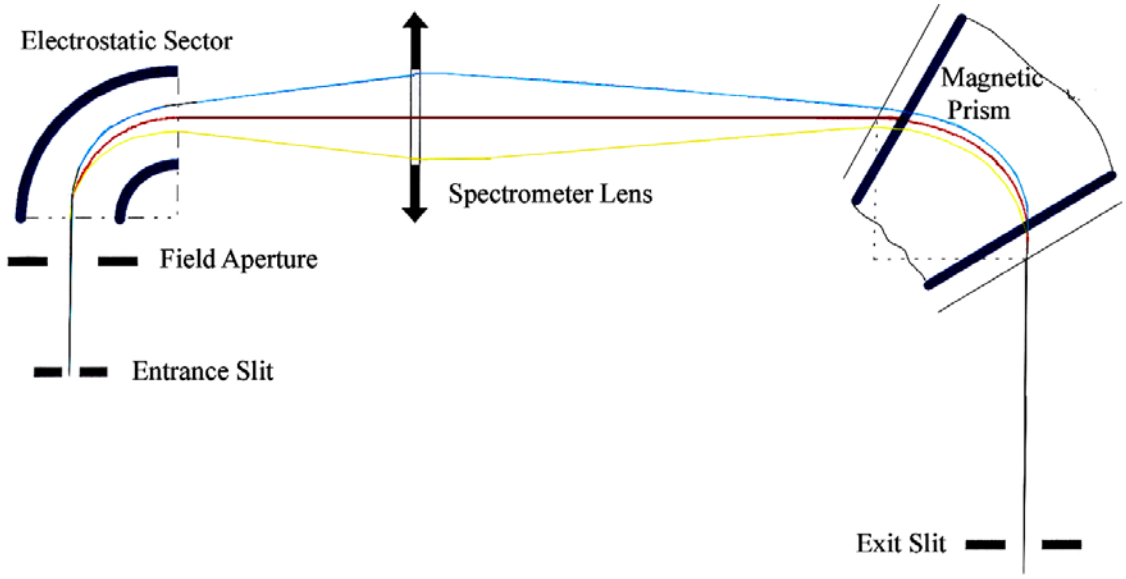

Figure 4-10. Trajectory of ions with different energies. The energy dispersion produced by the electrostatic sector and the magnetic prism work to cancel each other. Blue, red, yellow colors correspond to high, medium, low energies, respectively.[32]

Only the central ray with different energies is considered in Figure 4-10. However, a SIMS analysis includes ions with different trajectories through the electrostatic sector. In Figure 4-11, yellow and blue lines refer to energy trajectories other than the central ray (red line).[32] They are at the same energy and are brought into a common focus on the central ray by the electrostatic sector. All the ions are converted into one image point in the plane of the energy slit. The virtual image point produced by the lens will in turn act as an object point for the magnetic prism and be focused into a real image point by the prism.[32]

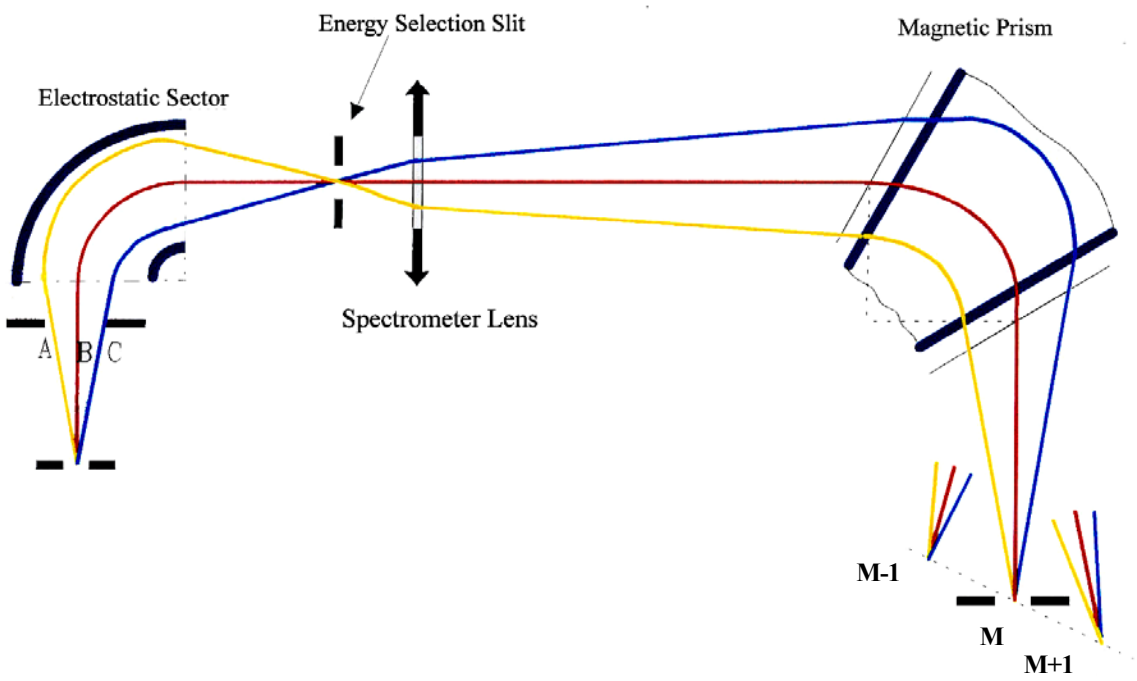

Figure 4-11. Mass separation of ions with the same energy but different trajectories.[32]

The high mass resolution capability permits elemental analysis through separation of the species of interest from interfering ions ($^{56}Fe/^{28}Si_2$, $^{31}P/^{30}SiH$, $^{32}S/^{16}O_2$). High mass resolution capability helps to broaden the applications for the instrument since in practical samples there are many different elements present and thus mass interferences are likely.

4.3.4 Secondary Ion Detection

The CAMECA IMS-6F is equipped with two types of detectors for secondary ion counting: a Faraday cup and an electron multiplier. The Faraday cup is used for high secondary ion count rates between 1E5 to 5E9 cts/sec, while the electron multiplier can be used to measure count rates between 1E-1 and 1E6 cts/sec. The combination of both the Faraday cup and the electron multiplier provides a high dynamic range capability for the secondary intensity measurement by giving the instrument the ability to detect secondary ions over a range of 10 orders of magnitude within a given analysis. There is another detector, a microchannel plate/fluorescent screen combination which provides the capability of secondary ion image detection.

4.3.4.1 Faraday Cup

The Faraday cup is a hollow cylinder with large ratio of length to input orifice diameter which is isolated from the instrument ground. The charges from the secondary ions entering the Faraday cup are thus accumulated. For accurate measurements of the secondary ion intensities, both the secondary ions and any secondary electrons must be prevented from escaping the Faraday cup. This is achieved by placing a repeller plate biased to a small negative potential in front of the Faraday cup. A schematic drawing of the CAMECA IMS-6F Faraday cup is shown in Figure 4-12.[33] A high impedance amplifier is used to convert the current from the entering secondary ions into a voltage. This voltage is sent to the input of a voltage to frequency converter.

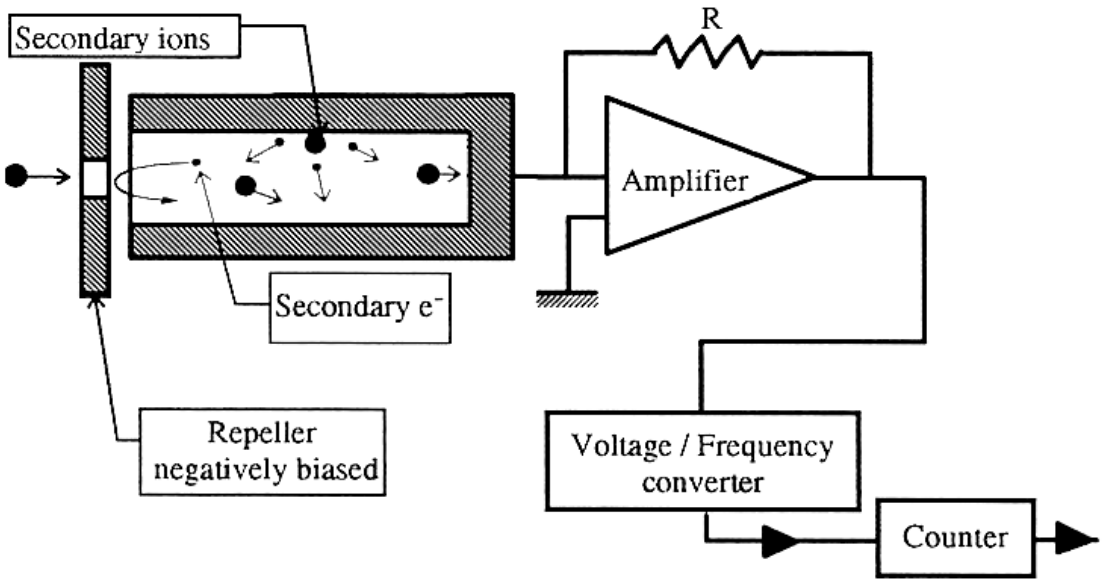

Figure 4-12. Schematic of the Faraday cup in the CAMECA IMS-6F.[33]

4.3.4.2 Electron Multiplier

A high sensitivity electron multiplier counting system that is capable of counting single ion impacts can be used for secondary ion count rates below about 2E6 cts/sec. The electron multiplier used on the CAMECA IMS-6F consists of a series of Cu/Be dynodes working in a direct pulse counting mode. (see Figure 4-13)[34,35]

Secondary ions colliding on the first dynode of the EM generate secondary electron emission. The secondary electrons are accelerated into the successive dynodes of the EM producing many more secondary electrons. An avalanche of secondary electrons develops, amplifying the secondary electron current. A gain of about 10^8 (number of electrons per secondary ion) is obtained. The group of electrons collected by the electron multiplier is measured as a pulse. Pulse counting is the most sensitive ion detection method. The amplitude of the pulses varies depending on the high voltage applied between the first and the last dynode, the mass and velocity of the secondary ions, the secondary beam position on the first dynode, and the age of the multiplier. Pulses of small amplitude according to the pulse height ratio usually represent the background noise and are eliminated by adjusting a

discriminator threshold. The optimized threshold corresponds to the first minimum of the pulse charge distribution.

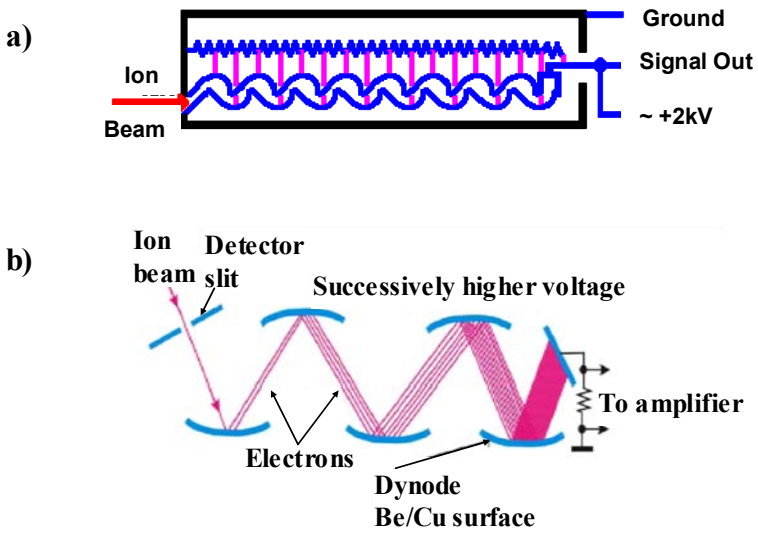

Figure 4-13. (a) Illustration of a discrete-dynode electron multiplier with; (b) an expanded view showing the cascade effect at each successive dynode.[34,35]

4.3.4.3 Microchannel Plate/Fluorescent Screen

The IMS-6F secondary ion image detector consists of a microchannel plate device coupled to a fluorescent screen (see Figure 4-14). The microchannel plates convert secondary ions to electrons and the fluorescent screen converts electrons to photons. The microchannel plate consists of an array of 10^4 - 10^7 small channels oriented parallel to one another. Each channel is a small hollow glass tube with a conductive inner surface layer. When a secondary ion strikes the inner surface, there is electron emission, these electrons are accelerated and multiplied by collision cascades in the channel. Electrons leaving the channels are further accelerated onto a fluorescent screen resulting in photon emission. The fluorescent screen image is acquired by means of a charge-coupled device (CCD) camera. This system is primarily used in alignment by providing a mass filtered image of the sample surface.

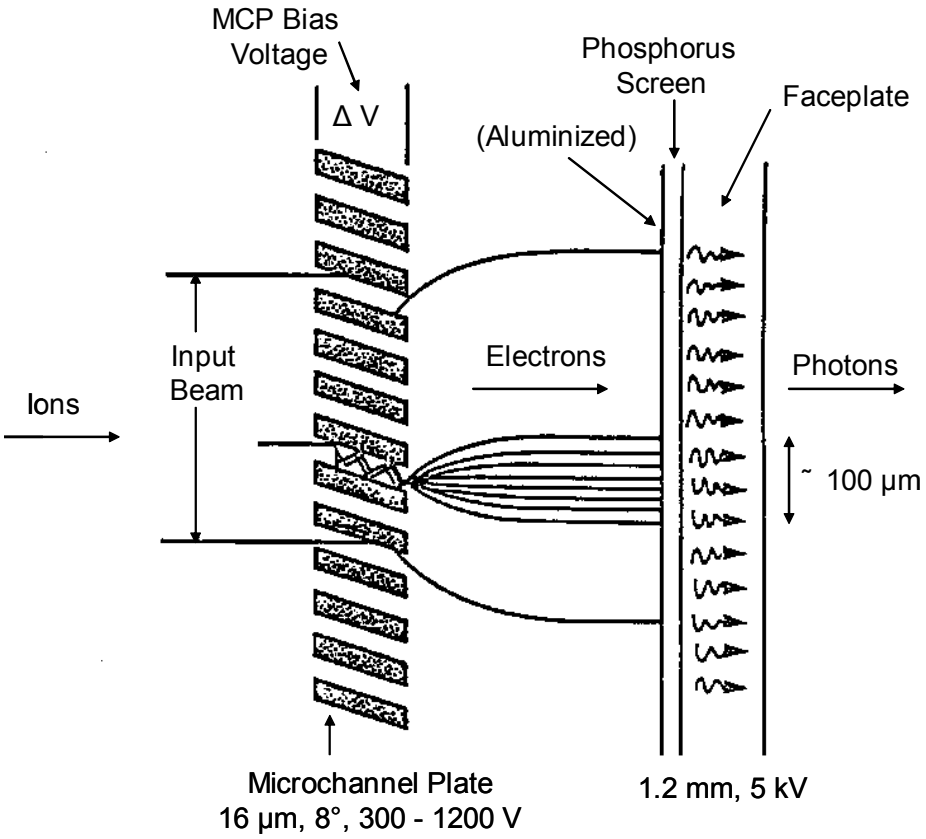

Figure 4-14. Schematic of a microchannel plate device coupled to a fluorescent screen.

4.4 Tencor P-20 Stylus Profilometer

Nanometer scale changes in surface roughness that occur during ion bombardment can be investigated using AFM. While AFM can be used to analyze shallow sputter crater depths, optical and stylus depth profilometers are more suitable for investigating the relatively large craters (>160µm^2) usually produced in SIMS. It is important to note that optical and stylus profilometers would not be the methods of choice to detect surface variations in surface topography.

Crater depths in this study are measured using a Tencor P-20 stylus profilometer and sputter rates were calculated assuming a linear sputter rate versus beam density. The stylus profilometer was first introduced by J.B. Williamson in 1967.[36] A stylus profilometer characterizes a surface by scanning a diamond tip across a surface with pressure to provide

information about surface topography. The Tencor P-20 profilometer uses a capacitive sensor to detect the vertical motion of the stylus due to the topography of the sample.[37] The changes in the capacitance are converted into variation in height. The measurement stage rests on an optical flat reference ensuring smooth and stable movement across the scan length. This allows the Tencor P-20 computerized system to provide accuracy of depth measurements of about 1nm for a flat and smooth sample. Also, it has a horizontal resolution of 0.01μm at 1μm/sec scan speed and a vertical resolution of 0.5Å with 3.25μm z range.[38]

4.5 References

[1] A. Benninghoven, Z. Physik. **230**, 403 (1970).

[2] H.W.Werner, in *Quant. Analysis with* EMP *and* SIMS, Jill-Conf. **8**, 239 (1973).

[3] A. Benninghoven, F. G. Rudenauer, and H. E. Werner, *Secondary Ion Mass Spectrometry, Basic Concepts, Instrumental Aspects, Applications and Trends*, Wiley, New York, p.290 (1987).

[4] P.C. Zalm, Mikrochim. Acta **132**, 243 (2000).

[5] E_source, Characteristics of different mass analyzers, Fraunhofer-Institute for Process Engineering and Packaging IVV,http://www.ivv.fraunhofer.de/ms/ms-analyzers.html.

[6] E_source, Atomic and Molecular Mass Spectrometry III, http://chz085.ust.hk/chem244/Lect13_0309Cao.ppt#1.

[7] E. Niehuis, T. Heller, G. Kampwerth and A. Benninghoven, in *Secondary Ion Mass Spectrometry SIMS VI*, Ed by A. Benninghoven, A.M. Huber and H.W. Werner. John Wiley & Sons, Chichester, p.255 (1987).

[8] X. Tang, R. Beavis, W. Ens, F. Lafortune, B. Schueler and K.G. Standing, Int. J. Mass Spectrom. Ion Proc. **85**, 43 (1988).

[9] U. Juergens, H.G. Cramer, T. Heller, E. Niehuis, Z. Zhang and A. Benninghoven, in *Secondary Ion Mass Spectrometry SIMS VIII*, Ed. By A. Benninghoven, K.T.F. Janssen, J. Teumpner and H.W. Werner. John Wiley & Sons, Chichester, p.277 (1991).

[10] B.W. Schueler, Microsc., Microanal., Microstruct. **3**, 119 (1992).

[11] B. Schueler, P. Sander and D.A. Reed, Vacuum **41**, 1661 (1990).

[12] J.C. Vickerman and D. Briggs, eds. *ToF-SIMS: Surface Analysis by Mass Spectrometry*. Chichester: IM ; Manchester: Surface Spectra, p.87 (2001).

[13] PHI, Our Techniques: TOF-SIMS, http://www.phi.com/techniques/tof-sims.html.

[14] C.W. Magee and W.L. Harrington, Appl. Phys. Lett. **33**, 193 (1978).

[15] R.G. Wilson, F.A. Stevie, and C.W. Magee, *Secondary Ion Mass Spectrometry: A Practical Handbook for Depth Profiling and Bulk Impurity Analysis,* Wiley, New York (1989).

[16] E_Source, Double-focusing Mass Spectrometer From Mass Spectrometry Terms, http://www.msterms.com/wiki/index.php?title=Double-focusing_Mass_Spectrometer.

[17] R. Fleming, Secondary Ion Mass Spectrometry Instrumentation Tutorial, http://www.eaglabs.com/en-US/references/tutorial/simsinst/caisinst.html.

[18] V. Krohn, J. Appl. Phys., **33**, 3523 (1963).

[19] C.A. Andersen, Int. J. Mass Spectrom. Ion Phys., **3**, 413 (1970).

[20] A. Benninghoven, F.G. Rudenauer, H. W. Werner, *Secondary Ion Mass Spectrometry*, John Wiley and Sons, (1987).

[21] K.H. Kingdon and I. Langmuir, Phys. Rev. **21**, 385 (1923).

[22] I. Langmuir and K.H. Kingdon, Proc. Roy. Soc. (London) A **107**, 61 (1925).

[23] J.A. Becker, Trans. Am. Electrochem. Soc. **55**, 153 (1929).

[24] M.J. Copley and T. E. Phipps, Phys. Rev. **48**, 960 (1935).

[25] C. Herrong and M.H. Nichols, Rev. Mod. Phys. **21**, 185 (1949).

[26] M.J. Dresser, J. Appl. Phys. **39**, 338 (1968).

[27] CAMECA, Microbeam Cesium Source Principle, IMS 6-F User's Guide, 1-65 (1996).

[28] G. Slodzian and J.F. Hennequin, C.R. Hebd. Seances Acad. Sci., Ser. B, **263**, 1246 (1966).

[29] C.A. Andersen, Int. J. Mass Spectrom. Ion Phys., **2**, 61 (1969).

[30] M.V. Ardenne, Technik. **11**, 65 (1956).

[31] CAMECA, Duoplasmatron Illustration, IMS 6-F User's Guide, 1-64 (1996).

[32] CAMECA, Illustration of mass spectrometer, IMS 6-F User's Guide, (1996).

[33] CAMECA, Illustration of Faraday Cup, IMS 6-F User's Guide, 1-77 (1996).

[34] Secondary Ion Mass Spectrometry Instrumentation Tutorial, http://www.eaglabs.com/training/tutorials/sims_instrumentation_tutorial/detector.php.

[35] Electron Multiplier for Mass Spectrometers, http://www.sge.com.

[36] J. B. Williamson, Proc. Inst. Mech. Eng. **182**, 21 (1967).

[37] Tencor P-20 Reference Manual, 4-1.

[38] Tencor P-20 Reference Manual, 3-1.

5 SIMS Depth Profiling of Phosphorus Implants under Cs^+ Bombardment

5.1 Introduction

The next generation of ultra-large-scale integrated (ULSI) devices will contain device features that are significantly less than 100nm. These devices will require shallow, low dose implants, in order to control the threshold voltage (V_t) adjust and optimize performance. Medium energy, low dose phosphorus (P) implanted in silicon (Si) is commonly used as the V_t adjust for p-FETs and flash memory cells. P will almost certainly continue to be widely used as an n-type dopant in Si. There are difficulties in characterizing low dose implants and aspects of Secondary Ion Mass Spectrometry (SIMS) depth profiling of low dose P in Si are studied in this work.

Depth profiles of low dose phosphorus (P) implants acquired by Intel showed an apparent increase in P dose as a function of sample age, seen primarily as a higher apparent P surface concentration. Although of secondary importance with respect to dose measurements, higher P background concentrations were also observed showing evidence of possible diffusion into the substrate. Possible explanations for the changes in apparent P distribution over time are surface oxidation, diffusion, and/or the influence of adjacent prior analyses. The goal of this study on the aging of low dose phosphorus implants is to investigate changes over time in the apparent phosphorus surface concentration that have been observed in SIMS depth profiles of phosphorus implanted silicon samples in Intel laboratories (see Figure 5-1).

This study consists of two complementary studies: the effect of time on the surface concentration of P for different phosphorus implant doses in silicon and the effects on phosphorus implants in silicon exposed to different processing methods. This study uses SIMS depth profiling to monitor changes in the concentration of P with depth for different implant profiles which were exposed to differing environmental conditions over time. Upon receipt by NCSU, the as received wafers were subdivided and portions of the wafers were

immediately analyzed to determine the as received P distributions. The samples were then stored under a variety of environmental conditions and analyzed periodically at which time unanalyzed and previously analyzed pieces were depth profiled.

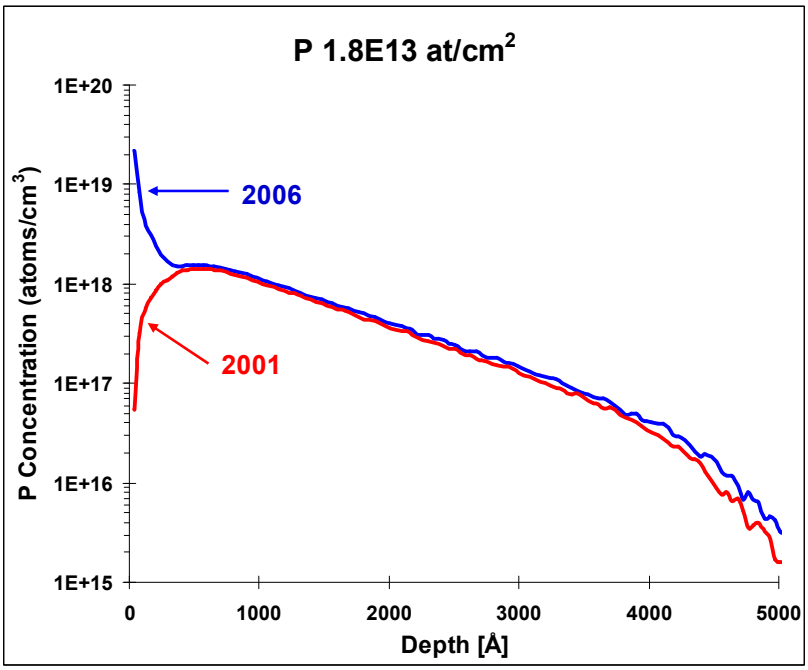

Figure 5-1. Sample 353 (P 1.8E13 at/cm^2, 35keV) as implanted and after 5 years.

5.2 Experiment

A set of samples provided by Intel are 10-30 Ohm-cm [100] p-type (B doped) Si wafers which were implanted with ^{31}P. A well characterized [100] P implanted wafer (NCSU standard) and a [100] P bulk doped wafer were also utilized in this study as external standards (see Table 5-1). Before implantation, the received test wafers underwent a pre-clean step that removes native oxide. For the initial study on the effect of time on the surface concentration of P for different phosphorus implant doses in silicon, wafers 344, 341, and 471 were analyzed over an extended time period. For reference purposes, the NCSU standard was frequently analyzed and the bulk doped sample was also analyzed during each analysis (see experiment below).

Table 5-1. Descriptions of wafers and standards analyzed to determine the effects on different P implant doses in Si .

Wafer Description	Implant Information
Wafer 344: P implant in Si	1.0E14 atoms/cm^2, 35keV
Wafer 341: P implant in Si	1.0E13 atoms/cm^2, 35keV
Wafer 471: P implant in Si	1.0E12 atoms/cm^2, 35keV
P implant in Si (NCSU)	1.05E14 atoms/cm^2, 50keV
Bulk doped P in Si (NCSU)	8.2E18 atoms/cm^3

In order to extend the sample set to study the effects on phosphorus implants in silicon exposed to different processing, five additional wafers were provided by Intel with all wafer processing (e.g. implantation, annealing) done at Intel. These additional wafers were implanted with 1E12 at/cm^2 P at 35keV. Two of these wafers were not subjected to any additional processing either prior to or post implantation. The remaining wafers used in this study were subjected to various processing methods in an effort to reduce the possibility of phosphorus redistribution toward the surface (see Table 5-2). Wafer 839 was implanted with P through a 50Å oxide layer. Wafer 840 was subjected to a 1080°C RTA following a pre-clean step to remove the native oxide. The intent of the RTA was to immobilize P through annealing with minimum P redistribution. Wafer 805 underwent pre-amorphization using a de-channeling implant (Si implanted into the Si substrate at 1.0E15 at/cm^2, 35keV) to amorphize the sample prior to P implantation (P in Si at 1.0E12 at/cm^2, 35keV). On completion of the above processing, the wafers were diced and immediately shipped to NCSU. Upon receipt by NCSU, the samples were immediately analyzed in the as received condition and placed in the selected storage conditions.

Table 5-2. Descriptions of wafers implanted with 1.0E12 at/cm^2 P at 35keV and the bulk doped standard analyzed to determine the effects of different processing methods.

Wafer Description	Implant Information
Wafer 672: P implant in Si	Implant Only
Wafer 798: P implant in Si	Implant Only
Wafer 839: P implant in Si	50Å Oxide
Wafer 840: P implant in Si	RTA (pre-cleaned, annealed at 1080°C)
Wafer 805: P implant in Si	Pre-Amorphization (Si 1.0E15 at/cm^2)
Bulk doped P in Si (NCSU)	8.2E18 atoms/cm^3

The storage conditions that have been employed in this project are: ambient air, high humidity, low humidity, elevated temperature (100°C or 200°C in ambient air), and liquid nitrogen. After the wafers arrived, multiple pieces were cut from each wafer for each of the 5 storage conditions (see Table 5-3). The pieces were cut into 1cm x 1cm pieces to be compatible with the CAMECA IMS-6F sample holder used for this analysis. After cutting and storage of the pieces to be analyzed, the remainder of each Intel wafer was stored in a Fluoroware container in ambient laboratory environment. Storage conditions are given in Table 5-3. The values given in Table 5-3 are the average temperature and relative humidity for each of the storage conditions (with the exception of the LN_2 stored samples). The relative humidity for the heated condition was calculated based on the lab temperature and humidity.

Table 5-3. The storage conditions used for the P implant aging study.

Condition *(temp/relative humidity)*	**Storage** *(environment/container)*
ambient (22°C)/ambient (42%)	Fluoroware / Fluoroware
ambient (22°C)/dry (24%)	dessicator / Fluoroware
ambient (22°C)/moist (93%)	dessicator with water / Fluoroware
Heat (100°C or 200°C)/ambient (<1%)	oven at 100°C or 200°C/glass Petri dish
liquid nitrogen	LN_2 Dewar/wire cage

The depth profile experimental conditions prescribed by Intel's best known method (BKM) SIMS depth profiling procedure for analysis of P was modified to provide a more detailed measure of the P secondary ion intensity at the sample surface (see Table 5-4). P sensitivity was improved by increasing the secondary ion count rate through the use of a larger field aperture. Depth resolution was improved through the use of a slower sputtering rate. All depth profiles were measured using a CAMECA IMS-6F. Table 5-4 lists the instrument conditions used to acquire the depth profiles including primary ion, total impact energy, primary ion accelerating voltage, and sample potential. The primary beam was rastered over 160μm x 160μm and secondary ions were collected from an optically gated area of 60μm in diameter. A mass resolution of 4000 M/ΔM, 750μm field aperture (FA2), 400μm contrast aperture (CD2), and a raster spacing of 300μm were used in all cases. Raster spacing refers to the distance between SIMS crater centers.

Table 5-4. CAMECA IMS-6F analysis conditions used for the P implant aging study depth profiles.

Primary Beam: Cs^+	Primary Voltage (E_p): 10kV	Secondary Voltage (E_s): -4.5kV
E_{Impact} = 14.5keV	I_p: 40nA	MR: 4000
α = 2	CD: 400μm (#1)	FA: 750μm (#2)
	Raster Size: 160μm	Raster Spacing: ≈ 300μm

The BKM used by Intel for this measurement specifies the measurement of only one species, P, with a matrix intensity measurement at the end of the SIMS analysis. To begin the initial study, it was of interest to acquire more than one species and, for these depth profiles, O, Si and P were acquired for one second each. As the study progressed, the conditions for the analyses were modified to acquire additional data points per unit depth to improve the precision of the P secondary ion intensity measurement near the surface. The changes in the analysis conditions included detecting only P (2 seconds per data point) with the Si matrix reference signal collected for 4 seconds at the end of the profile. Additionally, the range switch on the IMS-6F secondary magnet power supply was switched to the alpha (α) 2 setting to improve the digital tuning precision of the IMS-6F. Increasing alpha from a

setting of 1 to 2 doubles the calibration precision by doubling the number of data points across a mass peak, thus reducing calibration errors. Using the alpha 2 setting provided more stable and consistent Si and P signals through the entirety of each depth profile. In general at least one matrix species (e.g. Si) is measured together with the dopant signal (e.g. P) as a function of time throughout the SIMS depth profile. The ratio of dopant to matrix signal is then converted to dopant concentration by applying a RSF obtained using the calibration procedure described above (see section 3.4.2). A matrix species, such as Si in this study, is used to help quantify atomic concentrations and calculating implant doses; therefore, it is important for the matrix signal to be stable. Figure 5-2 compares the stability of the Si matrix reference signal as a function of time throughout the SIMS depth profile for the alpha 1 and 2 setting. Inconsistent Si signals are obtained using alpha 1 after a switch to alpha 2 a stable Si matrix reference signal is provided. This consistency in the Si matrix reference signal allows for more accurate phosphorus dose calculations. For example, the stability provided by the alpha 2 setting insured the P signal was consistently calibrated on the center of the P peak. Therefore, using alpha 2 allows for the dose measurement precision required for quantitative P depth profiling.

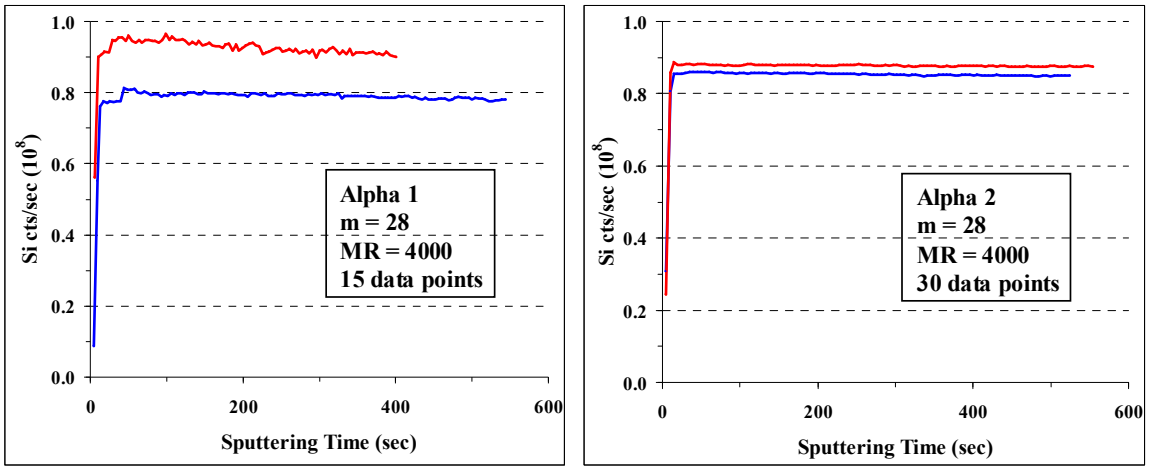

Figure 5-2. (left) Illustrates inconsistent Si signals with the alpha 1 setting and (right) the stable Si signal using alpha 2.

The analysis requirements specified by Intel's BKM for this investigation included Cs impact energy of 14.5keV. Because a primary goal of this study is to investigate the surface and near surface concentration of P implants in Si, analysis at a lower Cs energy was considered since low energy bombardment will improve depth resolution. However, lower energy decreases the detection sensitivity and limits the concentration that can be analyzed. Results using a lower energy of E_p = 5kV and E_s = -1kV with an impact energy of 6kV were compared to the results obtained using an impact energy of 14.5kV under the initial conditions. Under the low energy condition, adequate detection limits for the 1E12 at/cm^2 P in Si were not achieved. For the low energy analysis the detection limit is in the 10^{17} range. The capability to discern surface concentrations of the low dose (1E12 at/cm^2) P implants in Si requires a detection limit better than 10^{16}. Therefore, this study required high energy conditions (E_{Impact} = 14.5kV).

Using the primary ion beam conditions listed in Table 5-4, sputter rates ranging from 9 to 12Å/sec were obtained. The RSF was calculated from a P bulk doped Si wafer for quantitative measurement of P in Si. Samples stored in the ambient, dry, moist, and heat conditions were analyzed over an extended period of time. Samples stored in the liquid nitrogen were analyzed at the end of their respective study. During each analysis session, two pieces from the selected wafer storage conditions for each wafer were analyzed. With the exception of the initial analysis session, one piece of each wafer that had been exposed to Cs in all prior SIMS analyses was analyzed. Analyzed areas on previously exposed samples were selected to be as close as practical (approximately 300μm apart) to the previously analyzed areas. During each session, a previously unanalyzed and thus unexposed piece was also analyzed. After SIMS analysis, craters were measured using a Tencor P-20 stylus profilometer, and the previously exposed pieces were placed back into their respective storage conditions until the next analysis session.

5.3 Results and Discussion

5.3.1 Effects on Different Phosphorus Implant Doses in Silicon

In an effort to determine the cause of the apparent increase in P dose over time that has been observed by Intel, wafers 344 (1E14 at/cm^2), 341 (1E13 at/cm^2) and 471 (1E12 at/cm^2) were analyzed over a period of 31 weeks using the primary ion beam conditions listed in Table 5-4. Sputter rates ranging from 9 to 10Å/sec were obtained. The average RSF obtained using the P bulk doped sample as the reference was 1.13E23, with $^{28}Si^-$ as matrix species. The storage conditions that have been employed in this project (ambient air, high humidity, low humidity, elevated temperature of 100°C in ambient air, and liquid nitrogen) were chosen to provide a range of conditions which might affect and in some cases accelerate the apparent increase in P surface concentration. At least 7 analyses were performed on each of the three wafers over this period. Samples stored in the liquid nitrogen were analyzed after 31 weeks of storage. Sample 471, stored at an elevated temperature, was analyzed 8 times due to the substantial increases noted in P surface concentration. As can be seen in Figure 5-3, the elevated temperature conditions appear to have accelerated the apparent increase in P surface concentration. An example of this increase is shown for the 1E13 at/cm^2 wafer 341 in Figure 5-3. This increase was very similar to the results obtained by Intel (see Figure 5-1) on a 5 year old wafer 353. While the doses of wafers 341 (1E13 at/cm^2) and 353 (1.8E13 at/cm^2) are not identical, the difference is small and should not affect the comparison. In Figure 5-3, sample 341 (1E13 at/cm^2) provides a clear comparison between a sample unexposed (CsNo) and exposed (CsEx) to cesium with regard to the change in P surface concentration. The sample unexposed to Cs is represented by the as received depth profile of sample 341. Sample 341, previously exposed to Cs has been analyzed 7 times and stored in an oven at 100°C over 31 weeks.

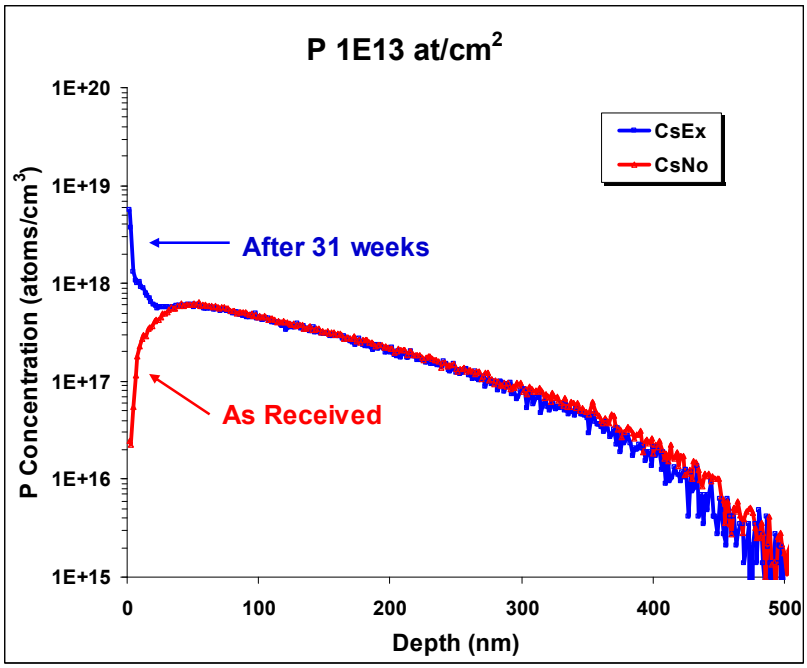

Figure 5-3. Depth profiles of sample 341 (P in Si of 1E13 atoms/cm^2, 35keV) unexposed and exposed to Cesium. The sample unexposed to Cs is represented by the as received depth profile of sample 341. The sample previously exposed to Cs has been analyzed 7 times and stored in an oven at 100°C over 31 weeks.

SIMS depth profile results obtained from the three wafers stored under the various conditions (see Table 5-3) were compared with depth profiles obtained from the as received wafers. For each of the 7 (or 8 as was the case for wafer 471) analyses performed over the subsequent 31 weeks, two pieces of each wafer were analyzed: one piece that had been analyzed during all previous analyses and thus exposed to Cs (referred to as CsEx) and one that had remained in its respective storage condition and thus had never been analyzed (CsNo). After each analysis, the CsEx samples were placed back into their respective storage conditions. The discussion below compares the SIMS results from the as received samples with results obtained from the CsEx and CsNo samples after 31 weeks of storage in the various conditions.

Wafer 344, which had the highest dose (1E14 at/cm^2) in this study, was clearly affected by storage at 100°C and CsEx because the P surface concentration increased by more than one order of magnitude (see Appendix Figure A-1). No significant changes were

observed for wafer 344 under any other storage conditions (see Appendix Figure A-2, Figure A-3). It is believed that the lack of observed changes in P surface concentration for wafer 344 under all but the 100°C storage conditions may be due to the already high surface concentrations of this high dose implant being sufficient to mask all but the largest changes.

For both wafer 341 (1E13 at/cm^2; see Appendix Figure A-4 through Figure A-8) and wafer 471 (1E12 at/cm^2 P dose; see Figure 5-4 through Figure 5-8), significant changes in apparent P surface concentrations were observed. For both of these wafers, the ambient, low humidity and high humidity storage conditions showed increases in the apparent surface P concentration, compared with the as received depth profiles with the largest changes occurring under the Heat storage conditions. Since wafer 471 provided the largest relative changes for the apparent P surface concentration, the remainder of the discussion will concentrate on this wafer. In each of the figures below, three P depth profiles are shown: as received ^{31}P (red); ^{31}P (blue) CsEx after 31 weeks in the various storage conditions; and ^{31}P (green) CsNo after 31 weeks in the various storage conditions.

Storage of wafers at 100°C was chosen in an attempt to accelerate changes that would occur at room temperature over an extended period of time. Both the CsEx (7 previous Cs exposures) and CsNo P depth profiles obtained from wafer 471 after 31 weeks aging at 100ºC (Figure 5-4) showed significant changes in the apparent P surface concentration. In the CsEx sample, surface P was measured at ≈ 8E18 at/cm^3, almost three orders of magnitude greater than the as received and the CsNo samples. The CsEx P depth profile in Figure 5-4 clearly demonstrates that prolonged sample storage at 100ºC along with previous Cs exposure results in a significant change in apparent P surface concentration, an increase which extends some tens of nm into the sample. Careful comparison of the CsNo sample P profile (Figure 5-4) stored under the same conditions with the as received P profile shows a much smaller but still significant change in surface apparent P concentration. These results indicate that while storage of the wafer for 31 weeks at 100ºC does result in some change in apparent P surface concentration, exposure to Cs in addition to storage at elevated temperature results in a much greater change.

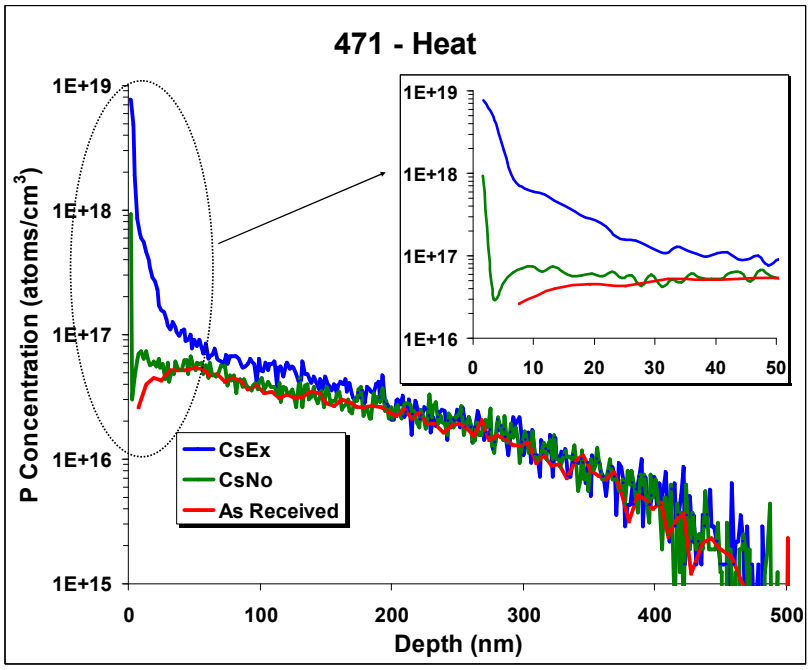

Figure 5-4. Depth profiles of sample 471 (P in Si of 1E12 atoms/cm^2, 35keV) as received, CsEx and CsNo samples after 31 weeks stored at 100°C.

Even though, the wafer 471 CsEx samples stored at high humidity, ambient, and low humidity (Figure 5-5 through Figure 5-7, respectively) showed much less of an increase in apparent P surface concentration than the samples stored under the Heat condition, a significant increase in the apparent P surface concentration was still observed for each of these conditions and this increase can be seen to extend 10's of nm from the sample surface. CsNo samples stored under the high humidity, ambient, and low humidity (Figure 5-5 through Figure 5-7, respectively) also showed small but still significant changes in surface P concentration when these profiles are compared to the as received P profile. Comparison of the CsEx and CsNo samples strongly illustrates the impact of Cs exposure prior to SIMS analysis. In addition to the previously discussed sample conditions, samples cut from each wafer were stored under LN_2 for 32 weeks. Figure 5-8 compares the P depth profile obtained from a piece of the as received wafer 471 to one obtained from a piece of this wafer stored under LN_2 for the 32 weeks (see Appendix Figure A-3 and Figure A-8 for wafers 344 and 341, respectively). No evidence of change in P surface concentration was observed. Based

on this observation, storage under LN_2 conditions eliminates changes in surface P concentration, at least over the 32 week period of this experiment.

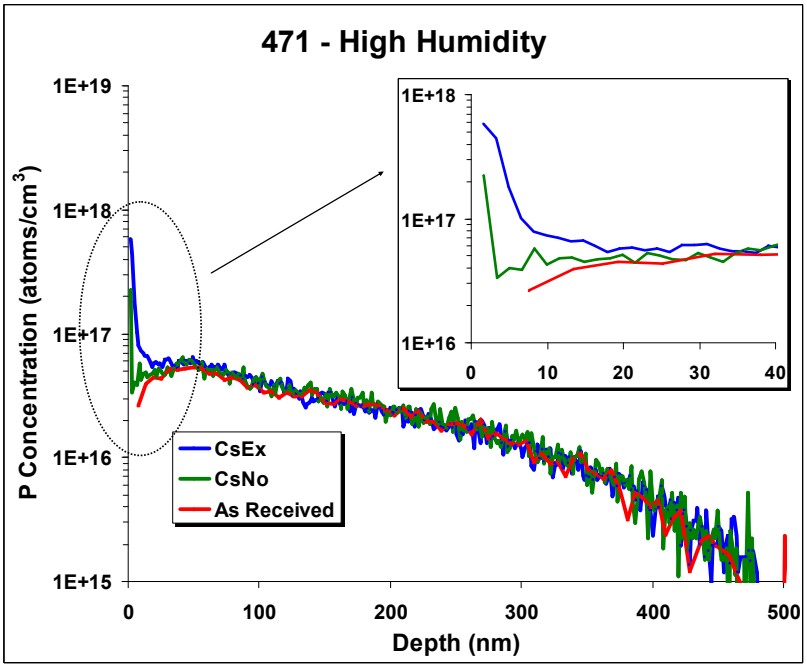

Figure 5-5. Depth profiles of sample 471 (P in Si of 1E12 atoms/cm^2, 35keV) as received, CsEx and CsNo samples after 31 weeks stored in a dessicator with water.

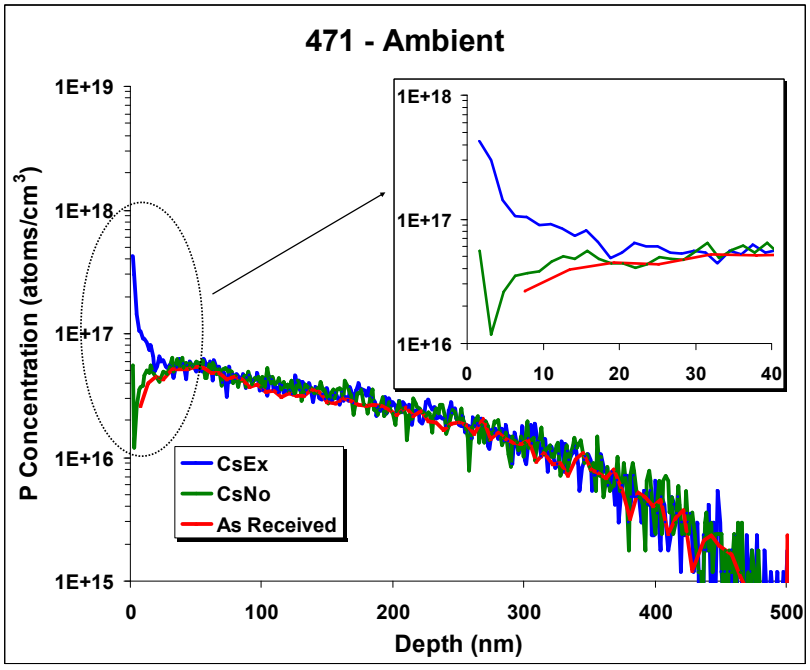

Figure 5-6. Depth profiles of sample 471 (P in Si of 1E12 atoms/cm^2, 35keV) as received, CsEx and CsNo samples after 31 weeks stored in an ambient laboratory environment.

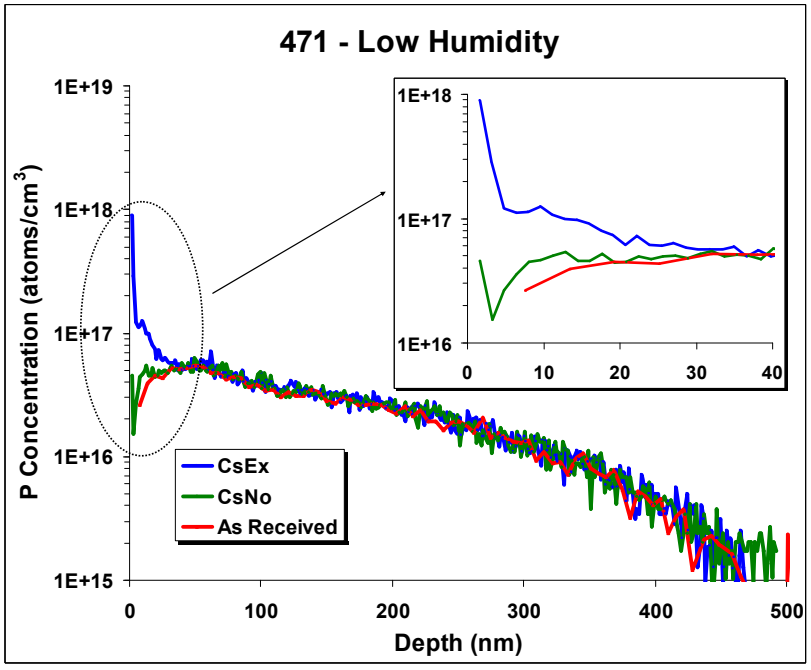

Figure 5-7. Depth profiles of sample 471 (P in Si of 1E12 atoms/cm^2, 35keV) as received, CsEx and CsNo samples after 31 weeks stored in a dry dessicator.

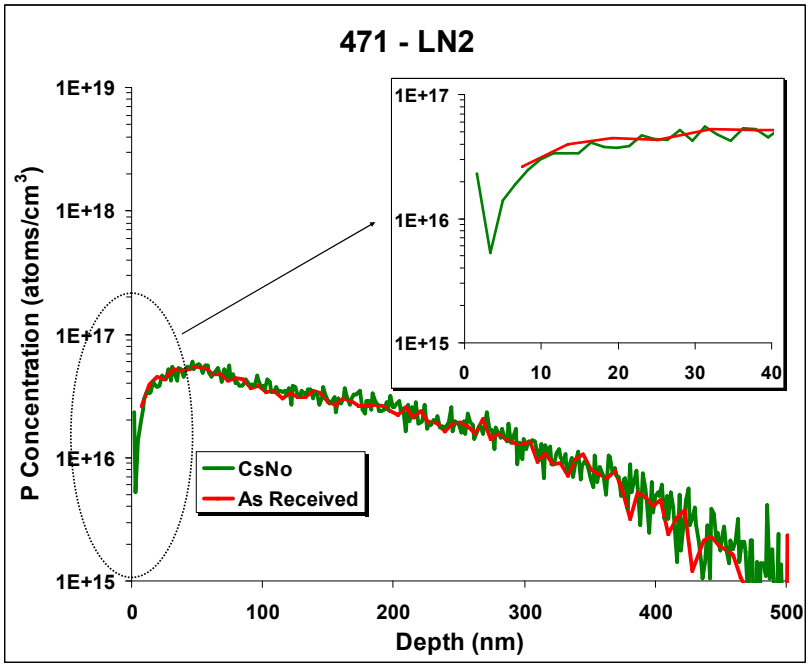

Figure 5-8. Depth profiles of sample 471 (P in Si of 1E12 atoms/cm^2, 35keV) as received and CsNo samples after 32 weeks stored under LN_2.

Total P dose, P dose from 0 to 36nm (selected based on the inflection point seen on the CsEx samples), and P dose from 36nm to the profile maximum were calculated for all P profiles. For various reasons including the noisy nature of the data (P count maxima were below 100 cts/s due to the low P dose of sample 471) and the use of multiple positions in various sample holders, there was significant scatter in the data. However, the following conclusions could still be drawn. For all of the CsEx samples profiled, the contribution to the total dose measurement from the apparent P dose in the first 36nm is sufficiently high to render these samples unusable as standards for high precision dose measurement or dose matching experiments. For the CsEx samples, the total calculated dose was sufficiently high that it is impossible to conclude, even in view of the low precision of the numerical data, that the increased surface dose resulted from redistribution of P from depths greater than 36nm. For the CsNo samples, the distortion of the P dose, while clearly discernable in Figure 5-4 through Figure 5-7, is sufficiently small and the noise in the acquired data was sufficiently large that no conclusion can be drawn as to the relative magnitude of the surface dose versus

the total dose calculation. However, it is clear that after only 31 weeks, measurable changes in the apparent P surface concentration have occurred. The only samples not showing any alteration of the surface after 31 weeks storage are those stored under LN_2.

5.3.2 Effects on Phosphorus Implants in Silicon Exposed to Different Processing Methods

While a significant amount of useful information was obtained by examining depth profile plots of data generated during the above study, the precision of the numerical information obtained was not sufficient to determine whether the increase in the apparent P surface concentration was due to redistribution of implanted P or the result of other factors. Information derived from a careful analysis of data and experimental conditions used in the previous study was used to design a follow up study with the goals of determining the source of the increase in the apparent P surface concentration and providing ways to mitigate this problem. Experimental requirements include sufficient precision for measurement of small changes in total dose and for measurement of dose redistribution.

In an effort to determine the cause of the apparent increase in P dose over time five wafers were provided by Intel with all wafer processing, e.g. implantation, annealing, done at Intel (see section 5.2). These wafers were implanted with 1E12 at/cm^2 P at 35keV. Two of these wafers were not subjected to any additional processing either prior to or after implantation. The remaining wafers used in this study were subjected to various processing methods in an effort to reduce the possibility of phosphorus redistribution toward the surface (see Table 5-2). Based on the previous results, three storage conditions have been selected: heat (200°C) to accelerate any redistribution, dry (in dessicator to minimize surface oxidation), and under LN_2 (see Table 5-3). The relative humidity for the heat condition was calculated based on the lab temperature and humidity.

Two sets of depth profile data acquisition parameters were used: 1) O and P were acquired at 1 second each with Si matrix signal acquired at the end of the depth profile; and 2) only P was acquired for 2 seconds per data point with Si measured at the end of the profile. These acquisition conditions were selected to provide the depth resolution sufficient

to examine the time dependent oxidation of the surface and to provide the highest possible P measurement precision. Both data acquisition methods were used in measuring wafers 672, 798, 839, and 840 in the as received condition. However, the O intensity was not measured on wafer 805 due to the shallow nature of the P implant into the preamorphized wafer. After an initial as received analysis, wafers 672 and 798 were not analyzed further due to their high and varied surface P concentration. The as received depth profile results from wafers 672 and 798, which had the same dose (1E12 at/cm^2) as wafer 471 (wafer from previous study), were clearly not similar to the results obtained previously from the as received wafer 471 (see Figure 5-9). It is clear from Figure 5-9 that the as implanted surface concentration of P in Si can vary even in wafers implanted under ostensibly identical conditions, i.e. 1E12 at/cm^2 P at 35keV. Therefore, wafers 672 and 798 can not generate valuable information for the increase in the apparent P surface concentration.

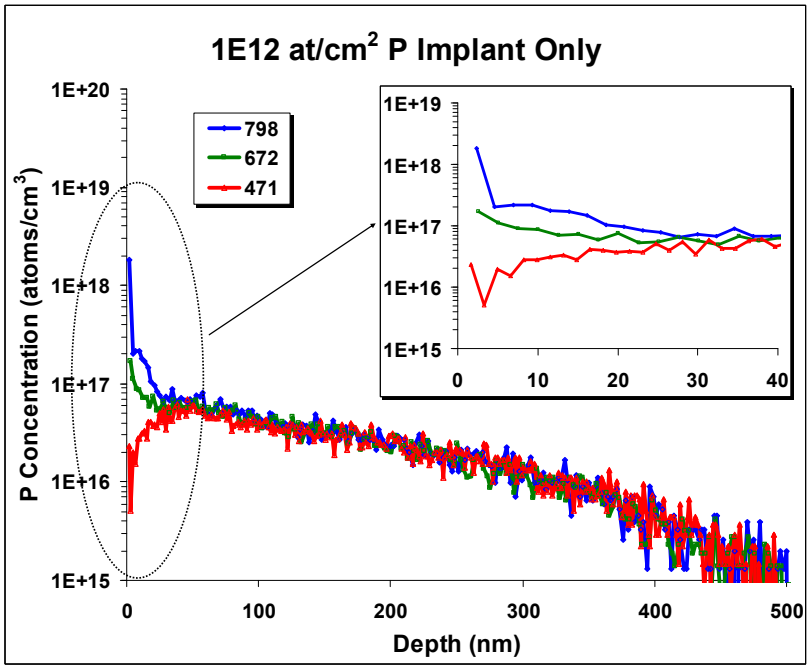

Figure 5-9. Depth profiles of samples 798, 672, 471 (P in Si of 1E12 atoms/cm^2, 35keV) as received.

As a result of those measurements, the subsequent sections present data for only wafers 839, 840, and 805 obtained by acquiring P only with Si measured at the end of the profile. Wafers 839 (1E12 at/cm^2, through a 50Å oxide layer), 840 (1E12 at/cm^2, RTA) and 805 (1E12 at/cm^2, pre-amorphization) were analyzed over a period of 24 weeks. At least 5 analyses have been performed on these three wafers over this period. For each of the analyses performed during the 24 week period, two pieces from the selected wafer storage conditions for wafers 839, 840, and 805 were analyzed. One piece is a previously unanalyzed and thus unexposed sample (referred to as CsNo). With the exception of the initial analysis session, the other analyzed piece is from a wafer that had been exposed to Cs (CsEx) in all prior SIMS analyses. Analyzed areas on previously exposed samples were selected to be as close as practical (approximately 300μm apart) to the previously analyzed areas. Data was obtained from both CsEx and CsNo samples taken from the wafers subjected to different processing methods in subsequent experiments. LN_2 stored wafers were analyzed only after being stored for 24 weeks to provide a clear measure of the change in P surface concentration, assuming that storage under LN_2 will eliminate time dependent changes as in the previous study (see Figure 5-8). Using the primary ion beam conditions listed in Table 5-4 (except for an increase in I_p from 40nA to 50nA to improve detection sensitivity), sputter rates ranging from 11 to 12 Å/sec were obtained. The average RSF obtained using the P bulk doped sample as the reference was 1.23E23, with $^{28}Si^-$ as matrix species.

SIMS depth profile results obtained from wafers 839, 840, and 805 stored under the various conditions (see Table 5-3) were compared with depth profiles obtained from the as received wafers. The discussion below compares the SIMS results from the as received samples with results obtained from the CsEx and CsNo samples after storage in the various conditions. In each of the figures below (except Figure 5-16), three P depth profiles are shown: as received ^{31}P (red); ^{31}P (blue) CsEx after storage in the various conditions; and ^{31}P (green) CsNo after storage in the various conditions.

Wafer 839, which had the P implanted in Si (1E12 at/cm^2) through a 50Å oxide layer, did not show any significant changes in P concentration beyond the surface oxide for the

CsNo (no Cs exposure) sample stored in the dry dessicator (see Figure 5-10). For the CsEx (previously exposed to Cs) sample stored in the dry dessicator, changes were observed near the surface (see Figure 5-10). However, the profiles shown in Figure 5-11 that were obtained from this wafer from both the CsNo and CsEx were clearly affected by storage in heat with the P surface concentration increasing approximately one order of magnitude. Note that the entire profile was quantified using the RSF generated from the bulk doped standard.

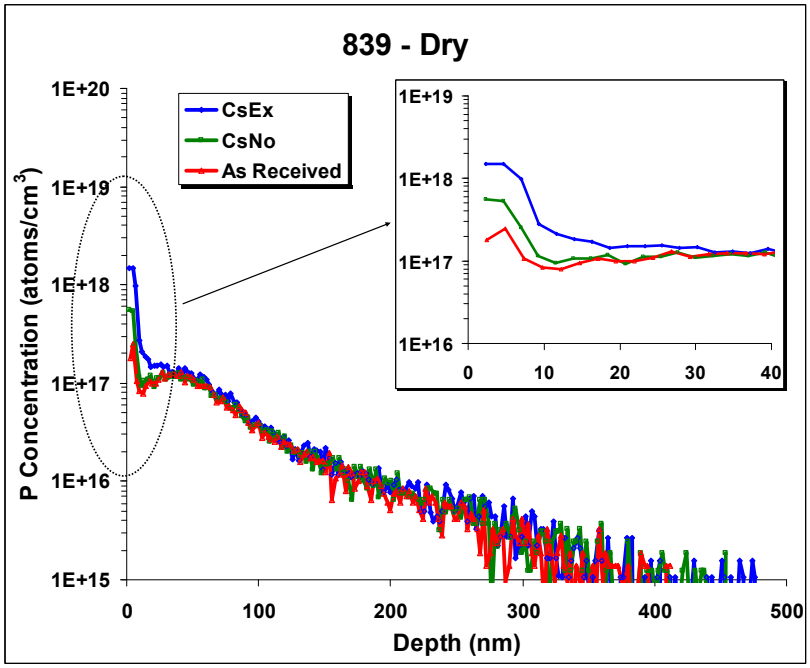

Figure 5-10. Depth profiles of sample 839 (P in Si of 1E12 atoms/cm^2, 35keV through a 50Å oxide) as received, CsEx, and CsNo samples stored in a dry dessicator.

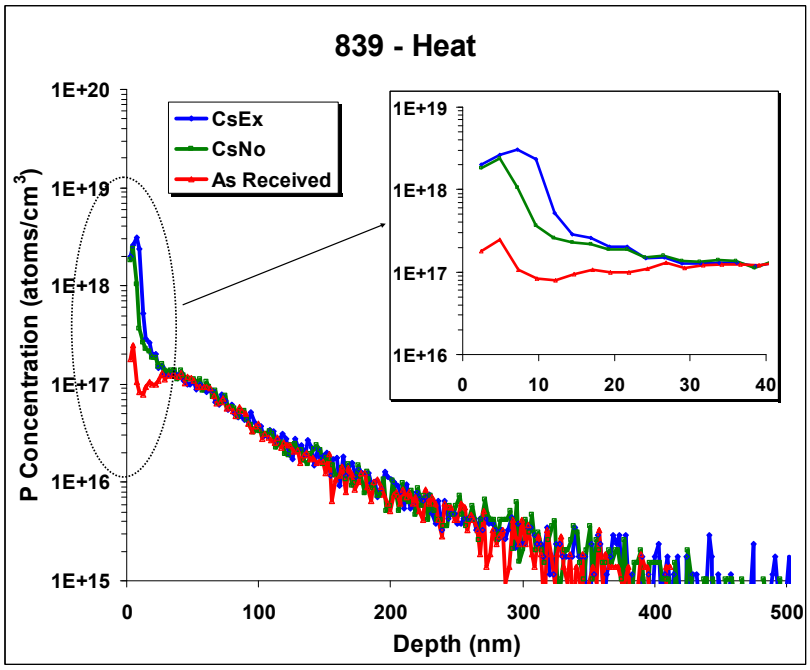

Figure 5-11. Depth profiles of sample 839 (P in Si of 1E12 atoms/cm^2, 35keV through a 50Å oxide) as received, CsEx, and CsNo samples stored at 200°C.

For wafer 840 (1E12 at/cm^2 after RTA; see Figure 5-12 and Figure 5-13), significant changes in apparent P surface concentrations were observed. For this wafer, both the low humidity and heat storage conditions showed increases in the apparent surface P concentration compared with the as received depth profiles, with the largest changes occurring under the Heat storage conditions.

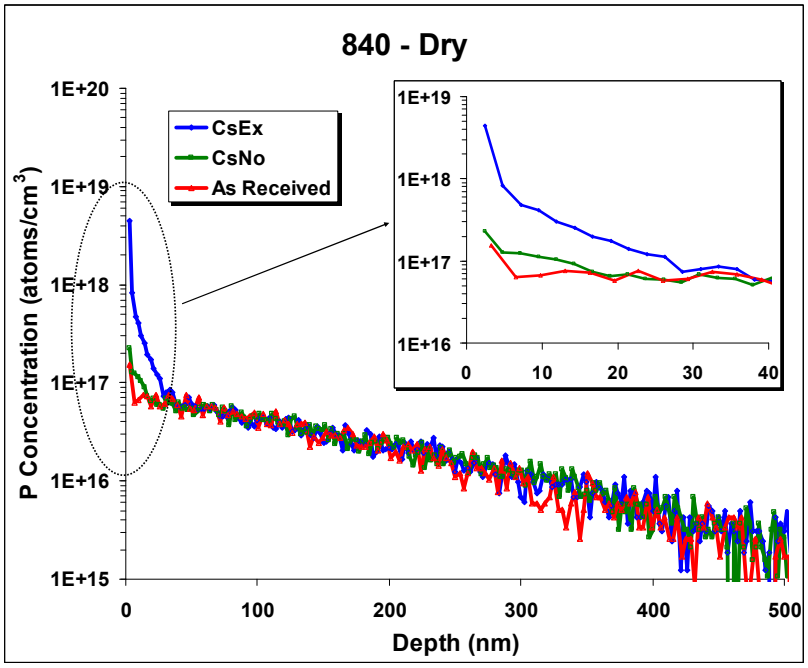

Figure 5-12. Depth profiles of sample 840 (P in Si of 1E12 atoms/cm^2, 35keV after RTA) as received, CsEx, and CsNo samples stored in a dry dessicator.

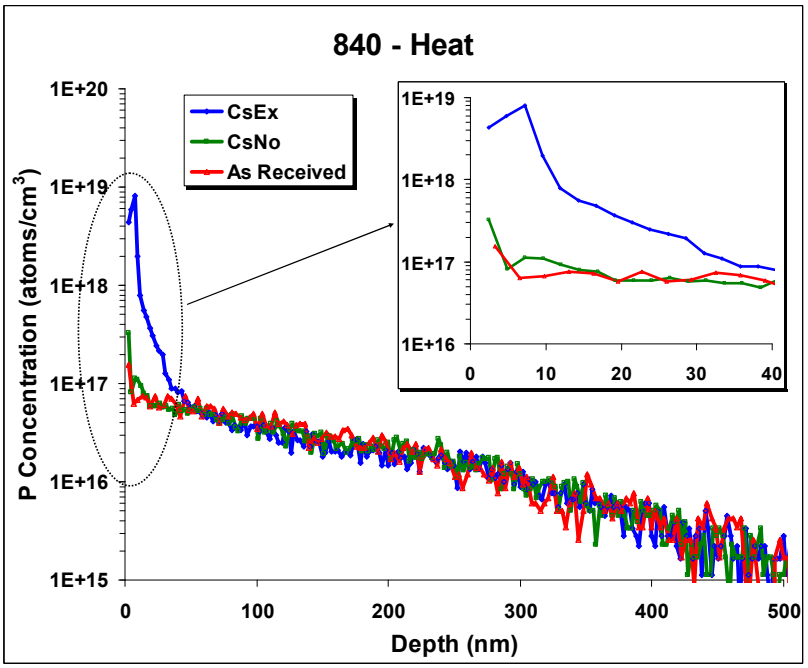

Figure 5-13. Depth profiles of sample 840 (P in Si of 1E12 atoms/cm^2, 35keV after RTA) as received, CsEx, and CsNo samples stored at 200°C.

No significant changes were observed for wafer 805, which had the P implanted in Si (1E12 at/cm^2) after pre-amorphization, when this wafer was stored in the dry dessicator (see Figure 5-14). However, while the wafer previously unexposed to Cs showed no significant change, wafer 805 previously exposed to Cs and stored in heat was significantly affected (see Figure 5-15).

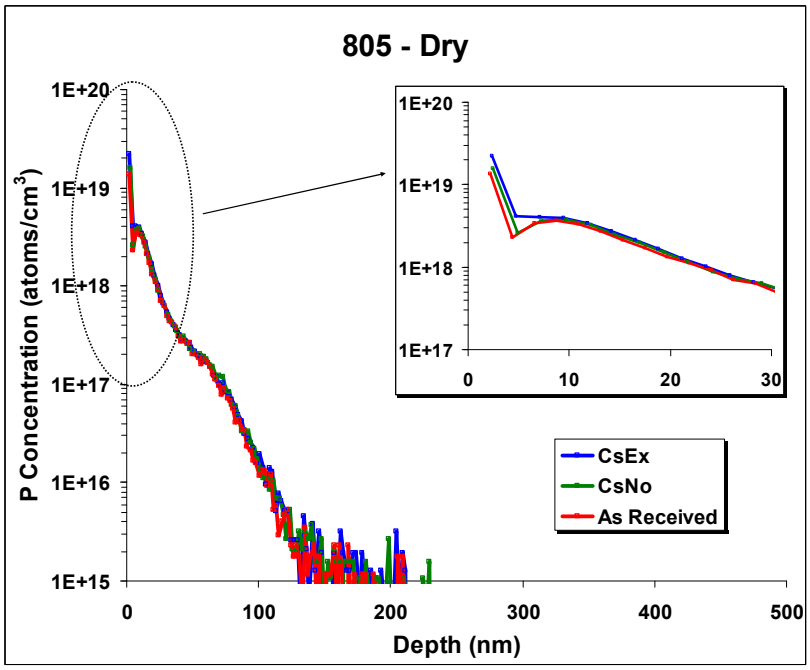

Figure 5-14. Depth profiles of sample 805 (P in Si of 1E12 atoms/cm^2, 35keV after pre-amorphization) as received, CsEx, and CsNo samples stored in a dry dessicator.

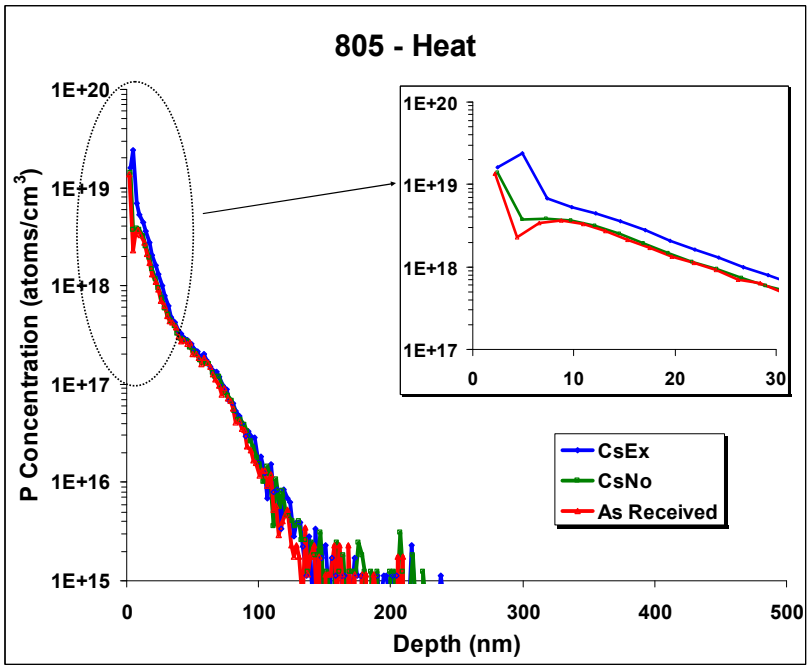

Figure 5-15. Depth profiles of sample 805 (P in Si of 1E12 atoms/cm^2, 35keV after pre-amorphization) as received, CsEx, and CsNo samples stored at 200°C.

Figure 5-16 illustrates the effect of pre-amorphization on the P implant compared with a P implant in Si without any additional processing. Both depth profiles were obtained were from the as received wafers. The profiles show differing implantation depths as would be expected with pre-amorphization limiting channeling and lateral straggle. Amorphization occurs when damage from the high dose implant (e.g. Si or Ge) changes the crystalline structure of a wafer to a more amorphous material. Therefore, channeling and straggle can be limited by disorder in the material and higher Si density.[1] So, it is not a surprise that the profile is shallower in depth after pre-amorphization. Also, as a secondary effect the Si atoms present in the implant layer can interact with the dopant and retard its diffusion during thermal steps such as high temperature annealing.[1]

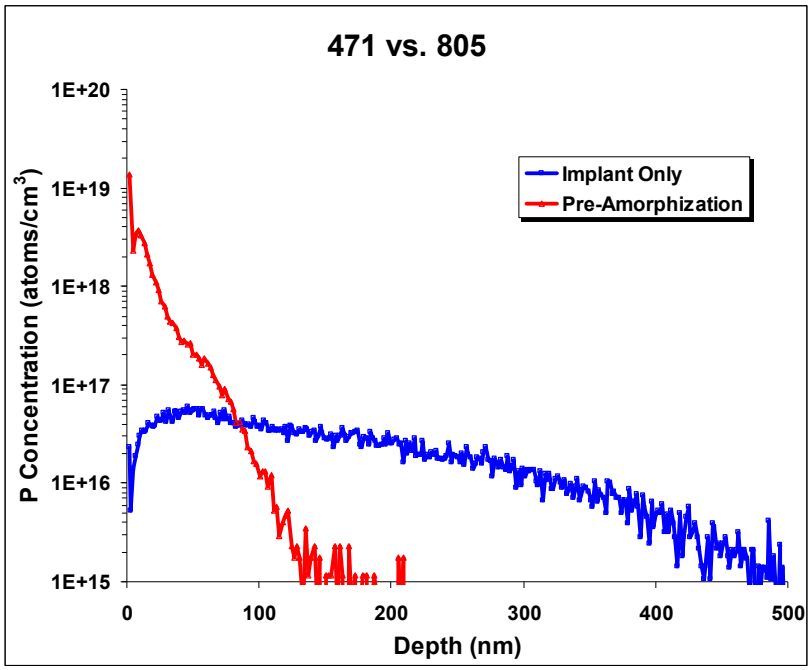

Figure 5-16. Depth profiles of sample 471 (P in Si of 1E12 atoms/cm^2, 35keV) and 805 (P in Si of 1E12 atoms/cm^2, 35keV after pre-amorphization) obtained from as received wafers.

For the second set of depth profile SIMS acquisition parameters, O and P were acquired at 1 second each with Si matrix signal acquired at the end of the depth profile. Examples of the results of these profiles are shown in Figure 5-17 and Figure 5-18. This SIMS depth profile acquisition condition was selected to provide information on time dependent oxidation of the surface while simultaneously providing high measurement precision for surface P. For the dry, heat, LN_2 wafers 839 and 840 measurements CsNo and CsEx, all measurements except 839 heat CsEx and 840 dry, heat CsEx showed insignificant increases in the surface oxidation. Figure 5-17 and Figure 5-18 illustrate the effects observed for wafers 839 (1E12 at/cm^2 through a 50Å oxide layer) and 840 (1E12 at/cm^2 after RTA) after storage in LN_2. No significant changes were observed when these wafers were stored in LN_2. However, while the sample previously unexposed to Cs showed no significant change, wafer 839 previously exposed to Cs and stored under LN_2 was significantly affected (see Figure 5-17). Figure 5-17 and Figure 5-18 show storage under LN_2 can be used as a storage condition to limit oxidation of the surface over time ($\leq$ 24 weeks). Therefore, Figure 5-17

provides evidence that oxidation of the surface is not a significant factor for the surface P concentration increases observed throughout this study.

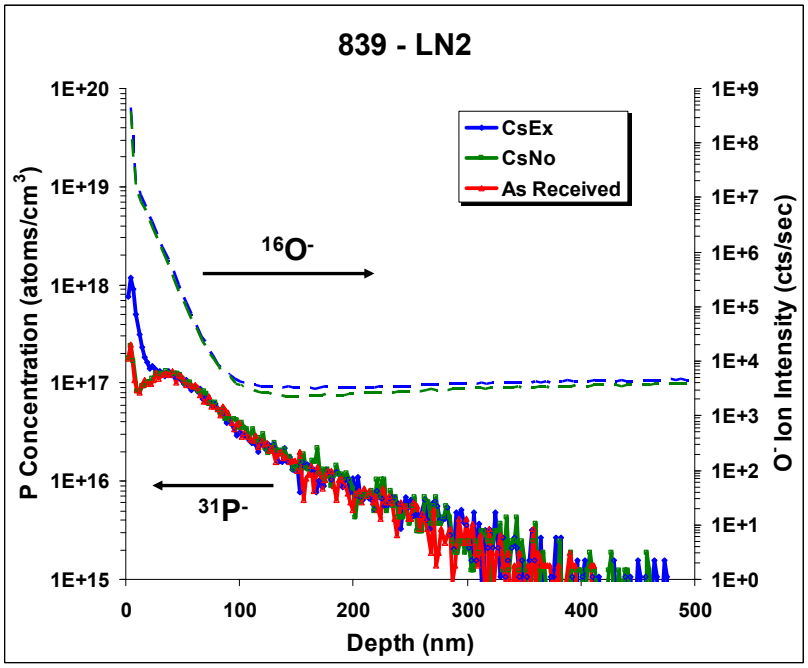

Figure 5-17. Depth profiles of sample 839 (P in Si of 1E12 atoms/cm^2, 35keV through a 50Å oxide) as received, CsEx, and CsNo samples stored in LN_2.

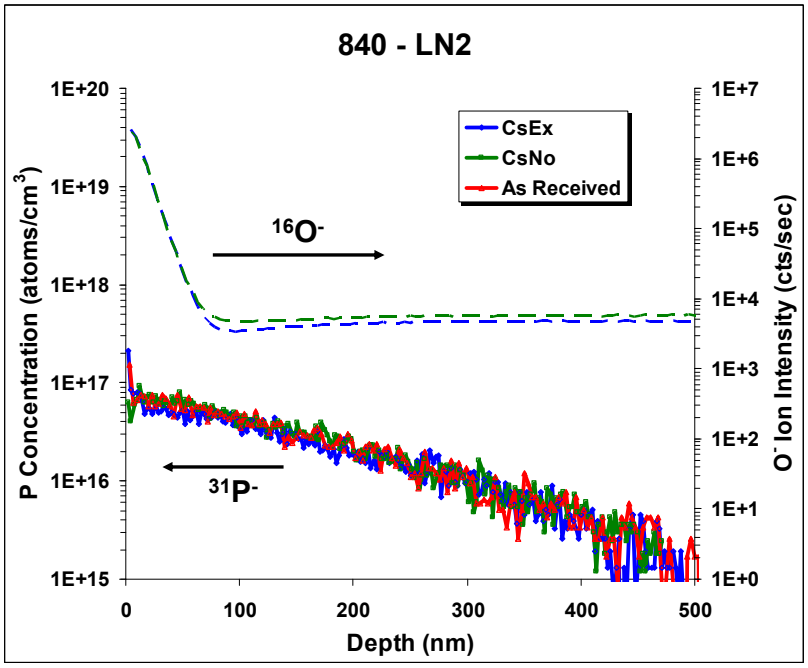

Figure 5-18. Depth profiles of sample 840 (P in Si of 1E12 atoms/cm^2, 35keV after RTA) as received, CsEx, and CsNo samples stored in LN_2.

Partly because P count maxima were below 100 cts/s as a result of the low P dose in this study, the data obtained is relatively noisy. Nevertheless, the following conclusions can still be drawn. In the previous study the total P dose, the P dose from 0 to 36nm (selected based on the inflection point seen on the CsEx samples), and P dose from 36nm to the profile maximum depth were calculated for all P profiles. However, for the wafers used in this study which have been subjected to different processing methods, an inflection point at a constant depth did not exist. Thus P doses were calculated as follows (see Table 5-5). The total P dose was calculated for all three wafers (839, 840, 805). In addition, for wafers 839 and 840, P dose was calculated for 0 to 40nm and 40nm to the total depth. For wafer 805 (after pre-amorphization), P dose was calculated for 0 to 10nm and 10nm to the total depth. Also, Table 5-5 provides the relative standard deviation (RSD) value for the as received P dose measurements. RSD is used to compare the uncertainty between different measurements by providing a value to the reproducibility of an analysis. RSD expressed as percentage (%) is

determined by dividing the standard deviation (σ) by the mean (χ) for the same set and then multiplying by 100%.

$$\%\text{RSD} = \frac{\sigma}{\chi} \times 100\% \qquad \textbf{Equation 5-1}$$

The RSD is calculated for wafers 839, 840, and 805 with the respect to each of the distinctive dose measurements previously discussed. The RSD determined the greatest variance in these dose measurements are within the near surface region, ≤ 40nm (wafers 839 and 840) and ≤ 10nm (wafer 805), of the analysis.

For the as received P dose measurements on wafers 839 and 840, there was less scatter in the ≥ 40nm data compared with the ≤ 40nm data. A similar result was found for the pre-amorphized wafer 805, which has a shallower and more rapidly changing P profile, in the P dose calculated for ≤ 10nm and ≥ 10nm. Therefore, it is recommended that a depth be selected (e.g. 40nm) and the dose at greater depths be integrated to increase the accuracy of P dose measurements. Eliminating a specific amount of the surface depth from dose calculations will avoid any risk of the aging effect or potentially deleterious effects of Cs exposure.

For wafers 839 and 840 stored under the dry, heat, and LN_2 conditions both unexposed (CsNo) and exposed (CsEx) to Cs, all measurements showed significant increases in both the total P dose and in the ≤ 40nm dose compared with the as received dose except for 839 dry CsNo, 839 LN_2 CsNo, 840 dry and LN_2 CsNo, CsEx. However, the ≥ 40nm showed dose changes less than 10% for dry, not exposed and exposed to Cs. When the samples are stored in heat at an elevated temperature of 200ºC, some of the dose appears to move toward the surface. In general, differences in the ≥ 40nm region between 839 and 840 were small, except for the heated CsEx of wafer 840.

For the pre-amorphized wafer 805, it is interesting to note that the as received total dose is significantly higher than the intended 1.0E12 implanted dose. In addition, the results for this wafer were consistent in that there were dose fluctuations of less than 10% for the ≥ 10nm as received data versus the ≥ 10nm data for all conditions with the exception of the heat CsEx.

Table 5-5. Calculated doses of wafers 839, 840, and 805.

Wafer	Condition	Doses: Total	≤ 40nm	≥ 40nm
839 1E12 at/cm^2 50Å Oxide	***As Received***	1.3E+12	5.8E+11	6.9E+11
	% RSD	9.7	20.0	3.3
	Dry, CsEx	2.0E+12	1.3E+12	7.5E+11
	Dry, CsNo	1.3E+12	6.2E+11	7.0E+11
	Heat, CsEx	3.7E+12	3.0E+12	6.9E+11
	Heat, CsNo	2.3E+12	1.6E+12	6.8E+11
	LN_2, CsEx	2.0E+12	1.1E+12	9.4E+11
	LN_2, CsNo	1.3E+12	5.7E+11	7.0E+11

Wafer	Condition	Doses: Total	≤ 40nm	≥ 40nm
840 1E12 at/cm2 RTA	***As Received***	1.2E+12	3.4E+11	8.8E+11
	% RSD	13.2	35.5	6.0
	Dry, CsEx	2.0E+12	1.1E+12	8.6E+11
	Dry, CsNo	1.2E+12	3.2E+11	8.6E+11
	Heat, CsEx	5.6E+12	4.9E+12	6.9E+11
	Heat, CsNo	1.2E+12	3.6E+11	8.1E+11
	LN_2, CsEx	1.1E+12	2.4E+11	9.0E+11
	LN_2, CsNo	9.7E+11	2.5E+11	7.2E+11

Wafer	Condition	Doses: Total	≤ 10nm	≥ 10nm
805 1E12 at/cm^2 Pre-amorph.	***As Received***	7.7E+12	3.2E+12	4.4E+12
	% RSD	4.1	18.4	10.4
	Dry, CsEx	9.9E+12	5.0E+12	4.9E+12
	Dry, CsNo	8.1E+12	3.5E+12	4.6E+12
	Heat, CsEx	1.6E+13	9.8E+12	6.5E+12
	Heat, CsNo	9.0E+12	4.1E+12	4.9E+12

5.4 Summary

The overriding conclusion from the study on the aging of low dose phosphorus implants is changes in the apparent P surface concentration are consistently observed in SIMS depth profiles over time and this change strongly affects the accuracy of P dose measurements. This study consisted of two complementary experiments: the effect of time on the surface concentration of P for different phosphorus implant doses in silicon and the effects on phosphorus implants in silicon exposed to different processing methods.

The result of the study on the effect of time on the surface concentration of P for different phosphorus implant doses in silicon showed that samples previously exposed to Cs (CsEx) should not be used as standards for P dose measurement or other P quantification experiments. While increases in apparent P surface concentration was observed in all instances where samples previously exposed to Cs were analyzed (no Cs exposure measurement was made for the LN_2 storage conditions), the largest surface P increases were seen in the lowest P dose sample (see Figure 5-4 through Figure 5-7), i.e. sample 471 (1E12 at/cm^2 P). For the CsEx samples, it is concluded that the large increases in apparent P surface concentration results from the effects related to the presence of implanted Cs near the sample surface. This Cs contamination can originate from a number of sources including Cs beam tails, Cs neutral beam, secondary sputtering from instrument optics and other structures, etc (see Chapter 6). The presence of Cs may not only alter the P secondary ion yield, but may also influence the oxidation of the sample surface additionally affecting P ion yield and sputter rate. In addition, the presence of Cs may enhance diffusion of P to the sample surface due to creation of vacancies or by altering the surface chemical potential in a manner that attracts mobile P.

Samples of wafer 344 (1E14 at/cm^2 P) and wafer 341 (1E13 at/cm^2 P) that were not exposed to Cs (CsNo) prior to analysis showed no measurable change in P surface concentration. Perhaps the lack of change is due to the masking of any fluctuation by their already high P surface concentrations (see Figure A-1 through Figure A-8). For wafer 471 (1E12 at/cm^2 P), changes in P surface concentration were observed for all but the sample stored under LN_2 (no Cs exposure carried out for the LN_2 storage conditions, see Figure 5-8).

Table 5-6 summarizes the results. Changes in the measured P surface concentrations of the wafer 471 samples stored under the various conditions may result from secondary ion yield enhancement due to surface oxidation and/or from P diffusion enhancement resulting from this oxidation.

Table 5-6. Results from the earlier phosphorus implant aging study (wafers 344, 341, and 471). Yes and No refer to the presence or absence of observed changes in P surface concentration.

CONDITIONS		1E14 at/cm^2	1E13 at/cm^2	1E12 at/cm^2
CsEx	Heat	Yes	Yes	Yes
	All*	No	Yes	Yes
CsNo	Heat	No	No	Yes
	All*	No	No	Yes
LN_2**		No	No	No

*Includes High Humidity, Ambient, Low Humidity
**No Cs exposure done for this storage condition

In the follow up study, both the CsEx and CsNo P depth profiles obtained from wafers 839 (50Å oxide) and 840 (RTA) stored at 200ºC (Figure 5-11, Figure 5-13) showed significant changes in the apparent P surface concentration. The CsEx P depth profiles in Figure 5-11 (wafer 839) and Figure 5-13 (wafer 840) clearly demonstrate that prolonged sample storage at 200ºC along with previous Cs exposure results in a large change in apparent P surface concentration which extends some tens of nm into the sample. Careful comparison of the CsNo sample P profile (Figure 5-11, Figure 5-13) stored under the same conditions with the as received P profile shows a smaller but still significant change in surface apparent P concentration. These results indicate that while storage of the wafer at 200ºC does result in some change in apparent P surface concentration, exposure to Cs in addition to storage at an elevated temperature results in a much greater change. The wafer 839 (50Å oxide) CsEx samples stored at low humidity Figure 5-10) did not show any

apparent P surface concentration increase below the 50Å oxide layer. However, wafer 840 (RTA) CsEx samples stored at low humidity (Figure 5-12) showed an increase in apparent P surface concentration similar to the samples stored under the Heat condition. A significant increase in the apparent wafer 840 (RTA) P surface concentration was observed for both of these conditions and this increase can be seen to extend 10's of nm from the sample surface. Wafers 839 (50Å oxide) and 840 (RTA) CsNo samples stored under low humidity (Figure 5-10, Figure 5-12) did not show any significant changes in surface P concentration when these profiles are compared to the as received P profile. Comparison of the CsEx and CsNo samples illustrates the deleterious effect of Cs exposure prior to SIMS analysis.

These results are significant with regard to practical P analysis as changes in apparent P surface concentration after ion implantation have been observed over time and these changes can strongly affect the accuracy of P dose measurements. The impact of the inaccuracy of the P measurement increases as the dose decreases. Thus, the use of low dose P implants without any pre or post processing as standards for P dose measurements or other P quantification experiments is problematic. If samples previously exposed to Cs are used as standards, P measurement accuracy is more severely impacted, again with the impact increasing as the P dose decreases. For wafers without any pre or post processing, results show that changes in the apparent P surface concentration and thus changes in measured P dose can be avoided (at least for samples stored for a period of up to 32 weeks) by using a fresh, not previously analyzed piece of a wafer that has been stored under LN_2 for each dose measurement experiment.

With regard to using processing methods to minimize apparent changes in P surface concentration, the use of pre-amorphization is problematic since the depth of the implant is drastically reduced causing potential problems with obtaining sufficient data points for generation of a useful RSF. However, preliminary results indicate that either pre-cleaning followed by RTA (wafer 840) or implantation through a 50Å oxide (wafer 839) can provide wafers that can be used for low dose P implant standards. If a new piece of standard can be used for each analysis, the RTA method appears to produce a useful standard. If the samples to be used as standards are previously exposed to Cs, then the dose integrated at depths

greater than 40nm must be used to avoid surface effects. For the sample with the 50Å oxide, prior exposure to Cs appears to have no effect over the period studied although the safest approach would be to avoid use of samples previously exposed to Cs. If Cs exposure cannot be avoided, it is recommended that a depth be selected e.g. 40nm and that only the dose at greater depths be integrated to avoid any risk of the potentially deleterious effects of Cs.

5.5 References

[1] Emanuele Rimini, *Ion Implantation: Basics to Device Fabrication*, Kluwer Academic Publishers, Boston (1995).

6 Quantification and the Effects of Cesium Surface Contamination in Si under Cs^+ Bombardment

6.1 Introduction

The impetus for the cesium exposure study is to resolve whether unintended cesium contamination occurring during SIMS analyses contributes to the observed changes in the real or apparent P concentrations (discussed in Chapter 5). This work is intended to determine whether dynamic SIMS depth profiling produces sufficient surface Cs concentration outside the intended analysis region to alter results from subsequent SIMS analyses. Measuring the unintended Cs surface concentration resulting from previous analyses should provide information on the amount of surface contamination that occurs during SIMS analyses through Cs^+ ion bombardment and whether the contamination is sufficient to generate significant surface ion yield variations. An analytical protocol was devised to perform this additional study.

6.2 Experimental Method

The Cs exposure study sample set consists of four sample types: 1) a previously analyzed piece of a Si [100] wafer implanted with 1E14 at/cm^2 P at 35keV that had been bombarded with Cs (analyzed 9 weeks earlier and stored in an ambient environment); 2) a piece of Si [100] wafer implanted with 1E14 at/cm^2 Cs at 400keV; 3) a Si [100] sample not exposed to Cs and 4) a Si [100] sample which was exposed to Cs.

Analyses were performed using a focused 20nA, low energy (i.e. 1.25keV impact energy) O_2^+ primary ion beam extracted from the duoplasmatron of the CAMECA IMS-6F and rastered over a 180 x 180μm^2 area. Table 6-1 lists the analysis conditions. Angles of incidence were calculated using a computer program written by Schumacher which includes the IMS-6F accelerating voltage conditions and primary ion column deflector voltage used for positioning the beam onto the primary column's optical axis of the IMS-6F mass spectrometer.[1]

Table 6-1. Analysis conditions used for the Cesium neutral beam study.

Primary Beam: **O_2^+**	Ep: **3kV**	Es: **1.75kV**
E_{Impact}: **1.25keV** Angle of Incidence: **48.5°**	Ip: **20nA**	Raster Size: **180µm**
	CD: **150µm**	FA: **750µm**
	MR: **1000**	Beam Density: **0.62µA/µm^2**

The secondary ions were acquired through a 60µm diameter optically gated area (750µm field aperture, FA2), 150µm image field, 150µm contrast aperture (CD2) centered on the rastered area. A mass resolution of 1000m/Δm used for the analyses obtained by adjusting the entrance and exit slits. Depths of sputtered craters were measured using a Tencor P-20 stylus profilometer.

The monitored species were ^{16}O, ^{28}Si, and ^{133}Cs. Depth profiles were acquired until the Si matrix secondary ions counts reached a steady state and the implanted Cs ion counts dropped to the background level. The Cs RSF used to quantify the Cs surface contamination was determined from a high energy Cs implant into a Si [100] wafer (Figure 6-1) normalized to Si^+.

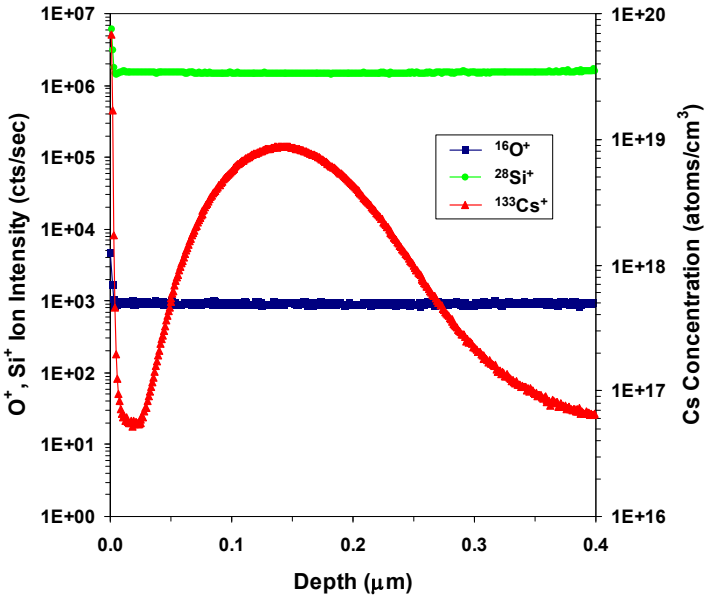

Figure 6-1. Depth profile of native Si implanted with 1x10^{14} atoms/cm^2 Cs at 400keV used as a standard to quantify the Cs concentration.

6.3 Results and Discussion

6.3.1 Mechanisms for Cs Contamination on the Sample Surface

Inadvertent Cs exposure can result from many sources including the tails of the Gaussian Cs primary ion beam, the Cs neutral beam, Cs resputtering from instrument optics, or redeposition of material sputtered during depth profiling. The Cs contamination from the sources listed above may result in changes to the Si surface that result in the movement of P to the sample surface and/or may alter the secondary ion yield of P beyond that normally anticipated from Cs implantation during depth profiling.

The Cs beam used for Cs SIMS depth profiling has radial Gaussian intensity distributions. When depth profiling, the sample is rastered to produce a SIMS crater, the Gaussian characteristic produces a crater with sloping sides. It is important to note that the walls of the crater do not ascend abruptly to the original surface, but flatten out gradually as a result of the Gaussian nature of the ion beam intensity distribution.[2] Since the ion beam has a Gaussian tail, a significant number of ions bombard and thus contaminate the sample outside the desired analyzed crater region. The exponential decrease in the tail leads to a contribution which is expected to diminish quickly with an increase in distance from the crater. Therefore, it is doubtful that the tail would induce any detectable damage at a distance beyond 2mm.[3] However, neutrals produced by the primary column may bombard the sample over a much larger area than the crater.[4] The Cs neutral beam results from charge exchange of primary ions in collisions with residual gas and/or with column optical components.[5] During SIMS analyses using Cs, sample material is sputtered and some of the sputtered atoms are deposited on adjacent lens surfaces. Consequently, sputtered ions are accelerated toward the lens where they can resputter previously deposited material from the lens back onto the analysis region.[6,7] This is known as the memory effect. In a CAMECA IMS-6F, the immersion lens cover plate is the main component involved in causing the memory effect (see Figure 6-2). Another source of Cs contamination of the sample surface may be from redeposition of material sputtered during depth profiling of adjacent areas. Analyses of Cs containing samples (e.g. Cs implant in Si and/or a previously analyzed sample with Cs) may

lead to redeposition of Cs on adjacent samples which could affect further analysis of those samples by SIMS.

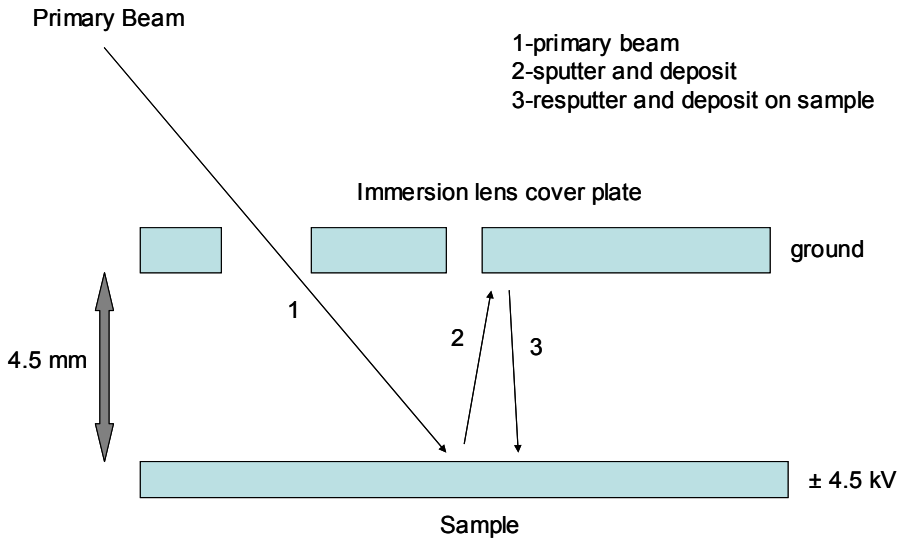

Figure 6-2. Illustration of the memory effect.

6.3.2 Visual Observation

During the analyses in this study and in previous SIMS analyses, it has often been observed that areas of a sample that are not covered by the sample holder mask become discolored at significant distances from the area analyzed. In the analyses described above (see Table 5-3), the Cs discoloration was distributed radially about the sputtered area in the shape of a concentric halo. Previous research has observed a circular and concentric halo with a diameter of 2 to 2.5mm surrounding a square shaped sputtered crater.[3,7,8] The halo appears bright whereas the surrounding sample surface appears dull. Clark states that initially it was thought that the halo was formed by the sputtering of the native surface oxide during the dynamic SIMS process.[3] However, the halo does not diminish over time, leading to the supposition that it is due to surface modification rather than simple removal of the native oxide.[3] Whether this change in contrast, which was seen in all samples regardless of storage conditions, is due to Cs beam tail or Cs neutral beam or whether it is due to increased oxidation or other factors is not known. In any case, the existence of this discoloration

indicates that changes have occurred to the sample surface and that the analyst must be wary of using previously damaged areas for quantitative analysis. The nature and cause of this discoloration was investigated.

6.3.3 Quantitative Analysis of Cs Contaminated Si

The Cs depth profiles in Figure 6-3 were obtained from a sample of a Si [100] wafer implanted with $1x10^{14}$ atoms/cm^2 P at 35keV. Part of this sample had been exposed during a previous P depth profile analysis using the Cs primary ion beam (see Table 5-3). Cesium exposed areas were easily differentiated from unexposed areas by a distinct change in contrast (see section 6.3.2) on the sample surface. The depth profile from the sample area previously exposed to Cs was acquired at approximately 300microns away from the previously analyzed area (see Figure 6-4). As can be seen from the depth profile in Figure 6-3, there is significant surface Cs contamination extending over 20nm into the sample. This level of unintended Cs contamination is clearly sufficient to alter P secondary ion yield and the presence of Cs may also contribute to P redistribution into this region. Contamination of unanalyzed areas adjacent to analyzed areas not covered by the sample holder mask results from a combination of Cs neutral beam (resulting from scattering and neutralization of Cs^+ in the primary column), Cs ion beam tails (beams have a Gaussian distribution even if well focused) and secondary sputtering of Cs from instrument optics. The surface Cs contamination shown in the depth profile for the unexposed area (see Figure 6-3), covered by the sample holder mask during the previous analysis with Cs^+ (see Figure 6-4), may be due to neutrals in the primary column. The level of surface contamination observed in the analyses of the unexposed area is not significant since the Cs concentration of less than 1 atomic percent is too low to alter P secondary ion yield.

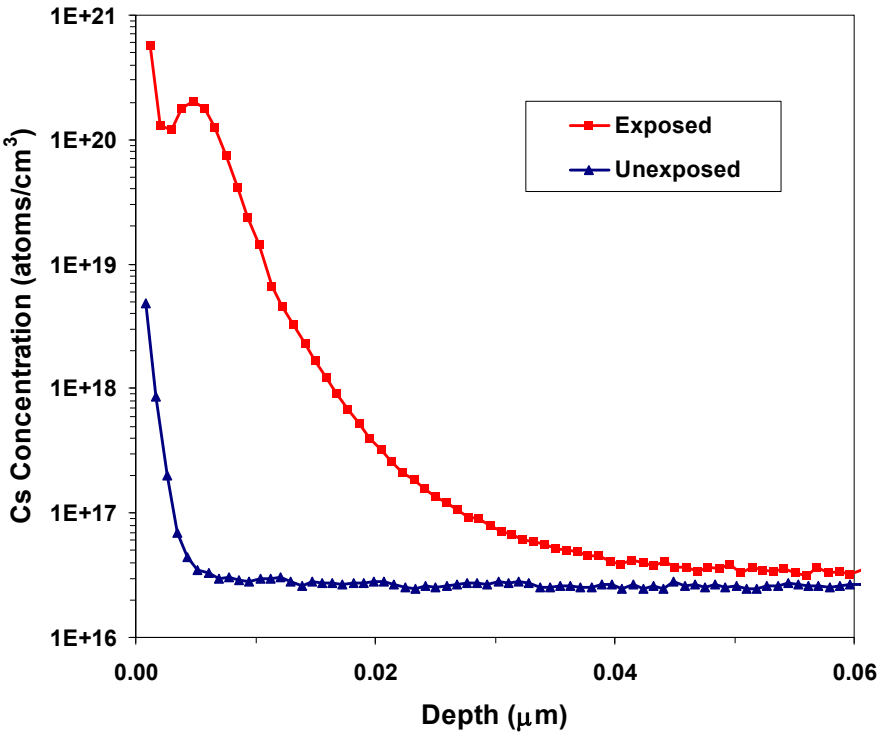

Figure 6-3. Cs depth profiles obtained from a Si wafer implanted with $1x10^{14}$ atoms/cm^2 P at 35keV across two different areas: exposed and unexposed to Cesium in relation to the sample holder drawings.

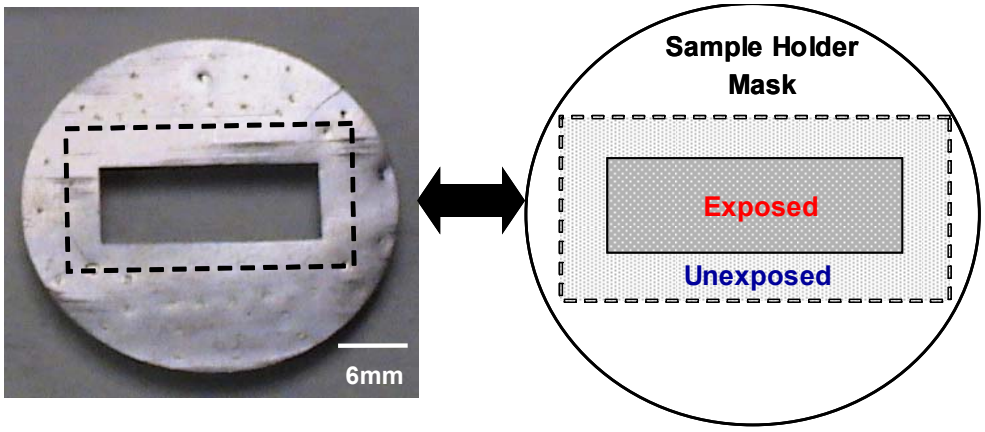

Figure 6-4. Sample holder image (left) and the Si [100] sample areas in reference to the discussion above (right).

6.3.4 Quantification of Cs Contamination via Secondary Sputtering and Redeposition

An additional experiment was used to further investigate the sources of Cs contamination including the issues of Cs resputtering and redeposition on unanalyzed areas. Two previously unanalyzed bare Si [100] wafers were used. The first Si sample was positioned in a sample holder along with a P implanted Si wafer that had been previously analyzed with Cs (see Table 5-3) and a Cs implant standard (see Figure 6-5).

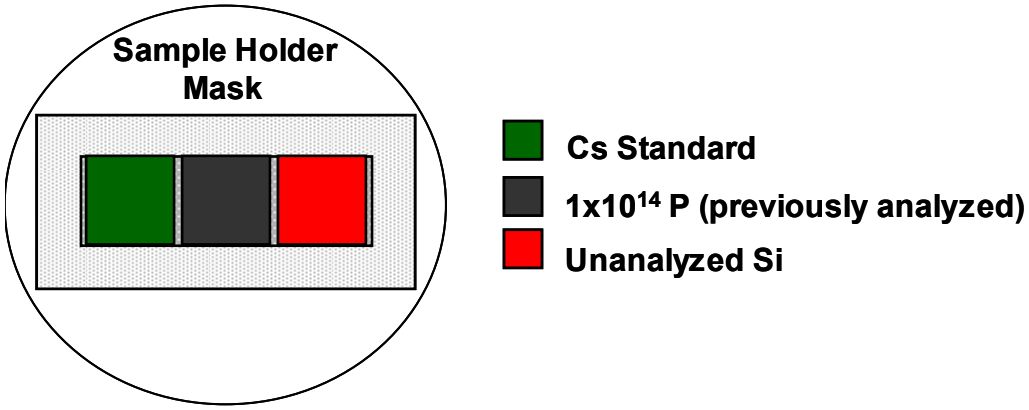

Figure 6-5. Physical layout of the SIMS sample holder used to examine for secondary sputtering and redeposition on previously unanalyzed areas.

The experiment was performed as follows. First, depth profiles of the Cs standard and the P implanted sample were acquired with O_2^+ (conditions in Table 6-1). Following these depth profiles, a Cs depth profile of the unanalyzed Si sample (mounted in same sample holder as the above two Cs containing samples) was acquired, again using O_2^+. Finally, a control sample of unanalyzed and thus unexposed Si mounted in a second sample holder was loaded into the sample chamber and immediately analyzed for Cs using the same O_2^+ depth profiling conditions as used above. The depth profiles of these two samples are shown in Figure 6-6. While lower than the Cs surface contamination of the exposed sample, there is significant Cs contamination on the unexposed sample. This indicates that there is a secondary source of Cs contamination, e.g. secondary sputtering of Cs from primary column or secondary ion extraction electrodes, not associated with Cs primary ion beam tails and/or Cs neutral beam. Furthermore, the level of Cs contamination observed in the unexposed

sample indicates that Cs contamination occurs not only when the Cs beam is used, but during O_2^+ analysis as well presumably as a result of sputtering of the primary optics by the O_2^+ beam, secondary sputtering (sputtering of sample chamber components by high energy secondary ions emitted from the sample) of secondary optics in the sample chamber, sputtering of sample chamber components by backscattered primary ions and/or redeposition from the analysis of Cs containing samples. Therefore, these profiles (see Figure 6-3 and Figure 6-6) support the contention that a combination of Cs neutral beam, tails of the Gaussian Cs primary ion beam, secondary sputtering of Cs from instrument optics, and redeposition of material sputtered during depth profiling contributes to Cs contamination of sample areas not being directly analyzed during depth profiling using the Cs primary ion beam.

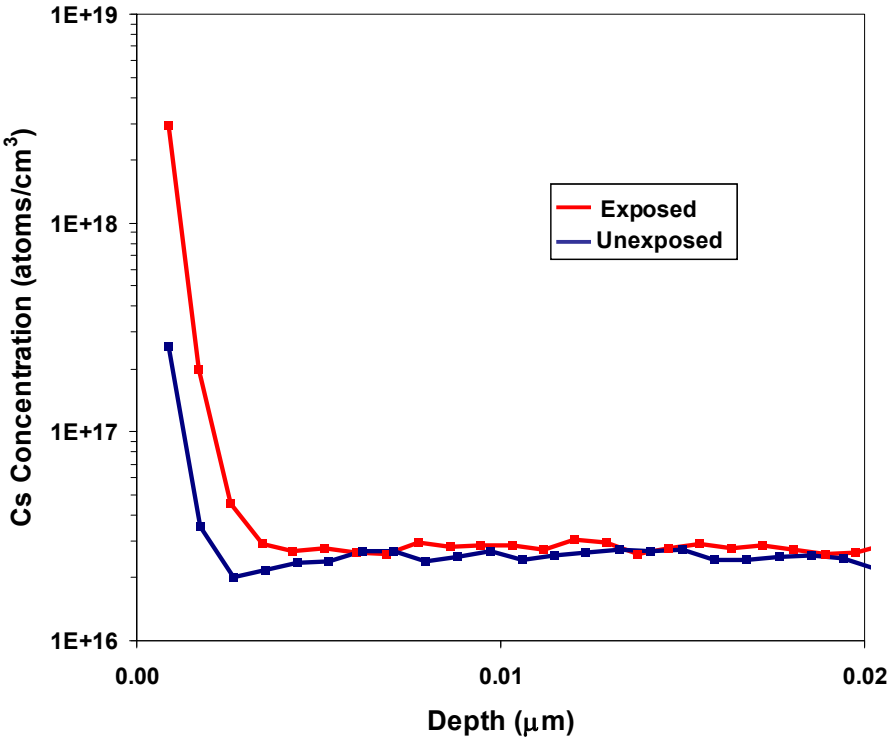

Figure 6-6. Depth profiles of fresh Si [100] samples; exposed and unexposed to secondary sources of cesium.

6.3.5 Quantification of the Cs Surface Concentration Induced by Adjacent SIMS Analysis

The purpose of this study is to obtain fundamental information about the distribution of Cs surface contamination after P depth profiling with Cs and its effect on subsequent analyses. The goal is to measure Cs surface concentration at various distances away from a previously analyzed area and to determine if there is an optimal separation between analyses.

A Si (100) wafer was pre-sputtered with Cs for 500 seconds at an impact energy of 14.5keV at 24.5° with respect to sample normal. SIMS analytical conditions were chosen to be consistent with previous Cs^+ analyses made during the P implant study (see Table 5-3). The specific time of 500 seconds was chosen to be consistent with the average analysis time required to obtain a depth profile of a P implant in Si for the P implant aging study (see Chapter 5). Following the pre-sputtering, nine SIMS depth profiles were performed on the same silicon sample at decreasing distances from the original crater, with the ninth depth profile taken at the position of the pre-sputtered crater (Figure 6-7). Depth profiles of Cs^+ and Si^+ secondary ions were obtained using a low energy O_2^+ primary ion. The impact energy of the oxygen primary ion was 1.25keV at an incidence angle of 48.5° in order to achieve high depth resolution and reduce the pre-equilibrium depth of the analysis beam.

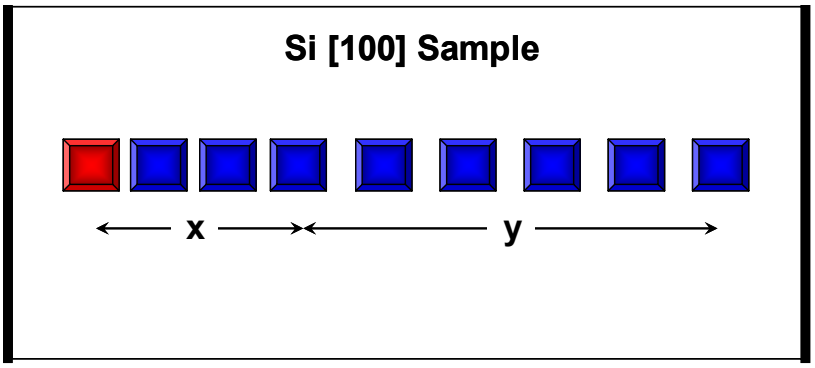

Figure 6-7. Physical layout of the post pre-sputtering SIMS craters (blue) on the silicon sample in terms of distance from the center of the original SIMS crater (red): craters in the x (1,500μm) and y (10,000μm) regions are equally separated from each other.

The analyses were started at the furthest distance away (≈ 11,500μm) from the pre-sputtered crater to decrease the amount of any redistribution of Cs sputtered from the sample. The surface Cs concentrations and Cs total doses were calculated using an RSF determined from a high energy Cs implant into a Si [100] wafer (see Figure 6-1) normalized to Si^+. Figure 6-8 shows the results of the Cs depth profiles from the adjacent areas in relation to the sputtered crater that was bombarded with Cs primary ions. These Cs depth profiles exhibited surface peaks within the first few nanometers and long Cs tails. In agreement with Yoshikawa and Tsukamoto, there is a shoulder region present in the Cs profiles.[9] This shoulder region may be produced by the implantation of Cs occurring during Cs pre-sputtering.

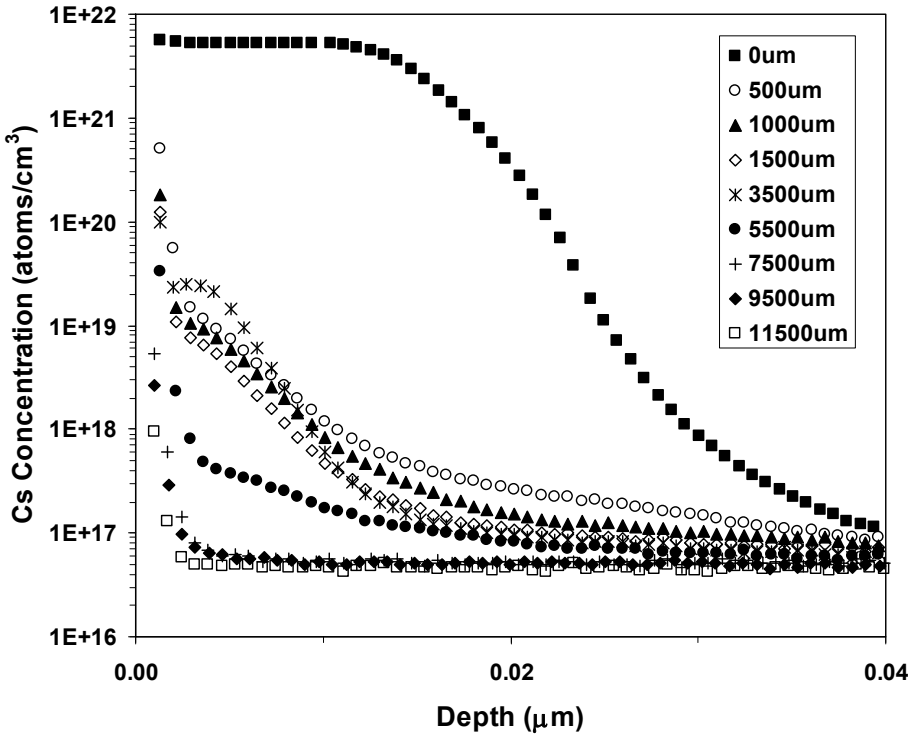

Figure 6-8. Cs concentration profiles on Si surface that was pre-sputtered by Cs primary ions.

Figure 6-9 shows a Si^+ and Cs^+ depth profile of the Cs pre-sputtered crater bottom at 14.5keV obtained using a focused 20nA, low energy (i.e. 1.25keV impact energy) O_2^+

primary ion beam (see Table 6-1). The depth profile clearly shows Si secondary ion intensities are lower in the shoulder region. At the surface, the Si intensity is about one order of magnitude lower than at the steady state region because the secondary Si yield is lower due to the high amount of Cs. Si intensity begins to level out at approximately 18 to 20nm. Referring to Figure 3-9, TRIM simulations show the projected range of Cs into Si for the pre-sputtered conditions of Cs primary ion bombardment. At impact energy of 14.5keV, TRIM predicts the total Cs ion range to be approximately 18nm consistent with the depth of the Cs shoulder in the depth profile in Figure 6-9. This evidence is supported by previous studies for oxygen and cesium bombardment. [9,10]

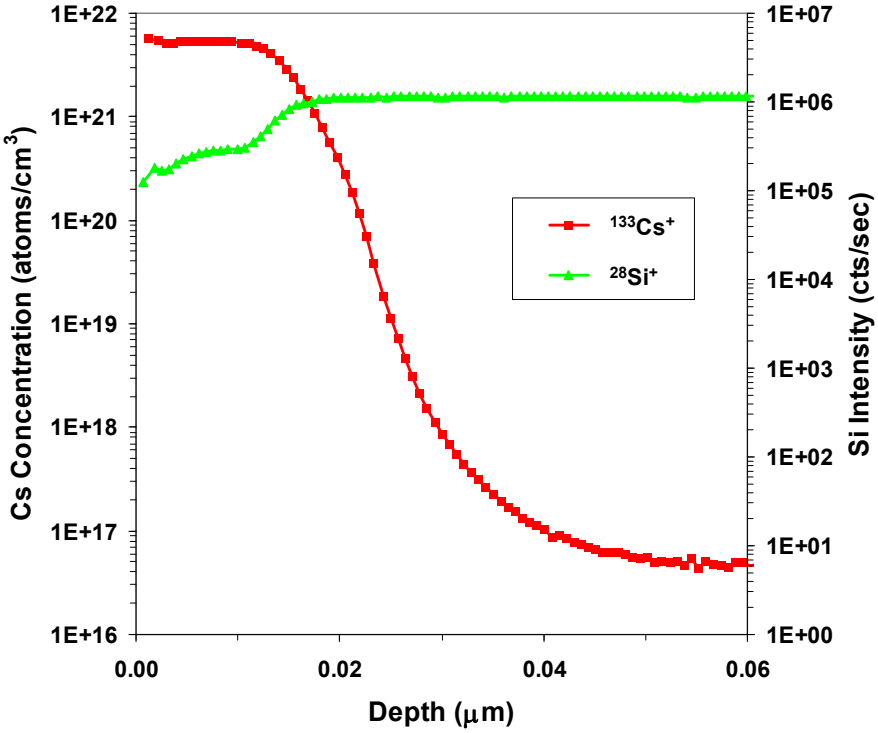

Figure 6-9. Cs^+ and Si^+ depth profiles of the Si surface which was pre-sputtered by Cs primary ions.

The surface Cs concentration in the shoulder resulting from Cs implantation during sputtering is approximately $6x10^{21}$ atoms/cm^3. Therefore, the Cs concentration reaches approximately ten atomic percent at the pre-sputtered crater based on the density of native Si

which is $5x10^{22}$ atoms/cm^3. Figure 6-10 presents the surface Cs concentration with respect to the distance from the pre-sputtered crater on the Si sample. The first cesium data point was used to determine the surface concentration value. Higher surface Cs concentration may cause the ion yield or sputtering yield of areas exposed to Cs to change from those of lower surface Cs concentration regions.[9] Cesium concentration at 1.5mm away from the pre-sputtered crater is $1x10^{20}$ atoms/cm^3 and less than one atomic percent. However, normal separation between analyzed craters is 300microns in the P implant aging study. Based on these results, an estimate of the surface Cs concentration at 300microns from the crater may be as high as $\approx 1x10^{21}$ atoms/cm^3 or approximately 2%. Unfortunately, results obtained below do not provide conclusive evidence that the distance between craters should be increased during repeated analyses; for instance, the P implant aging study (see Chapter 5). These results below are based on Cs contamination after only one previously analyzed area; however, in the P study samples are repeatedly analyzed further increasing the potential for unwanted Cs contamination. For example, with crater spacing increased to 1000microns, a decrease in the surface Cs concentration would not significantly change contamination problems observed after repeated analyses on a specific sample. During repeated analyses, areas across the sample are going to be continually exposed to Cs and the amount of Cs contamination will be higher than the observed values in Figure 6-10.

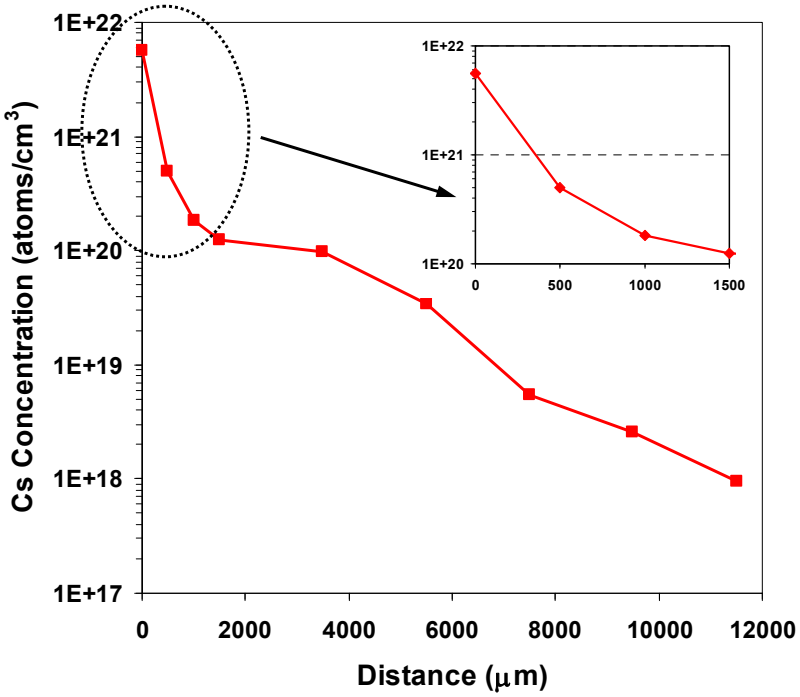

Figure 6-10. Surface Cs concentration with respect to the distance from the pre-sputtered crater by Cs primary ions on a Si [100] sample.

6.4 Summary

The cesium surface concentration in Si resulting from the use of Cs^+ primary ions was studied to gain an understanding of effects observed in secondary ion yield data obtained in the P implant study.

Cs primary ion bombardment for depth profiling in SIMS has been employed for many years to increase negative secondary ion yields. Secondary ion yield is dependent on the chemical composition of the sputtered surface of a matrix. The presence of Cs on the surface lowers the sample's work function and increases the negative ion yield which increases P secondary ion yield. This increase in ion yield can have deleterious effect resulting from inadvertent Cs exposure which may contribute to the observed changes in the real or apparent surface P concentrations on samples previously analyzed using Cs.

It appears that the large increases in apparent P surface concentration almost certainly result from the effects related to the presence of unintended implanted Cs near the sample surface (see Figure 6-10). This Cs contamination can originate from a number of sources

including Cs beam tails, Cs neutral beam, secondary sputtering from instrument optics and other structures, etc. Although this was not observed in the P study in Chapter 5, the presence of Cs may enhance diffusion to the sample surface due to creation of vacancies or by altering the surface chemical potential in a manner that attracts mobile P and perhaps the sputter rate. Clearly the strongest effect of unintended Cs contamination appears to be the altering of P secondary ion yield. An additional effect may result from increased oxidation of the sample surface additionally affecting P ion yield.

It was shown in depth profiles of sample surfaces that had been previously analyzed using the Cs primary beam that Cs contamination on the order of more than an atomic percent can extend laterally to at least 500μm away from the previously analyzed crater and probably significantly farther if the same sample is repeatedly analyzed. For example, during the P implant aging study (see Chapter 5) samples are repeatedly analyzed and continually exposed to Cs. Therefore, the Cs contamination will be higher than the one atomic percent observed in Figure 6-10 even with crater spacing increased. From the P implant aging study, CsEx samples clearly showed that this level of Cs is sufficient to significantly affect P secondary ion yield and perhaps P distribution for all samples held at 100°C and for all storage conditions for the two low dose samples. It has also been determined that, in addition to Cs neutral beam contamination, other sources of Cs sample contamination are present from sources that probably include primary beam sputtering of primary column optics, secondary sputtering of sample chamber components, sputtering of sample chamber components by backscattered primary ions, and/or redeposition of material from analysis of Cs containing samples (see Figure 6-3 and Figure 6-6). The relative degree to which these sources contribute has not been determined. However, the results suggest that the majority of the contamination is produced by the Cs neutral beam. The known occurrence of Cs contamination indicates SIMS analyses need to be completed with vigilance and with understanding of processes that may produce surface artifacts.

6.5 References

[1] M. Schumacher, CAMECA Instruments, computer program.

[2] D.W. Hoffman, Surf. Sci. **50**, 29 (1975).

[3] M.H. Clark, K.S. Jones, and F. A. Stevie, J. Vac. Sci. Technol. **20**, 1663 (2002).

[4] W. Vandervorst, H.E. Maes, and R. De Keersmaecker, Surf. Interface Anal. **4**, 245 (1982).

[5] K. Miethe, W.H. Gries, and A. Pöcker, in *Proceedings of SIMS V*, Volume 44 in Springer Series in Chemical Physics (Springer, Berlin, 1986), p.347.

[6] R.G. Wilson, F.A Stevie, and C.W. Magee, Secondary Ion Mass Spectrometry: A Practical Handbook for Depth Profiling and Bulk Impurity Analysis, Wiley, New York, (1989).

[7] K. Wittmaack and J.B. Clegg, Appl. Phys. Lett. **37**, 285 (1980).

[8] W.H. Gries and K. Miethe, J. Vac. Sci. Technol. **5**, 1740 (1987).

[9] S. Yoshikawa and K. Tsukamoto, in: Junction Technology, IWJT. Extended Abstracts of the Second International Workshop on. 45 (2001).

[10] J.C.C Tsai and J.M. Morabito, Surface Science, **44**, 247 (1974).

7 Conclusions and Future Work

7.1 Summary

A change in apparent P surface concentration after ion implantation has been observed over time and this change can strongly affect the accuracy of P dose measurements. The impact of inaccuracy in the P measurement increases as the dose decreases. If samples previously exposed to Cs are used as standards, P measurement accuracy is more severely impacted, again with the impact increasing as the P dose decreases. The results of this study show that changes in the apparent P surface concentration and thus changes in measured P dose can be avoided (at least for samples stored for a period of up to 32 weeks) by using a fresh, not previously analyzed piece of a wafer that has been stored under LN_2 for each dose measurement experiment. The source of the observed increase in apparent P surface concentration can result from redistribution of the implanted dose, contamination from the environment, a change in P secondary ion yield, or a combination of these and/or other factors.

The use of low dose P implants in Si without any pre or post processing as standards for P dose measurements or other P quantification experiments is problematic. Also, the as received P depth profiles of 1E12 at//cm^2 implanted nominally identical samples (wafers 672 and 798) demonstrated that the as implanted surface concentration of P in Si can vary even in wafers implanted under presumably identical conditions. The use of pre-amorphization to reduce surface effects is problematic since the depth of the implant is significantly reduced causing potential problems with obtaining sufficient data points for generation of a useful RSF.

With regard to use of low dose P implants as standards, preliminary results indicate that either pre-cleaning followed by RTA (wafer 840) or implantation through a 50Å oxide (wafer 839) can provide wafers that can be used for standards. If a new piece of standard can be used for each analysis, P implanted Si wafers that have undergone RTA following implantation can be used to provide a useful standard. If the samples to be used as standards are previously exposed to Cs, then the dose integrated below 40nm must not be included to

avoid surface effects. For the Si wafers with P implanted through a 50Å oxide, prior exposure to Cs appears to have an insignificant surface effect over the period studied although the safest approach would be to avoid use of samples previously exposed to Cs. If Cs exposure cannot be avoided, it is recommended that a depth be selected e.g. 40nm and that only the dose at greater depths be integrated to avoid any risk of the potentially deleterious effects of Cs.

In depth profiles of samples whose surfaces had been previously analyzed using the Cs primary beam (CsEx), Cs contamination on the order of more than an atomic percent can extend laterally at least 500μm away from the center of the previously analyzed crater. CsEx samples clearly showed that the level of Cs observed is sufficient to significantly affect P secondary ion yield and perhaps affect P distribution for all samples stored at 100°C and for the low dose samples (without any pre or post processing) under all storage conditions. It has also been determined that, in addition to Cs neutral beam contamination, other sources of Cs sample contamination are present which probably include primary beam sputtering of primary column optics, secondary sputtering of sample chamber components, sputtering of sample chamber components by backscattered primary ions, and/or redeposition of material from analysis of Cs containing samples. The relative degree to which these sources contribute has not been determined.

7.2 Future Work

The time study of the P dose measurement changes should continue in order to determine if the above results can be extended. Further work is required to determine if there is any movement of P from the bulk to the surface, if the increase in apparent surface concentration is due to contamination from the SIMS instrument, a change in the P ion yield, or any or all of the previous possibilities.

APPENDIX

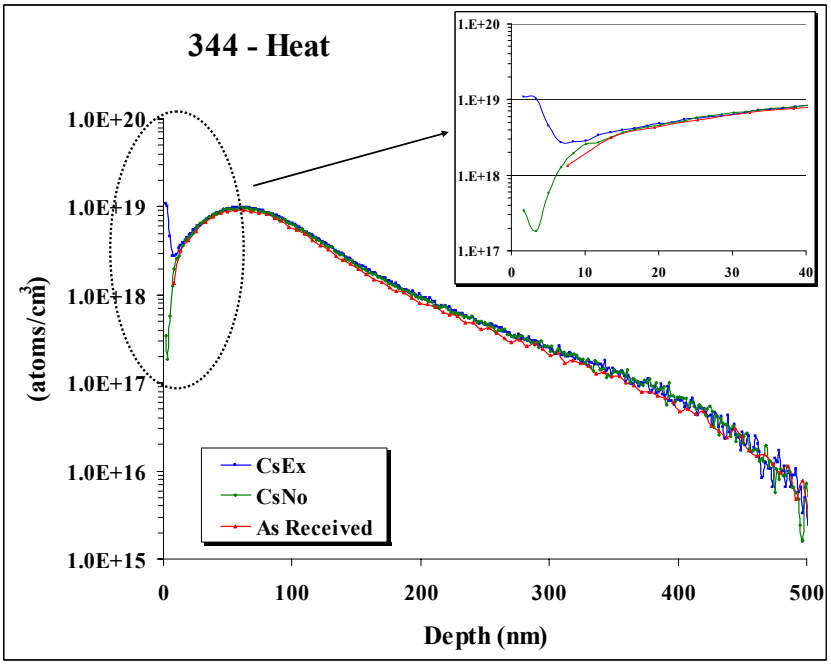

Figure A-1. Depth profiles of sample 344 (P in Si of 1E14 atoms/cm^2, 35keV) as received, CsEx and CsNo samples after 31 weeks stored in an oven at 100°C.

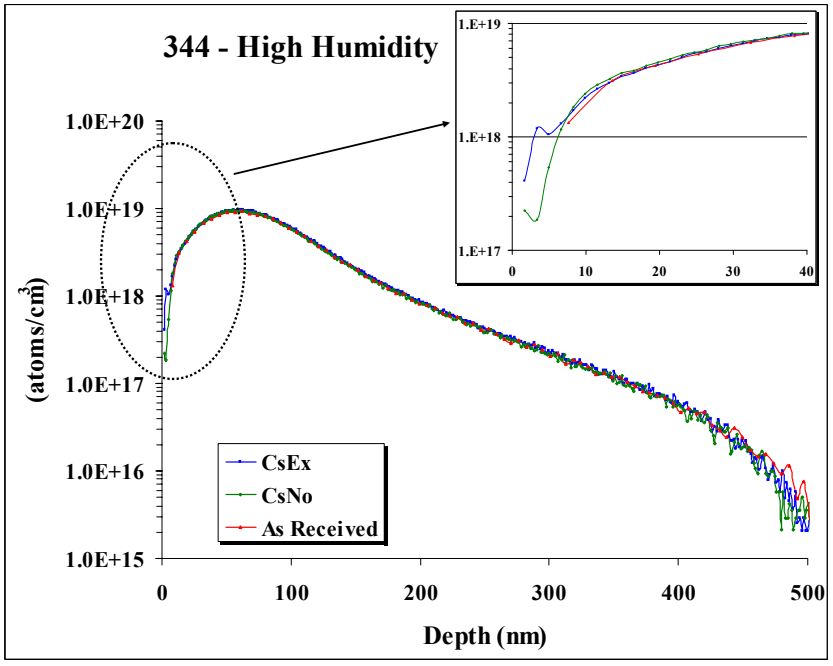

Figure A-2. Depth profiles of sample 344 (P in Si of 1E14 atoms/cm^2, 35keV) as received, CsEx and CsNo samples after 31 weeks stored in a dessicator with water.

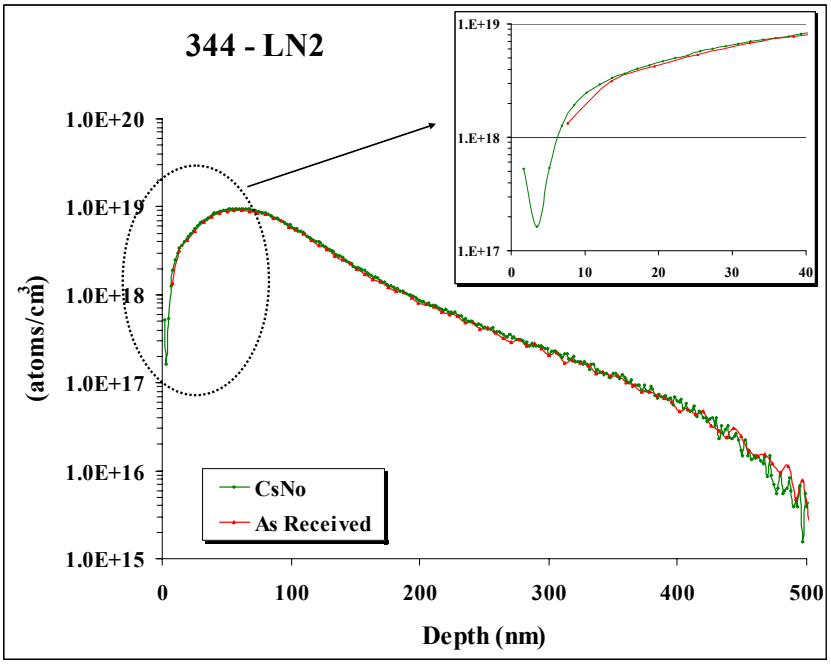

Figure A-3. Depth profiles of sample 344 (P in Si of 1E14 atoms/cm^2, 35keV) as received and CsNo samples after 32 weeks stored under LN_2.

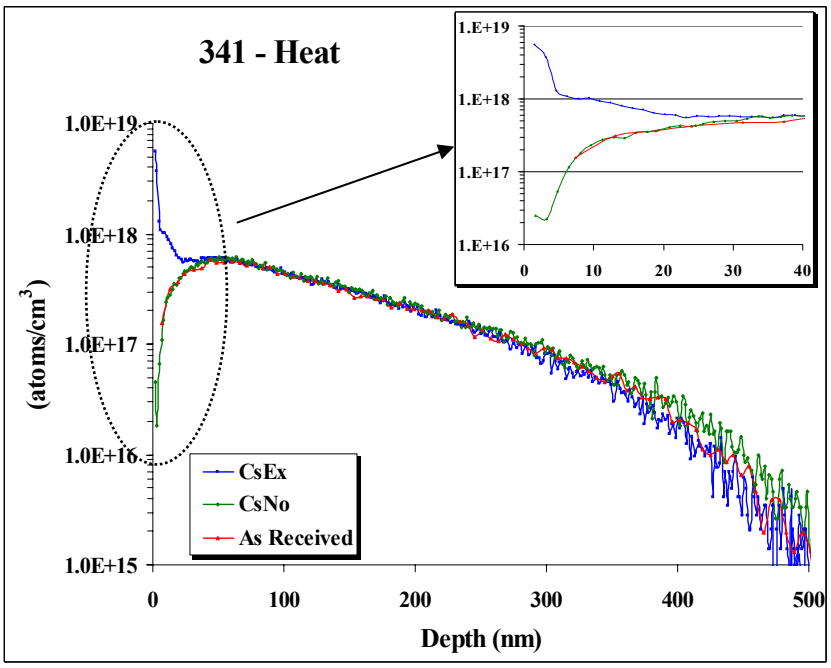

Figure A-4. Depth profiles of sample 341 (P in Si of 1E13 atoms/cm^2, 35keV) as received, CsEx and CsNo samples after 31 weeks stored in an oven at 100°C.

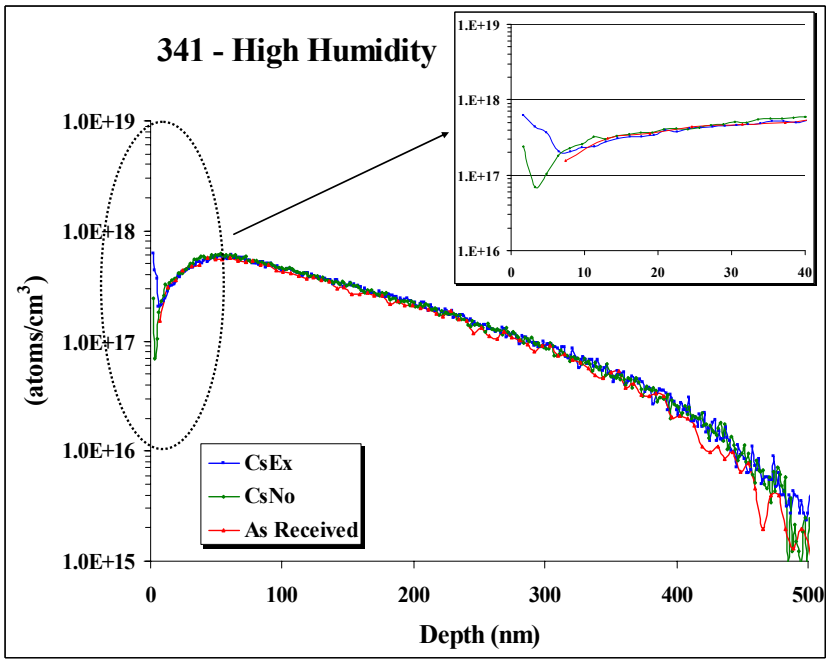

Figure A-5. Depth profiles of sample 341 (P in Si of 1E13 atoms/cm^2, 35keV) as received, CsEx and CsNo samples after 31 weeks stored in a dessicator with water.

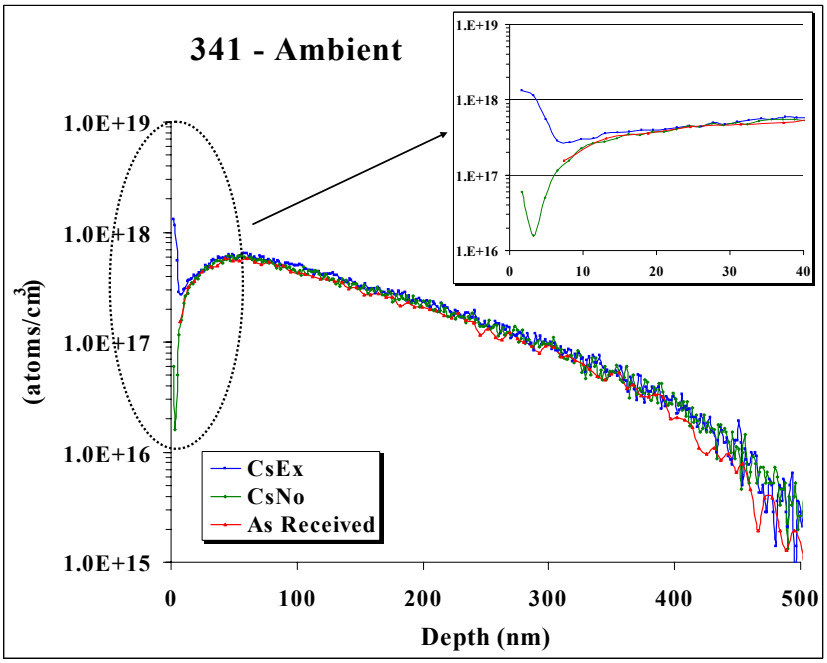

Figure A-6. Depth profiles of sample 341 (P in Si of 1E13 atoms/cm^2, 35keV) as received, CsEx and CsNo samples after 31 weeks stored in an ambient laboratory environment.

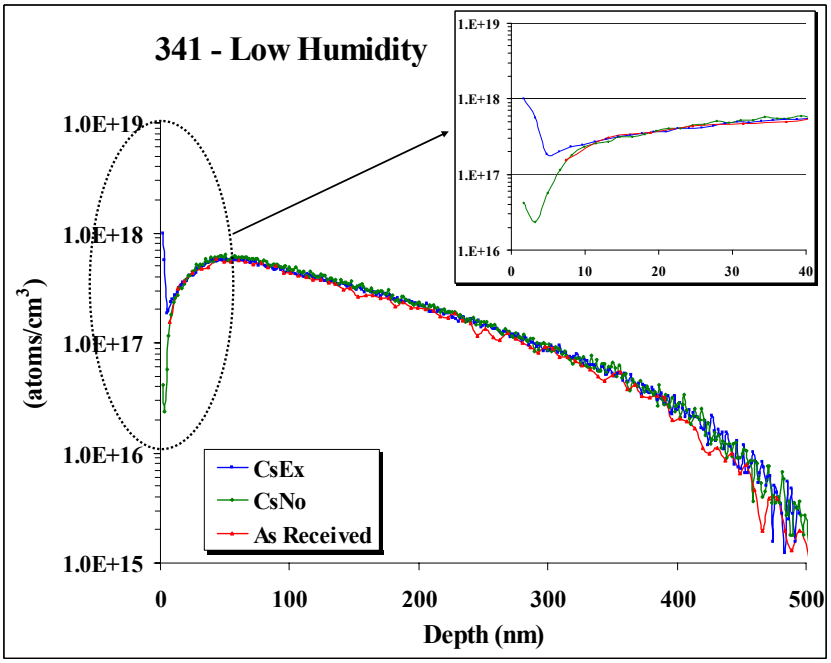

Figure A-7. Depth profiles of sample 341 (P in Si of 1E13 atoms/cm^2, 35keV) as received, CsEx and CsNo samples after 31 weeks stored in a dry dessicator.

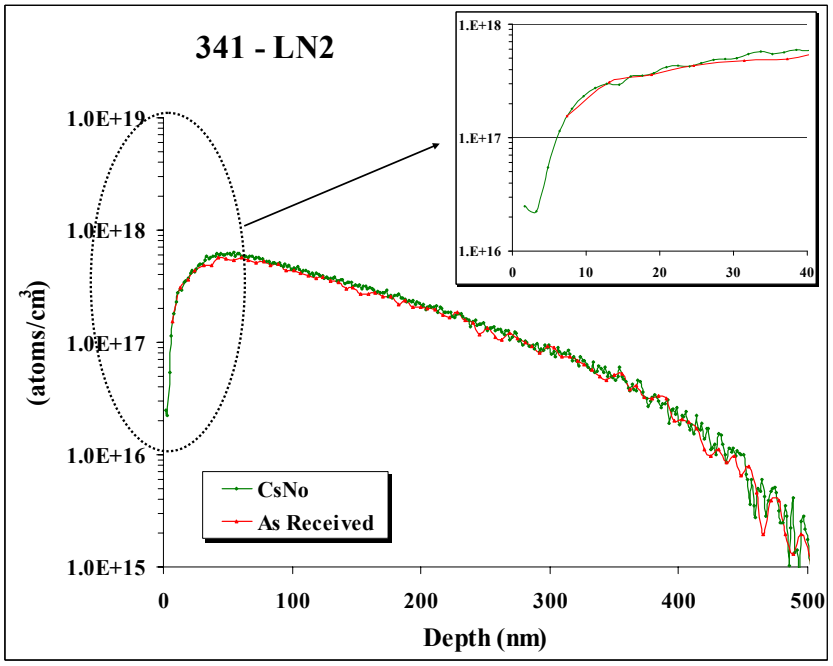

Figure A-8. Depth profiles of sample 341 (P in Si of 1E13 atoms/cm^2, 35keV) as received and CsNo samples after 32 weeks stored under LN_2.